CERN LIBRARIES, GENEVA

CM-P00051230

OPAL-PN020
DECEMBER 20, 1990

Final State Photon Radiation in Multihadronic Decays of the Z^0

C.Markus, P.Mättig, S.Schreiber, and W.Zeuner

Abstract

Final state photon radiation is measured with more than 170,000 multihadronic Z^0 decays. The observed yield of 184.4±14.3 photons emitted from quarks is in agreement with the expectation from the JETSET calculation of 150.2±6.0. Also the energy spectrum, the spectrum of the transverse momentum with respect to the thrust axis, and the topology of the recoil event are in agreement with the expectation. Interpreting these results in terms of the weak coupling $c_i = v_i^2 + a_i^2$, one finds for the up and down type quarks

$$c_d = 1.20 \pm 0.16 \quad c_u = 1.61 \pm 0.21$$

in agreement with the standard model results. The theoretical error is still under study.

1 Introduction

In this letter we present a measurement of final state photons emitted from quarks [1] in multihadronic decays of the Z^0. As discussed in detail in [2] the final state radiation provides a way of disentangling the weak couplings of up and down type quarks. Briefly, it exploits the fact that photons couple to the square of the charge of the emitting fermion. As a result up type quarks are enriched in a theoretically known ratio in events with a hard photon relative to the overall multihadron sample. The respective yields allow one to infer the weak couplings.

A clean, almost background free signal is observed. For the current analysis the theoretical estimate of the expected photon yield can just be pursued with the JETSET model [3]. In view of the approximations used in this model it is difficult to determine the absolute theoretical error. The analysis is not yet finalized, the results will therefore be given with respect to the JETSET expectation only.

A first measurement exploiting this method based on about 27,000 multihadronic Z^0 - decays can be found in [1]. The current analysis is based on a sevenfold increase of data allowing, together with smaller systematic uncertainties, a much higher precision.

2 Data selection

This analysis is based on an integrated luminosity of about 8 pb^{-1} collected with the OPAL detector [5] at LEP over the first year of operation. The data were recorded at center of mass energies E_{cm} between 88.28 and 95.04 GeV around the Z^0 - pole.

The most important components of OPAL for this study are the main central drift chamber and the barrel part of the electromagnetic calorimeter. The central detector provides a measurement of the momenta of charged particles over almost the entire solid angle in a magnetic field of 4.326 kG. The electromagnetic calorimeter covers the solid angle up to $|cos\theta| \leq 0.98$, where θ is the polar angle with respect to the beam direction. Its barrel part is used for photon identification in this analysis and consists of 9440 lead-glass blocks of 24.6 radiation lengths, pointing towards the interaction region and each subtending an angular region of approximately 40x40 mrad^2. The presampler for electromagnetic showers and the hadron calorimeter served as cross checks for the photon identification. The presampler is located between the coil and the lead glass calorimeter. It consists of a set of 16 double-planed chambers containing Iorroci tubes with both wire and cathode-strip readout. The hadron calorimeter, consisting of nine planes of streamer-tube chambers within the iron return yoke of the magnet, is located directly behind the electromagnetic calorimeter. Apart from measuring hadron energies it allows one to scan the longitudinal shower development.

Multihadronic events are required to have at least five well measured tracks and more than seven clusters in the electromagnetic calorimeter. An accepted track, reconstructed from at least 20 hits in the main drift chamber, must have a minimum transverse momentum

to the beam of 250 MeV, a reconstructed distance of closest approach to the beam axis of less than 5 cm, and a longitudinal displacement along the beam direction from the nominal interaction point of less than 30 cm at the point of closest approach to the beam. A cluster in the lead-glass calorimeter consists of at least one block and a total energy of more than 100 MeV in the barrel region ($| cos\theta | < 0.82$) and at least two adjacent blocks with a minimum total energy of 200 MeV in the endcap region ($| cos\theta | > 0.82$). The energy sum ΣE_{clu} of all accepted clusters must exceed $0.11 \cdot E_{cm}$. It must be balanced along the beam direction as $| \Sigma(E_{clu} \cdot cos\theta) | / E_{cm} < 0.65$. These requirements were satisfied by 172,309 events. The acceptance for multihadronic events is estimated to be 0.975 with a systematic uncertainty of 0.007 and a fraction of background from τ pairs, and two-photon processes of less than 0.003 [6].

These events were searched for isolated photon candidates of more than 10 GeV energy within a fiducial region of $| \cos\theta | \leq 0.72$. The latter cut is chosen to minimize the material in front of the lead glass and thus to retain a good discrimination power against π^0 - background. No tracks and no other electromagnetic clusters were allowed within a cone of half-angle 20 degrees centered at the photon direction. To reduce the background from narrow neutral jets, to select only photons emitted from quarks that couple directly to the Z^0, and to avoid biases against any flavour [2], only photons with a transverse momentum p_T with respect to the thrust axis of more than 5 GeV were selected. After these cuts 222 clusters are retained.

Background to direct photons stems from neutral hadrons and particularly from photons due to π^0 decays. It is further suppressed by requiring the properties of the electromagnetic cluster to be consistent with that expected from a single photon. In a first step clusters were selected that consist of no more than 15 lead-glass blocks and have a width, defined by

$$M^{EB} = \sqrt{\frac{\Sigma E_i \cdot ((\phi_i - < \phi >)^2 + (\theta_i - < \theta >)^2)}{\Sigma E_i}}, \qquad (1)$$

of less than 30 mrad. Here ϕ_i and θ_i are the polar and azimuthal angles of each block i in the cluster and E_i is the energy deposited in the block. $< \phi >$ and $< \theta >$ describe the centroid of the cluster, and the summation runs over all blocks in the cluster. The corresponding distribution of the photon candidates are displayed in figs. 1a,b.

The final cut refers to the sharing of energy among the blocks which has to be consistent with that expected from a photon. For this purpose a cluster shape variable

$$C = \frac{1}{N_{block}} \sum \frac{(E_i^{exp} - E_i^{obs})^2}{\sigma_i^2} \qquad (2)$$

is calculated for each cluster, where E_i^{exp}, σ_i and E_i^{obs} denote the expected energy, its variation and the observed energy of block i, respectively. The summation is over all blocks of the cluster. C is then required to be less than 1.5. The distributions in C of the isolated clusters before the cuts on the cluster properties are displayed in figs. 2a-c for the three energy intervals $10 < E_{clu} < 20$, $20 < E_{clu} < 30$, and $E_{clu} > 30$ GeV. These cuts leave 195 photon candidates in the sample.

3 Efficiency and Background Contributions to the Photon Sample

The efficiency of the photon selection was determined from a sample of unambiguous photons from radiative lepton-pair events and the process $e^+e^- \rightarrow \gamma\gamma$ [7] recorded during the same running period. 181 photons were collected for this reference sample. The total efficiency for photon identification is 89.8±2.7% and comprises losses due to conversions before and inside the chamber (5.7±2.2%) and the requirements on the cluster shape (5.0±1.6%). The cluster shape observed in these events are also shown in figs. 2a-c and are seen to agree very well with the photon candidates in the multihadronic events. Also shown are results of the simulation of photons which reproduce well the observed spectrum.

The remaining background from neutral narrow jets to the observed candidate events was estimated with several independent methods. By assuming isospin symmetry, the background yield was obtained from the number of narrow *charged* jets. Cross checks were performed by using the different distributions in C of genuine photons, of π^0's and of other hadronic contributions to the isolated clusters and by studying the response in the hadron calorimeter and the barrel presampler.

Multihadronic Z^0 - decays as generated with the models of [3] and [8], interfaced with a detailed simulation of the OPAL - detector, served as a tool for understanding which kind of fragmentation background could potentially contribute to the selected sample. Only π^0's were found to produce isolated clusters surviving all requirements. The background expected from these simulations is 8.3±3.8 events. This number will not be used in the following analysis. Rather the background will be estimated from the data themselves. Other sources of isolated clusters with properties resembling those of genuine photons were found to be due to K_L^0's, neutrons and decays of high momentum particles like η's and K^{*0}'s decaying into two neutral particles and yielding overlapping showers in the lead glass calorimeter. These two background contributions, single and unresolvable pairs of neutral particles, were estimated using charged particles within a subsample of 115,095 events.

As a first background source single charged particles were considered. Ten isolated tracks were retained. To guarantee those to be well measured strict cuts were applied leading to a track finding efficiency of 0.93±0.01 obtained from μ - and electron pair events. To translate the yield of isolated charged particles into the yield of isolated neutral clusters several corrections have to be applied. Isospin symmetry implies $n_{\pi^0}=1/2 \cdot n_{\pi^\pm}$, $n_{K_L^0}=1/2 \cdot n_{K^\pm}$, $n_{neutron}= n_p$, where at least the first two relations are experimentally supported (for a review see [9]). The efficiency to reject π^0's using the cluster shape has been found with a detailed simulation of the OPAL detector as 0.6, 0.36, and 0.15 in the respective energy intervals $10< E_{clu} <20$ GeV, $20< E_{clu} <30$ GeV, $E_{clu} >30$ GeV. The lead glass response of π^0's obtained from a simulation is shown in figs. 1a-c. The corresponding efficiency to reject K_L^0's and neutrons, was found to be 0.986±0.005 and 0.993±0.005 respectively. Using in addition the relative fractions of pions, kaons, and protons for particle energies above 10 GeV [10] leads to an estimated background of 2.6±0.8 (stat. err.) events from single isolated neutral particles, most of them being at energies somewhat above 10 GeV. Uncertainties in

these corrections stem mainly from the measured ratio of neutral over charged pions (±25%), and from the $\pi^{\pm}$ fraction in the stable charged particle yield ($\sim$ 10%). A total systematic error of 50% will be assigned to this background source.

As a second kind of hadronic background the overlap of two particles in one cluster was considered. Due to the various possible contributions and due to the lack of precise measurements, respectively uncertainties in modelling the hadronization process, the estimate is less certain. In a first step potential sources of neutral particles yielding photon - like electromagnetic clusters were simulated with 300-500 single decays of each $K^{*0} \rightarrow K^0_L\pi^0$ and $K^0_s \rightarrow \pi^0\pi^0$. Depending on the decay, 1.6 and 16% of the particle combinations were finally retained. All of those had a decay opening angle of less than 40 mrads. In a second step the background from overlapping neutral particles was estimated by searching for two *charged* particles within 40 mrads [1] which,when combined, satisfy the kinematic requirements imposed on the isolated photons. Apart from ten e^+e^- - pairs of single photons, which are consistent with the expected number of converted photons, 21 isolated charged particle combinations were found. Correcting these for isospin symmetry, experimental distortions and the rejection efficiency for their neutral counter parts from the cluster shapes, one estimates a background of 0.75 neutral clusters. To take into account the uncertainty in the precise nature of the two overlapping particles and in the experimental corrections a systematic uncertainty of ±100% was assigned to this contribution.

Other hadronic background contributions not covered by the charged particle analysis are electromagnetic decays like $\eta \rightarrow \gamma\gamma$. From simulation studies it was found that for energies between 10 and 50 GeV, 0.980±0.006, of these decays are rejected. As a result these contributions in the selected isolated clusters are negligible.

In total a background of 3.1±2.2 is estimated from the analysis of charged particle jets.

This background estimate was cross checked with other methods. A first check is based on the different distributions of photons, π^0's (see figs. 1a-c), and overlapping neutral hadrons in the cluster shape parameter C. The observed distribution was used to unfold these contributions. To obtain the hadronic background in the selected sample, the distribution n^{obs} in C were split into the five intervals 0.-0.5, 0.5-1., 0.5-1.5, 1.5-4 and larger than 4 and expressed with a linear equation system

$$N_i^{obs} = p_i^{\gamma} \cdot N^{\gamma} + p_i^{\pi^0} \cdot N^{\pi^0} + p_i^{nh} \cdot N^{nh}.$$

Here p_i^c are the probabilities to find a particle c in the interval i, and $N^{\gamma}, N^{\pi^0}, N^{nh}$ the numbers of γ's, π^0's and neutral hadrons as free parameters. The p_i^c's were taken from the photon reference sample, and from the simulation respectively. The linear equation system was solved separately for $10 < E_{clu} < 20$ and $20 < E_{clu} < 30$. Assuming the π^0 fraction for $E_{clu} > 30$ GeV to be the same as for the lower energies, the background is given as 0.6±5.2 (stat.) consistent with the result of the charged jet analysis. The systematic uncertainties of the fit results were estimated by varying $p_i^{\gamma}(C)$ and p_i^{nh} taking into account statistical uncertainties and possible variations of the neutral hadronic component and are estimated to be ±10 clusters.

[1] This requirement was imposed in the plane transverse to the beam direction only. To take into account the worse resolution along the beam direction, the total opening angle had to be smaller than 10 degrees.

Table 1: Observed Photon candidates and expected contributions

	nb. of events
observed yield	195.0 ±14.0
expected fragm. background	3.4±2.2
expected initial state photons	7.2±0.8
Remaining photons	184.4±14.3
expected final state photons	150.2±5.9

The photon candidates were further checked by studying their response in the presampler and in the hadron calorimeter. The width and the size of the signals in the presampler are consistent with the observations for photons in the reference sample. Only a small fraction of genuine photons should leak into the hadron calorimeter. Five candidates were found to have more than 2 GeV energy deposition in the hadron calorimeter. From the longitudinal shower profile two of those are judged inconsistent with electromagnetic origin. These numbers are consistent with the background estimation as obtained from the reference sample of 1.5±1.0 for genuine photons and 0.75±0.75 for neutral stable hadrons.

For the further evaluation the background from hadronic origin is assumed to be 3.4±2.2.

4 The Final State Photon Sample

Additional background to the final state photons is due to initial state photons. On the Z^0 these are strongly suppressed, however, 26.9% of the data for this analysis were collected slightly off the peak. At these energies the fraction of initial state photons is significantly increased. Taking the energy dependence into account, the number of initial state photons as expected by using the Monte - Carlo generator of [11] is 7.2±0.8.

The various contributions to the selected sample are listed in table 1. Subtracting the background from fragmentation and initial state radiation leads to 184.8±14.4 photons from other sources. Assuming standard model couplings the simulation [3] with parameters optimized to describe the event shapes [12] predicts 150.2±2.2 (statistical error) final state photons for the number of multihadronic events produced. The systematic uncertainties of this expectation are due to the event selection and to the theoretical model. Various studies were performed to establish their size.

Potential theoretical and phenomenological uncertainties of the predictions of the photon yield are discussed in detail in [2]. Since the photon *yield* will be taken as a measure for parameters of the standard model, the discussion of the quality of the theoretical description

Table 2: Ratio of measured and expected final state photon yield for different isolation cones

	cone 15°	cone 20°	cone 25°
n(obs.)/n(exp.)	1.21	1.20	1.23

will start with the *shape* of the distribution. Uncertainties of the absolute prediction will be discussed in the next section.

The requirement of having *no* track and *no* other electromagnetic cluster (after cuts) within a cone of half opening angle of 20° is rather severe and could distort the acceptance estimate. From randomly triggered events it was found that less than 0.7% of events with hard photons are lost because of noise induced clusters inside the isolation cone. The uncertainties in losses due to soft hadrons scattered into the isolation cone were estimated by examining the particle flow just outside the isolation cone and by modifying the isolation angle. No significant deviation from the Monte - Carlo comparison was observed. The particle flow $1/N_{ev}dN/dcos\alpha$, α being the angle of each track or cluster to the photon candidate, for α between 0 and 90 degrees is shown in fig.3a. There are 7.2±4.5% more Monte - Carlo events than real data in the interval of α 20 - 25 degrees which would indicate an underestimation of the acceptance. On the other hand, the ratio of the number of events observed to those expected increases by 4.3±3.2% with a change of the maximum energy in the isolation cone from 0 to 0.5 GeV, indicating an overestimation of the acceptance. The same trend is observed when changing the isolation cone to 15 and 25 degrees leading to a 2.6%, respectively 4.3% larger ratio (table 2). To take into account possible uncertainties due to soft particles biasing the isolation requirement, an error of 3% will be assigned to the prediction of isolated photons. Combined with the 2.7% uncertainty for the photon detection, the total uncertainty of the selection is ±4.0%.

Apart from the modelling of soft hadronization, uncertainties in the simulation may be due to the treatment of hard higher order QCD corrections. As shown in [15,16] the jet topology of the total multihadronic events is well described by the simulation. In figs. 3b,c specific tests of the topology of events with hard photons are displayed. The jet rates as calculated using the JADE jet finding algorithm [17] are shown as function of $y_{cut} = M^2/E^2_{vis}$, with M the maximum allowed jet mass and E_{vis} the sum of track momenta and cluster energies in each event. The candidate photon has been excluded from the jet finding. The simulation describes the measurement very well. A more concise estimate of the relation of photons and jets is given by the minimum invariant mass per event of a photon and a jet. The comparison of data and simulation shows a good agreement (fig.2c, for y_{cut}=0.005). Both distributions indicate potential losses due to jets falling into the isolation cone to be negligible.

The quality of the simulation can be further studies from figs. 4a,b displaying the energy and the p_T - spectrum of the observed photons together with the expectation and the background contribution. For fig. 4b also photon candidates with $p_T < 5$ GeV are included that are retained by all other cuts. No statistically significant difference between data and simulation is observed. The measured photon yield between energies of 10 and 20 GeV is 2.6

Table 3: Ratio of measured and expected final state photon yield for different minimum photon energies

	7.5 GeV	10.0 GeV	12.5 GeV
n(obs.)/n(exp.)	1.20	1.20	1.22

Table 4: Ratio of measured and expected final state photon yield for different minimum transverse momenta of the photon

	0 GeV	2 GeV	4 GeV	6 GeV	8 GeV	10 GeV
n(obs.)/n(exp.)	1.20	1.19	1.19	1.19	1.18	1.17

standard deviations above the expectation.

Apart from these specific investigations the systematic uncertainties can be estimated globally by varying the kinematical cuts and calculating the final photon yield. Tables 3 and 4 summarize the effects of variations of the minimum photon energy (7.5 - 12.5 GeV) and the transverse momentum of the photon with respect to the thrust axis (0 - 10 GeV). Listed is the ratio of observed and expected photon yield for each choice of cut variable. All the background estimates discussed in the previous section, the calculations for initial state radiation and final state photons were performed in full for each cut value. All the results agree within statistics. Although the observed yield of photon candidates varies by more than a factor two, the ratio changes by at most 2.5%.

Combining the above studies a systematic error of ± 6.0 events was assigned to the selection efficiency for the 150.2 events expected from the JETSET simuation. It is due to uncertainties in the efficiency of photon detection, to the modelling of the soft hadronization and to the limited Monte - Carlo statistics. This result has to be compared with the 184.4 ± 14.2 observed final state photons.

5 Determination of the Quark Couplings

To interpret this measurement in terms of the weak quark couplings and possible non - standard contributions, the theoretical uncertainty of the model has to be evaluated. This has not been finalized yet. Therefore all numbers in this section refer to the expectation from JETSET with the parameters optimized as given in [12].

The observed yield is 2.2 standard deviations larger than expected. Any additional contribution, as conceived, e.g., in composite models [18], of more than $\sigma_{\gamma+had} = 13.3$ pb can be excluded with 95% confidence. Here an isotropic distribution of the photon was assumed and no correction for potential losses due to kinematical cuts were applied. In terms of contri-

butions to Z^0 decays, non standard - model sources with $BR(Z^0 \rightarrow hadrons + \gamma) > 3 \cdot 10^{-4}$ can be excluded. No significant deviation from the standard model expectation has been observed in any of the kinematical distributions. In the following it will be assumed that only standard model sources contribute to the observed photon sample.

Corrections to the final state photon sample come from photons emitted from non - primary quarks, produced in the parton cascade by $g \rightarrow q\bar{q}$. They are expected to contribute less than $5 \cdot 10^{-3}$ to the photon sample [3]. The interference of final and initial state photons which is not included in the Monte - Carlo generator [3] was estimated by integrating the matrix element [2] [13] in lowest order correction in α. It was found to contribute 0.1% of the whole $q\bar{q}\gamma$ sample on the Z^0 pole (where most of the data were collected) and -7.8% and +1.8% at $E_{cm} = 88.16$ and 94.16 GeV respectively.

Apart from these small effects, the photon rate is determined within the standard model essentially by two parameters:

- the ratio of electromagnetic and strong coupling α_{em}/α_s
- the relative fraction of up - and down type quarks

As discussed in [2] within the model [3] the yield depends on the value of the strong coupling scale Λ_{shower}. The electromagnetic coupling constant was used in the Thomson limit $\alpha_{em}(0)$ [14].

As yet only one QCD - program includes final state photons. From measurements of the jet rates [15] and from the overall event topologies [12] the model specific QCD-scale Λ_{shower} has been determined as Λ_{shower}=310±50 or 290^{+20}_{-10} MeV. Its uncertainty corresponds to an uncertainty of ±1 photons. Setting the weak couplings equal to their standard model values, the observed photon yield could be explained if $\Lambda_{shower} \sim 100$ MeV. With such a value it is difficult to obtain a consistent description of the event topologies.

Several cross checks were performed to establish the correctness of the ansatz in [3]. No significant discrepancy between simulation and data has been observed. The estimate of a theoretical error, however, is not yet completed.

Apart from the QCD coupling strength, the photon rate is sensitive to the amount of up - and down type quarks in multihadronic events and thus to the electroweak couplings

$$c_i = v_i^2 + a_i^2 \tag{3}$$

of down and up type quarks to the Z^0 [2]. The axial and vector couplings are defined by

$$v_i = 2 \cdot I_{3,i} - 4 \cdot Q_i \cdot \sin^2\theta_w \quad and \quad a_i = 2 \cdot I_{3,i} \tag{4}$$

where i denotes down or up type quarks, I_3, Q, and θ_w the third weak isospin component, the charge of the quarks and the weak mixing angle respectively.

[2] No QCD or hadronization corrections were included.

Combining the measurement of the photon rate with the total hadronic decay width, one can obtain the weak couplings of up - and down type quarks. From the hadronic decay width of the Z^0 one obtains

$$3 \cdot c_d \; + \; 2 \cdot c_u \; = \Gamma_{had} \cdot \frac{24 \cdot \pi\sqrt{2}}{N_c \cdot G_\mu \cdot M_Z^3} \cdot \frac{1}{1 \; + \; \frac{\alpha_s}{\pi}} \tag{5}$$

Here Γ_{had}= 1778±26 MeV [19] is the hadronic width N_c is the number of colours, G_μ the Fermi coupling constant at the muon mass, M_Z the mass of the Z^0 , and α_s the strong coupling constant measured as 0.118±0.008 [20,21] at $\sqrt{s}=M_{Z^0}$. This leads to

$$3 \cdot c_d \; + \; 2 \cdot c_u \; = \; 6.90 \pm 0.11$$

Because the photons couple with the square of the electric charge of the quarks, the proportion of u-type quarks is enhanced by a factor of four relative to the d-type quarks in events with final state photons. Their yield is therefore proportional to $(3 \cdot c_d + 8 \cdot c_u)$. From the observed number of events it is given as

$$(3 \cdot c_d + 8 \cdot c_u)_{exp} \; = \; \frac{(N_{\gamma q\bar{q}})_{exp}}{(N_{\gamma q\bar{q}})_{MC}} \cdot (3 \cdot c_d + 8 \cdot c_u)_{MC} \; = \; 16.75 \pm 1.41 \tag{6}$$

The indices 'exp' and 'MC' stand for either the experimental values or those obtained from the simulation [3]. The number of events after selection and including inefficiencies in the photon detection is denoted by $N_{\gamma q\bar{q}}$. $(N_{\gamma q\bar{q}})_{MC}$ is the number of photon events expected by the Monte - Carlo program normalized to the observed number of multihadronic events.

These two measurements can be solved for c_d and c_u leading to

$$v_d^2 + a_d^2 \; = \; 1.20 \pm 0.16 \;\; and \;\; v_u^2 + a_u^2 \; = \; 1.64 \pm 0.24$$

These results, together with the one standard deviation intervals from the hadronic width and the number of final-state bremsstrahlung photons, are depicted in fig. 5. It should be noted that these results, and the values for the branching ratios and widths of up - and down - type quarks are correlated. The somewhat larger than expected photon rate reflects itself in an up - type coupling that is higher, and a down - type coupling that is smaller than the corresponding standard model expectations of c_d=1.18 and c_u=1.15 for $sin^2\theta_w$=0.23.

These results can be expressed in terms of the hadronic branching ratios for up and down type quarks using

$$B_i \; = \; \frac{(v^2 + a^2)_i}{3 \cdot (v^2 + a^2)_d \; + \; 2 \cdot (v^2 + a^2)_u} \tag{7}$$

yielding

$$B_d \; = \; 0.175 \pm 0.024 \qquad B_u \; = \; 0.238 \pm 0.034$$

The corresponding partial widths Γ_d, Γ_u obtained from

$$\Gamma_i \; = \; B_i \cdot \Gamma_{had} \tag{8}$$

are

$$\Gamma_d \; = \; 311 \pm 42 \qquad \Gamma_u \; = \; 423 \pm 60 \qquad MeV$$

To repeat, at this stage of the analysis these numbers are valid only within the JETSET model with optimized parameters. No theoretical error can yet be assigned.

References

[1] T.F.Walsh and P.Zerwas, Phys.Lett. *44B* (1973), 195; S.J.Brodsky, C.E.Carlson, and R.Suaya, Phys.Rev.*D14* (1976), 2264; K.Koller, T.F.Walsh, and P.Zerwas, Z.Physik *C2* (1979), 197

[2] P.Mättig and W.Zeuner, CERN-PPE 90-144 submitted to Z.Phys. C

[3] T.Sjöstrand, Comp. Phys. Comm *39* (1986), 347; JETSET, Version 7.2

[4] OPAL - collaboration, M.Z.Akrawy et al., Phys.Lett. *B246* (1990) 285

[5] OPAL - collaboration, K.Ahmet et al. CERN-PPE 90-111

[6] OPAL - collaboration, M.Z.Akrawy et al., Phys.Lett *231B* (1989) 530

[7] OPAL - collaboration, M.Z.Akrawy et al., Phys. Lett. *241B* (1990) 133

[8] G.Marchesini and B.R.Webber, Nucl.Phys. *B310* (1988), 461; HERWIG, Version 3.2

[9] P.Mättig, Phys.Rep. 177 (1989) 141

[10] TPC - collaboration, H.Aihara et al., Phys.Rev.Lett 61 (1988) 1263; TASSO - collaboration, W.Braunschweig et al. Z.f.Phys C42 (1989) 189

[11] F.A.Berends, R. Kleiss, S.Jadach, Nucl.Phys. *B202* (1982), 63

[12] OPAL - collaboration, M.Z.Akrawy et al., Z.f.Phys. C47 (1990) 505

[13] E.Laermann, T.F.Walsh, I.Schmitt and P.M.Zerwas, Nucl.Phys. *B207* (1982), 205

[14] Private communication Y.Dokshitzer, R.Kleiss, and P.Zerwas

[15] OPAL - collaboration, M.Z.Akrawy et al., Phys.Lett. *B235* (1990) 389

[16] OPAL - collaboration, M.Z.Akrawy et al., CERN-EP 90-97

[17] JADE - collaboration, W.Bartel et al., Z.f.Phys. C33 (1986) 23; JADE - collaboration, S.Bethke et al., Phys.Lett. B123 (1988) 235

[18] F.Boudjema et al., in Proceedings of the Workshop on Z - Physics at LEP 1, ed. G.Altarelli, R.Kleiss, and C.Verzegnassi, CERN 89-08

[19] OPAL - collaboration, Contribution to the Singapore conference

[20] OPAL - collaboration, M.Z.Akrawy et al., CERN-EP 90-143

[21] M.Jacob, talk given at the Singapore conference

6 Figures

Figure 1: Comparison of cluster properties of candidate photons in multihadronic events (points with error bars) with those of photons of the reference sample of $e^+e^- \rightarrow \gamma\gamma$ and $l^+l^-\gamma$ (dotted area); a. number of lead glass blocks per cluster b. cluster width in rads.

Fig.2: Cluster shape distribution of candidates in hadronic events (points with error bars), in the reference sample (hashed area), expected from the simulation of photons (strong line) and expected from the simulation of π^0's (weak line). The distributions are normalized to the number of photon candidates with C<1.5. a. 10< E_γ <20 GeV, b. 20< E_γ < 30 GeV, c. E_γ > 30 GeV.

Fig.3: Comparison of data and simulation for properties of events with an isolated photon candidate. a. Particle flow around the photon candidate, b. Jet rates in the hadronic system as a a function of $y_{cut} = M^2_{jet}/E^2_{vis}$ c. Minimum mass per event between photon and jet for $y_{cut} = 0.005$.

Fig.4: Kinematical properties of the photon, comparison between data and simulation. Also indicated is the expected background from initial state photons and hadrons. a. photon energy, b. transverse momentum of the photon wrt. the thrust axis.

Fig.5: Correlation of couplings of up and down type quarks. Shown is are the relations obtained within one standard deviation from the measured hadronic width and from the photon yield as predicted by JETSET7.2. Also indicated is the standard model expectation.

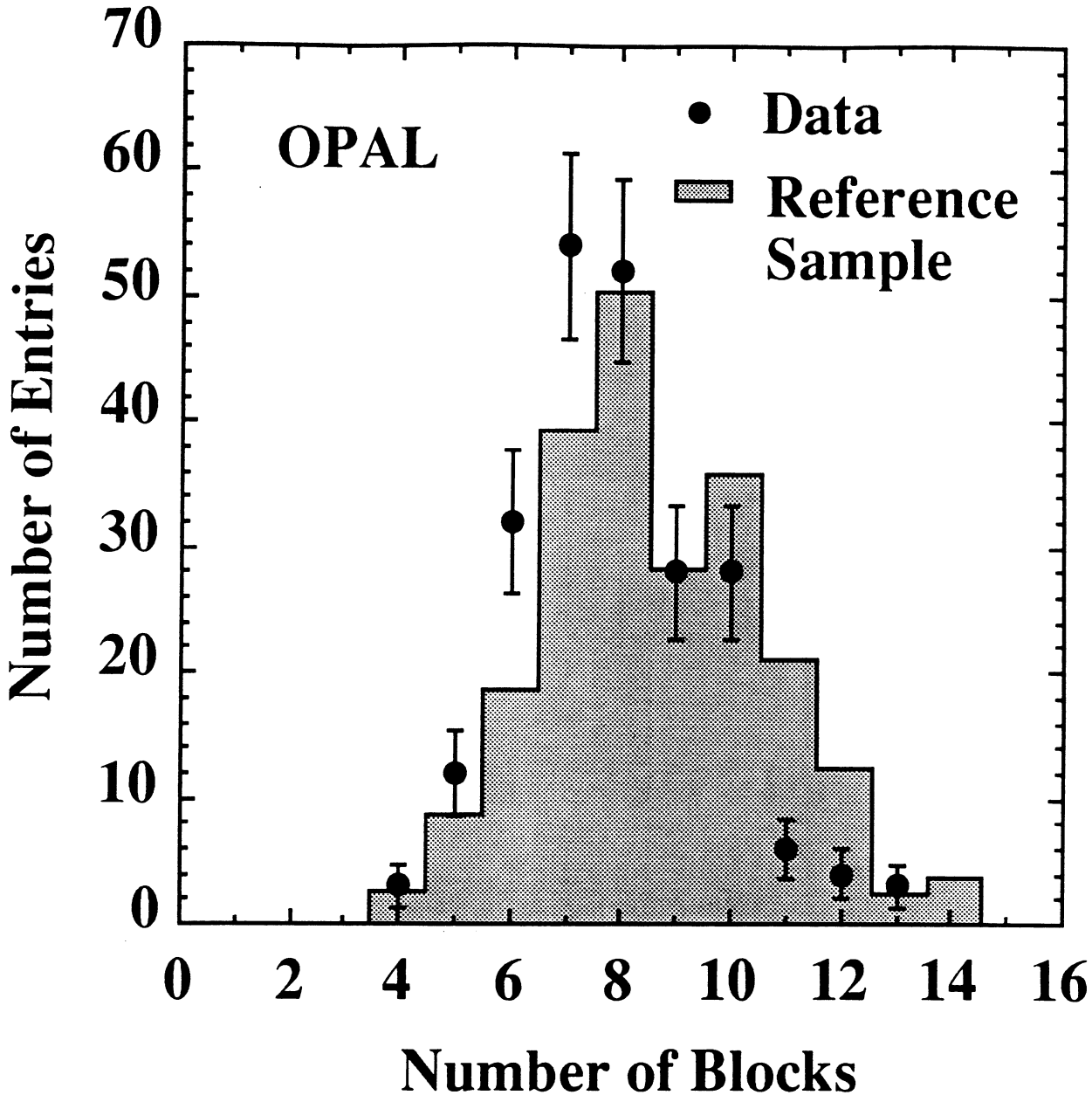
OPAL
Data
Reference Sample
Number of Entries
Number of Blocks
0
10
20
30
40
50
60
70
0
2
4
6
8
10
12
14
16

Fig. 1a

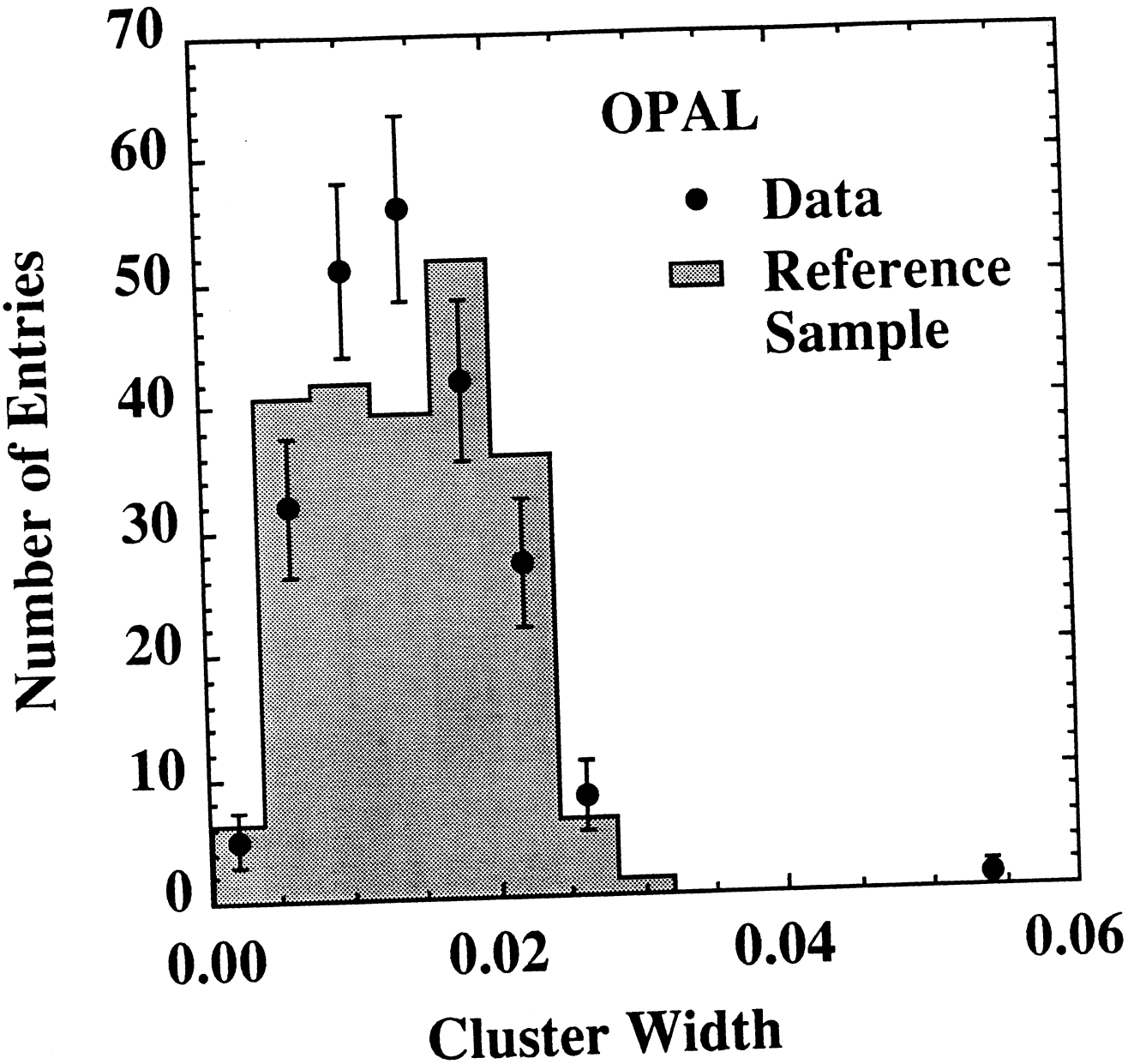
OPAL
Data
Reference Sample
Number of Entries
70
60
50
40
30
20
10
0
0.00
0.02
0.04
0.06
Cluster Width

Fig. 1b

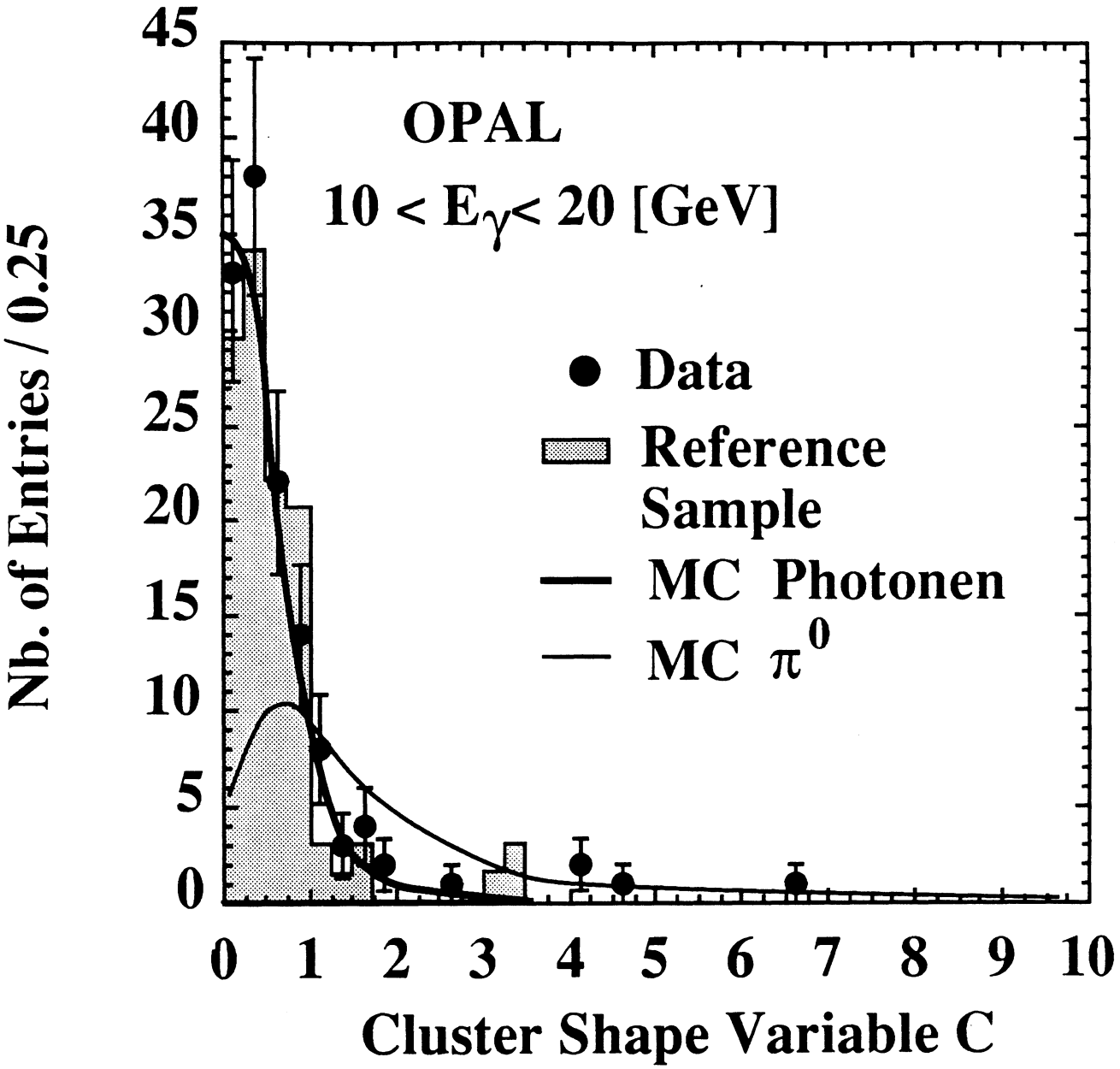
OPAL
10 < Eγ< 20 [GeV]
Data
Reference Sample
MC Photonen
MC π0
Nb. of Entries / 0.25
Cluster Shape Variable C
0
5
10
15
20
25
30
35
40
45
0 1 2 3 4 5 6 7 8 9 10

Fig. 2a

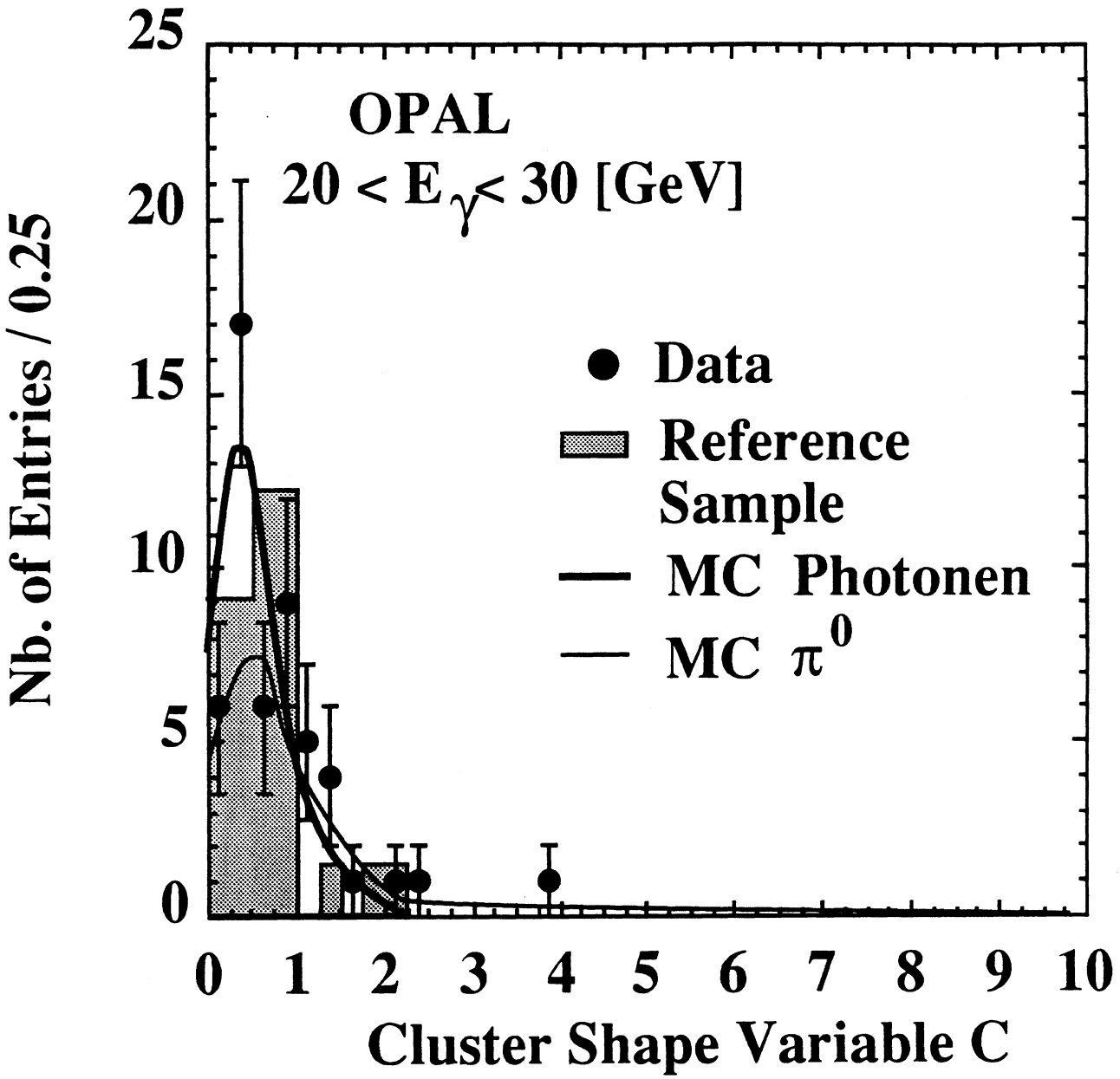
OPAL
20 < E$_\gamma$ < 30 [GeV]
Data
Reference Sample
MC Photonen
MC π^0
Nb. of Entries / 0.25
Cluster Shape Variable C
0
5
10
15
20
25
0 1 2 3 4 5 6 7 8 9 10

Fig. 2b

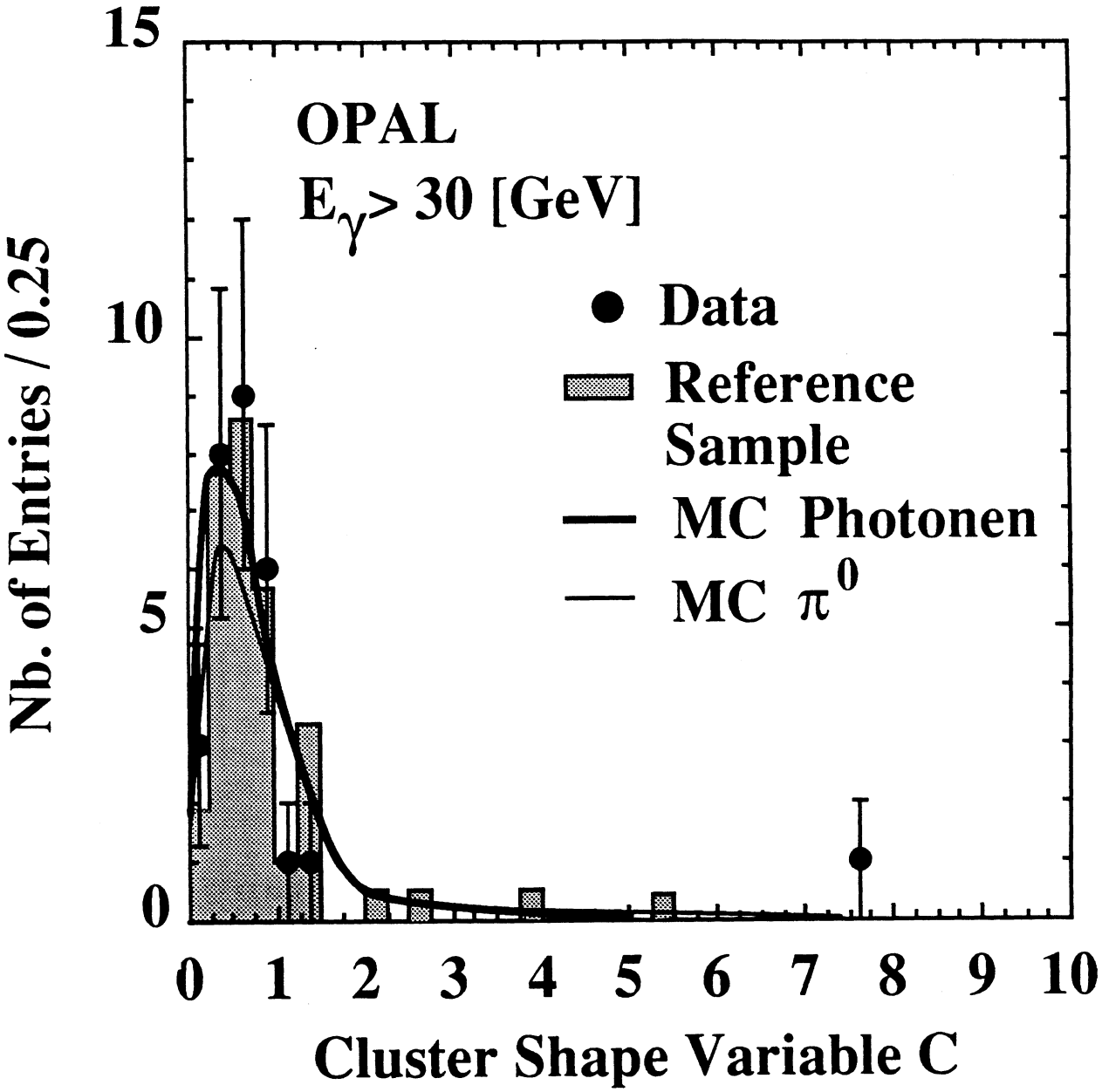
OPAL
E_γ> 30 [GeV]
Data
Reference Sample
MC Photonen
MC π^0
Nb. of Entries / 0.25
0
5
10
15
0 1 2 3 4 5 6 7 8 9 10
Cluster Shape Variable C

Fig. 2c

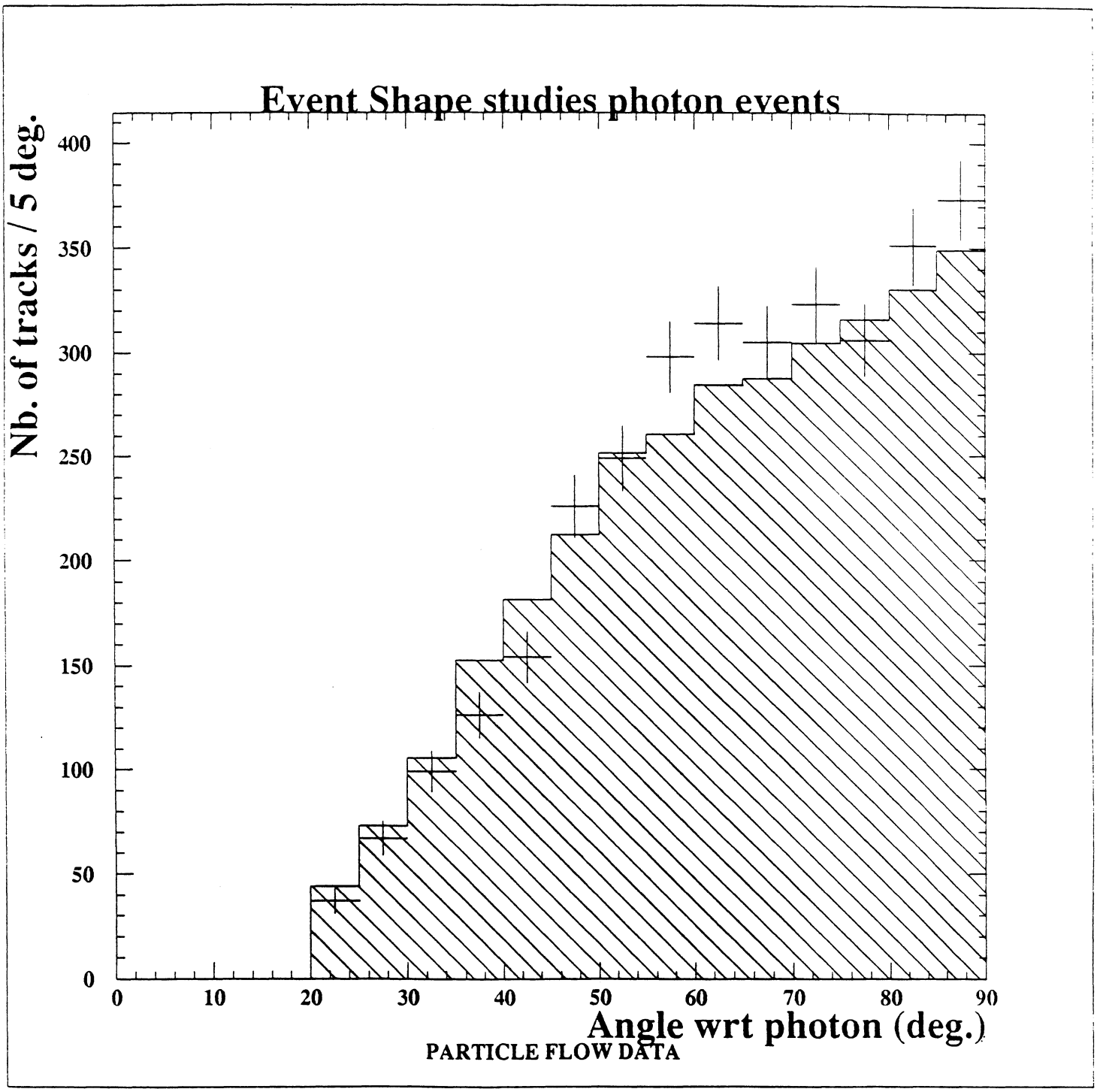
Event Shape studies photon events
Nb. of tracks / 5 deg.
0
50
100
150
200
250
300
350
400
0
10
20
30
40
50
60
70
80
90
Angle wrt photon (deg.)
PARTICLE FLOW DATA

Fig. 39

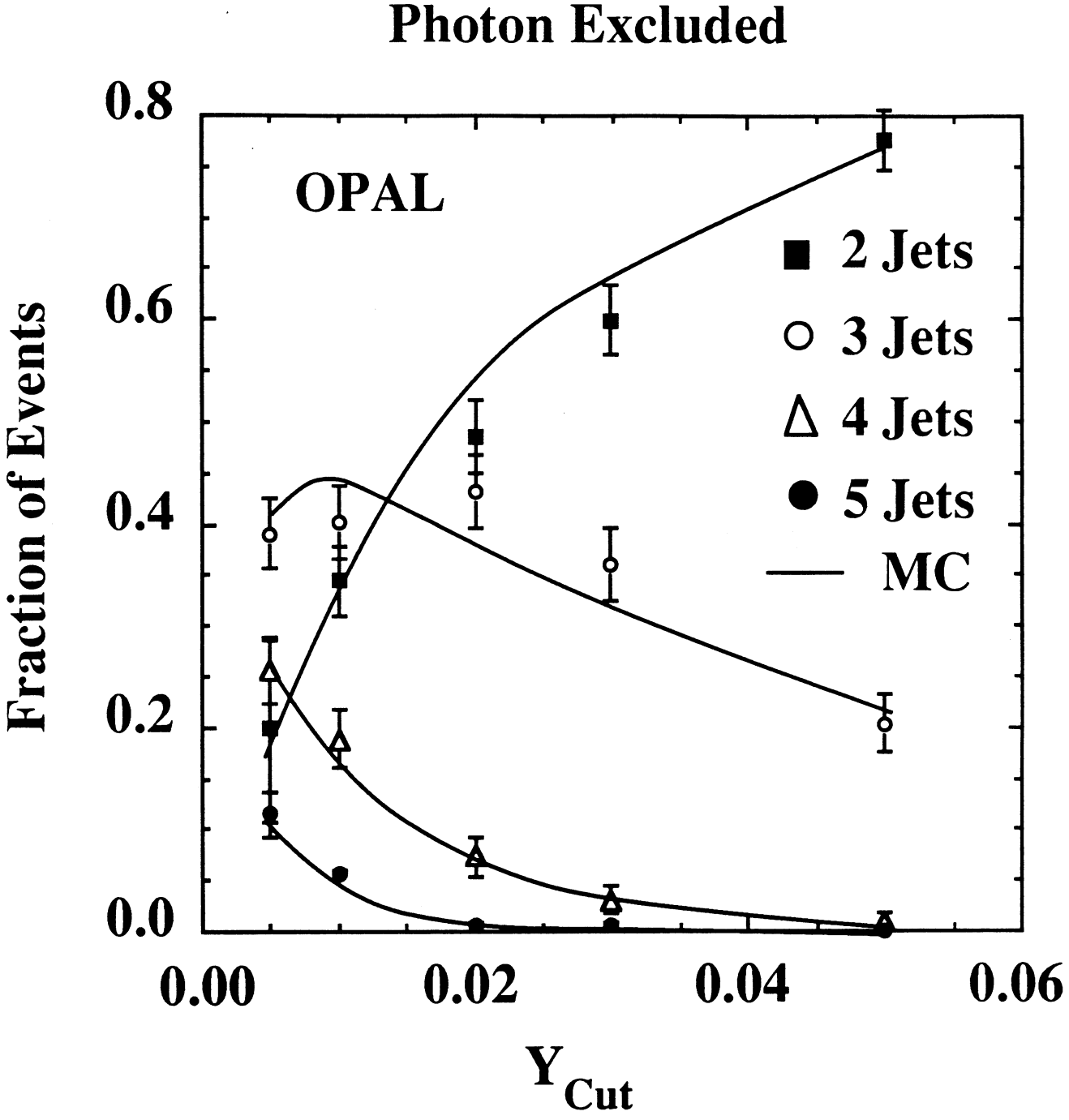
Photon Excluded
OPAL
2 Jets
3 Jets
4 Jets
5 Jets
MC
Fraction of Events
0.0
0.2
0.4
0.6
0.8
0.00
0.02
0.04
0.06
Y Cut

Fig. 3b

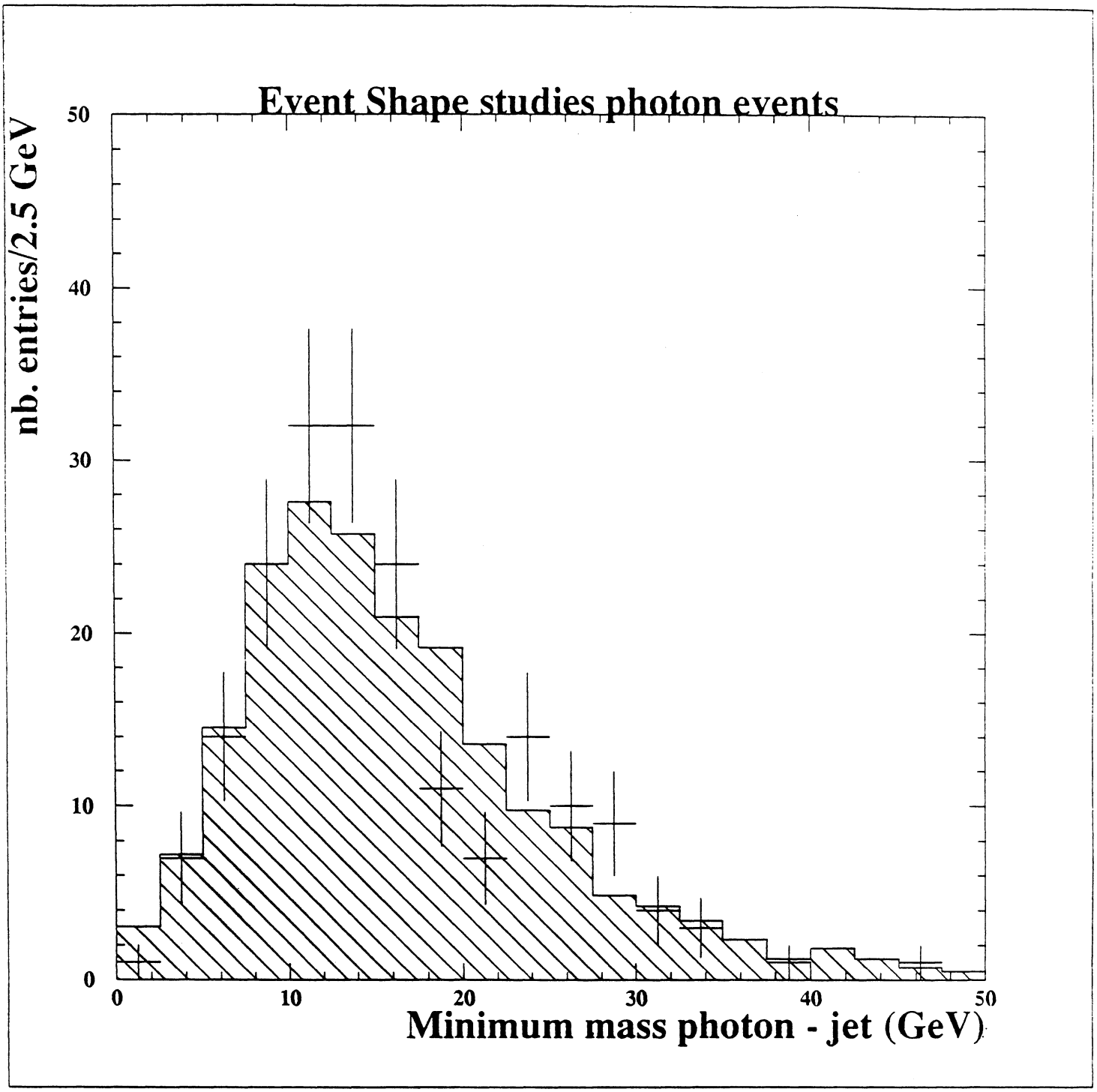
Event Shape studies photon events
nb. entries/2.5 GeV
0
10
20
30
40
50
0
10
20
30
40
50
Minimum mass photon - jet (GeV)

Fig 3c

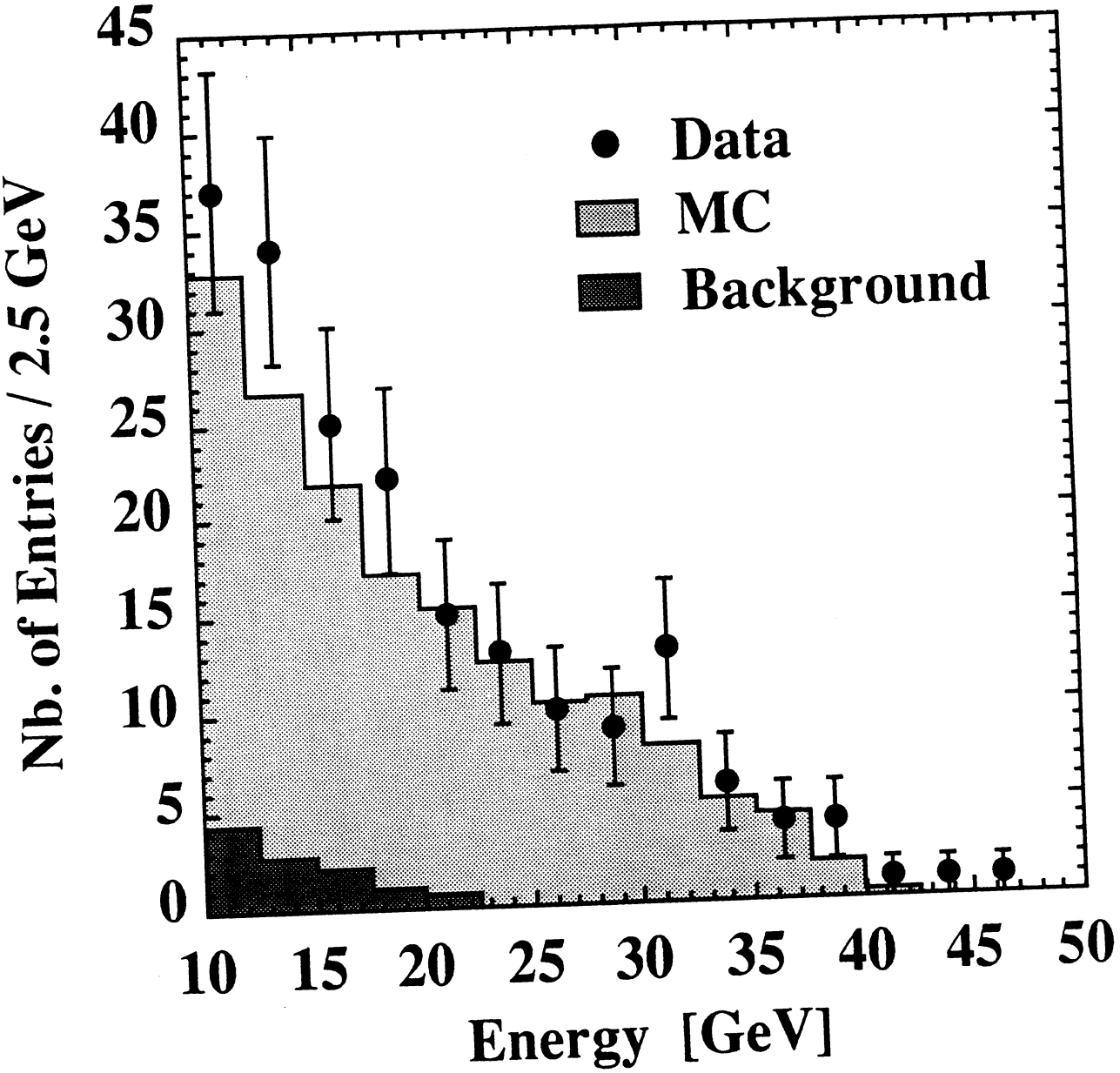
Nb. of Entries / 2.5 GeV
45
40
35
30
25
20
15
10
5
0
Data
MC
Background
10
15
20
25
30
35
40
45
50
Energy [GeV]

Fig. 4a

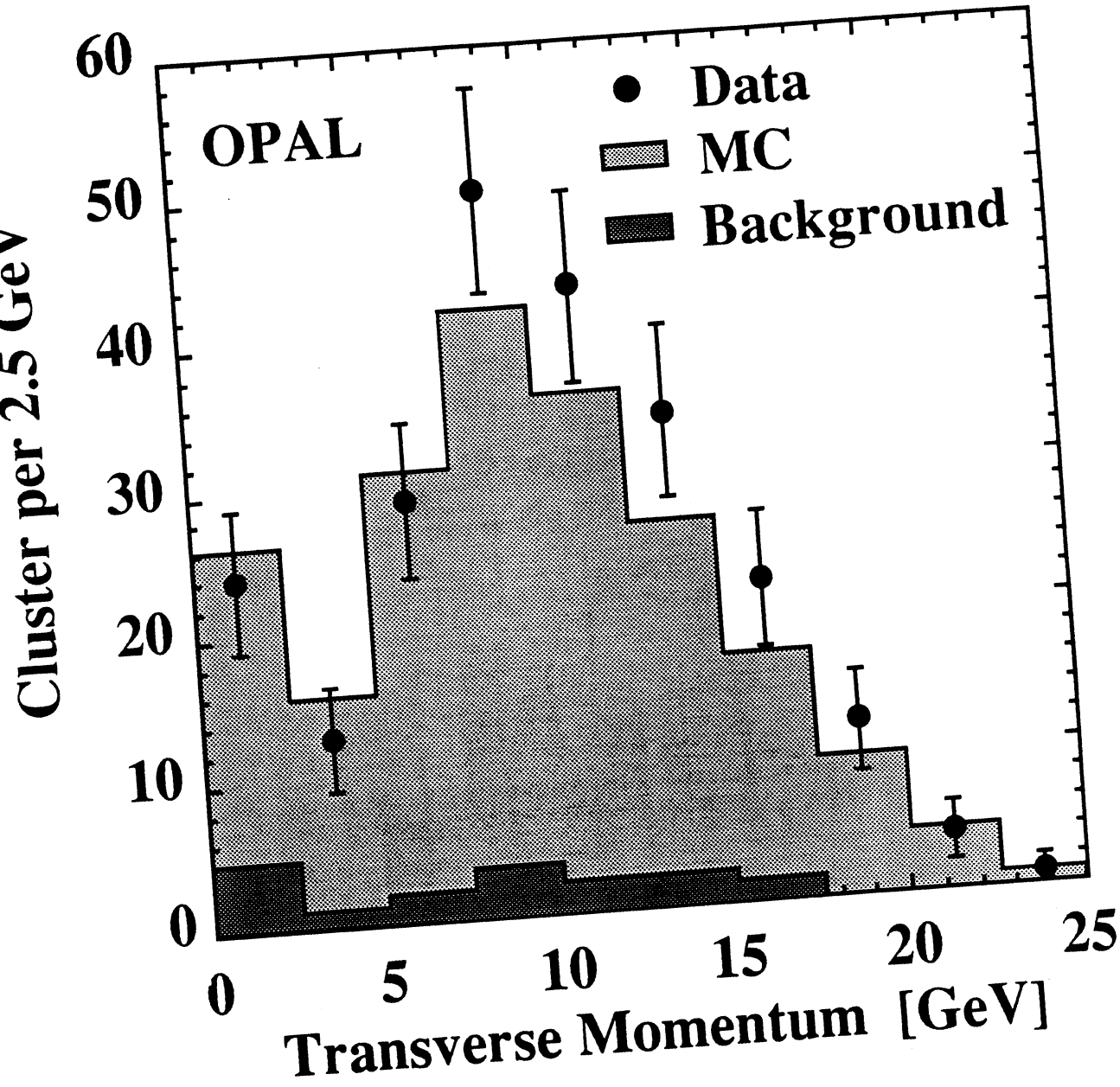
OPAL
Data
MC
Background
Cluster per 2.5 GeV
60
50
40
30
20
10
0
0
5
10
15
20
25
Transverse Momentum [GeV]

Fig. 4b

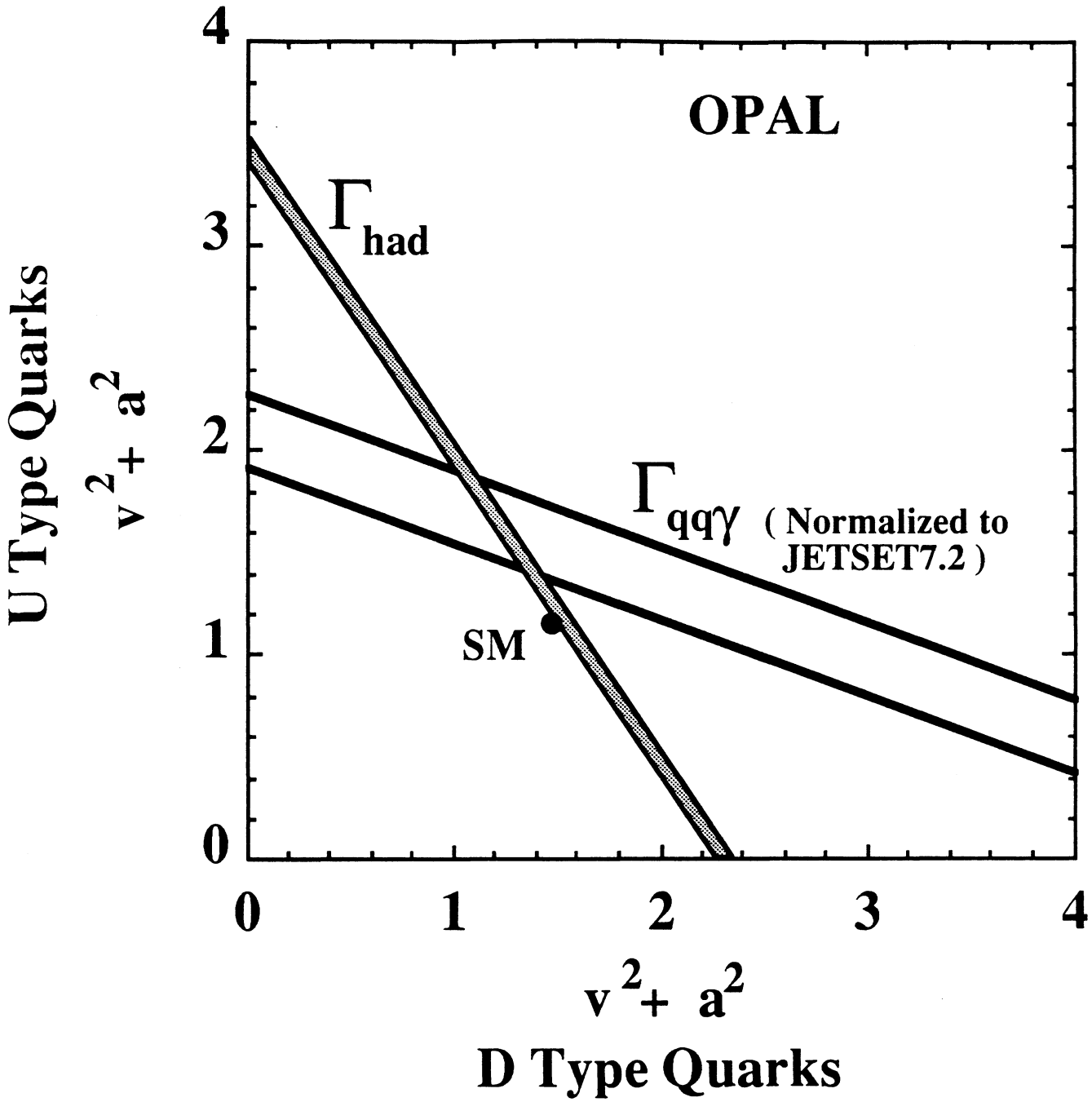
OPAL
Γ_{had}
$\Gamma_{qq\gamma}$ (Normalized to JETSET7.2)
SM
U Type Quarks
$v^2 + a^2$
D Type Quarks
$v^2 + a^2$
0
1
2
3
4

Fig. 5

Description of

$e^+e^- \rightarrow e^+e^-$ analysis for 1990

OPAL technical note TN027 19.December 1990

T. Kawamoto

University of Tokyo

Abstract

An analysis of cross section and forward-backward asymmetry for $e^+e^- \rightarrow e^+e^-$ is described. Within the kinematical acceptance of $|\cos\theta_{e^-}| < 0.7$ and $\theta_{acol} < 10°$, a total of 4701 (4892) candidate events were selected for cross section (asymmetry) measurement from the data taken in 1990. The systematic error was estimated to be 0.66 % for the cross section and 0.0046 for the asymmetry.

1 Introduction

This is a description of $e^+e^- \rightarrow e^+e^-$ analysis for study of Z^0 line shape and lepton forward-backward asymmetry. The event selection of $e^+e^- \rightarrow e^+e^-$ is nearly identical to the analysis in the previous publications [1]. New features are described in the next sections. The cross section was measured with a set of simple kinematical cuts; angular acceptance and acollinearity, so that the efficiency of the event selection within this acceptance can be nearly 100 %.

2 Event selection

The selection criteria are listed below:

1. Multiplicity
   - $2 \leq N_{clusters} \leq 8$
   - $2 \leq N_{tracks} \leq 8$

   The EM clusters are counted if $E > 0.2$ GeV and $N_{blk} \geq 2$. The tracks had to satisfy $d_0 < 2$ cm,$Z_0 < 100$ cm, $P_t > 0.002E_{beam}(\approx 0.10$ GeV),$N_{hits} \geq 16$ and R_1 (radius of first hit) < 60 cm.

2. At least two EM clusters with $E > E_{th}$ are found in $|\cos\theta_{cl}| < 0.85$. E_{th} is set at $0.5E_{beam}$ in the barrel region ($|\cos\theta_{cl}| < 0.715$) and lower threshold energies were used for the 'overlap region' where the energy resolution is worse. The cluster energy cuts are listed in Table 1 as a function of $|\cos\theta_{cl}|$.

3. Sum of the EM energy,$E_{sum} > 0.80E_{cm}$. Again in the 'overlap region' the energy cut was lower as shown in Table 1.

4. Electrons were separated from photons by requiring matched charged tracks to the energy clusters. Among three highest energy clusters, at least two 'charged clusters' (energy clusters associated with charged tracks) were required within $|\cos\theta_{cl}| < 0.85$. The condition of track matching was : $|\Delta\phi| < 3°$ and $|\Delta\theta| < 10°$, where $\Delta\phi(\Delta\theta)$ is the difference of $\phi(\theta)$ of the extrapolated track to the calorimeter and the energy cluster; $\Delta\phi = \phi_{track} - \phi_{clust}$ and $\Delta\theta = \theta_{track} - \theta_{clust}$. The polar angle($\theta$) of electrons were determined from the position of energy cluster while the azimuthal angle(ϕ) was taken from the measurement of the charged tracks (at the origin) in order to avoid the effect of magnetic field. The minimum energy of the third cluster was set at $0.05E_{beam}(\approx 2.2$ GeV) and the minimum P_t of the matched track was 0.5 GeV. For low energy electrons ($P <\approx 2$GeV) matched cluster may not be found,in this case, if the direction of the track at the origin was pointing to one of the high energy cluster within $\Delta\phi$ and $\Delta\theta$ cut, this particle was taken as a electron(positron). The P_t of the track could be as low as $0.002E_{beam}$ for this second criteria. If a track was assigned to two clusters, the combination with smaller opening angle ($\sqrt{\Delta\phi^2 + \Delta\theta^2}$) was taken. When three were three charged clusters, two highest energy clusters were taken as e^+e^- candidates.

5. Electron and positron were distinguished by the sign of the charge of the track. When more than one track were associated to the cluster, the sign of the track with the highest momentum was taken. There were a small fraction of events with same sign was assigned to both of the tracks. Only those events with opposite sign pair were used for the analysis.

6. Acceptance cuts

   - The acollinearity angle between e^+ and e^-, $\theta_{acol} < 10°$.
   - Direction of e^-, $-0.7 \leq \cos\theta_{e^-} \leq 0.7$.

The multiplicity cuts 1) reject multihadronic events and a part of $e^+e^- \to \gamma\gamma$ events. The cluster energy cut 2) and the total energy cut 3) remove $e^+e^- \to \tau^+\tau^-$ and $e^+e^- \to e^+e^-e^+e^-$ backgrounds. The requirement of two back-to-back charged clusters eliminate remaining backgrounds from $e^+e^- \to \gamma\gamma$ and $e^+e^- \to e^+e^-(\gamma)$ events in which e and γ are back-to-back. The acceptance $|\cos\theta_{e^-}| < 0.7$ assures a uniform EM calorimetry and enrich the e^+e^- final states from Z^0 decays by reducing the contribution from t-channel exchange which dominates at small angle region.

In addition following detector status were required:

- EB $\geq 2, \geq 2$ (detector,trigger)
- EE $\geq 3, \geq 2$
- CJ ≥ 3, X
- FD ≥ 3 (for cross section)

After applying these selection cuts, a total of 4701(4892) candidate events were selected for cross section (asymmetry) measurement.

Table 1: Cluster energy and total EM energy cut as a function of $\cos\theta$ of the cluster. For the total energy cut, the $\cos\theta$ of the second highest energy cluster was used.

$\cos\theta$	E_{cl}/Ebeam	E_{sum}/Ecm
0.000 - 0.715	0.5	0.8
0.715 - 0.780	0.3	0.6
0.780 - 0.835	0.2	0.3
0.835 - 0.910	0.5	0.8
0.910 -	0.3	0.8

3 Efficiency

For the study of the efficiency of the event selection and the background estimation, Monte Carlo events of 20,000 e^+e^-, 30,000 $\tau^+\tau^-$ and $\approx 100,000$ multihadrons were used. In figure 1, the cluster energy distribution for $e^+e^- \to e^+e^-$ Monte Carlo is compared with data, shown separately for different $\cos\theta$ regions. The cluster energy of Monte Carlo was rescaled by factor 0.99 and a gaussian smearing of $\sigma = 3\%$ was applied to obtain good agreement between data and Monte Carlo. In the region $0.7 < |\cos\theta| < 0.78$ agreement of data and Monte Carlo is not perfect, which suggests that the materials in front of the calorimeter are not well simulated in this region. The present analysis is not sensitive to this problem since most of the EM clusters are in $|\cos\theta| < 0.7$.

3.1 Multiplicity cut

The measured distributions of track and cluster multiplicity are shown in figure 2 and compared with Monte Carlo expectations. The $e^+e^- \rightarrow e^+e^-$ Monte Carlo predict no event outside the multiplicity cuts. Check was done for the data by visual scanning of the events which satisfy all other cuts but do not satisfy the multiplicity requirement. No e^+e^- candidates were found for $N_{tracks} > 8$ or $N_{clust} > 8$. It was assumed that the inefficiency due to the multiplicity cut was negligible.

3.2 The Cluster energy cut

Most of the electrons(positrons) in the $e^+e^- \rightarrow e^+e^-$ final state have nearly full beam energy. However $\approx$ 4 % of the events have electron(positron) with energy less than 1/2 of the beam energy due to hard photon radiation in the final state (figure 3). In most cases, photons are emitted collinear to the final state electron(positron) and they together detected as a single high energy EM cluster. Even for the case when e and γ are separated each other, one of them should have the energy greater than 1/2 of the beam energy if a single hard photon emission is assumed and acollinearity between e^+ and e^- is restricted to small value. Hence the effect of the cluster energy cut is not as big as 4 %. The expectation by $e^+e^- \rightarrow e^+e^-$ Monte Carlo of the measured cluster energy distribution is shown in figure 4. Only those events which satisfy in 4-vector level the kinematical cuts (angular acceptance and acollinearity) are plotted. Also shown is the distribution of data after all other cuts. There were 6 events found out of 4700 events(0.13 %) from the data in which one of the clusters has energy just below the cut at $0.5E_{beam}$. This is consistent with Monte Carlo expectation (0.09 ± 0.04%). The correction for this effect is 0.13 % with a systematic uncertainty of 0.08 %.

Possibility of loosing events due to bad energy measurement (energy measured was << actual energy due , for example, to dead channels, wrong gain calibration, wrong HV, etc) was checked in following way: (1) Total energy cut was removed, (2) Two EM clusters were required in $|\cos\theta| < 0.7$. At least one cluster should have $E > 0.8E_{beam}$. Energy of the second cluster can be as low as 0.1 GeV. (3) Tracks with momentum P> $0.8E_{beam}$ were required for both of the two highest energy clusters. The energy distribution of the second cluster was checked if there is any indication of $e^+e^- \rightarrow e^+e^-$ events with badly measured cluster energy. Figure 5 shows the correlation plot of E_1 and E_2 (two highest cluster energies). There were 6 such events with $E_3 < 0.5E_{beam}$ found out of 2983 events(= 0.2 %) The $e^+e^- \rightarrow e^+e^-$ Monte Carlo predict 0 events whereas $\tau^+\tau^-$ Monte Carlo predict 4.2 ± 1.7 events which is consistent with the observed number of events. As the worst case we assigned the limit on the loss of $e^+e^- \rightarrow e^+e^-$ due to this possible detector effect to be < 0.12 %.

3.3 Total EM energy cut

This cut is to remove remaining backgrounds coming mainly from τ pair production. Figure 6 shows the normalized total EM energy distribution after all other cuts are applied and compared with Monte Carlo prediction. A good agreement of Monte Carlo and data was obtained by applying additional energy smearing and renormalization of overall energy scale. A gaussian smearing of 3 % to the cluster energy(simulating calibration error of individual channels) and overall energy scale correction of 0.99 was applied. The cut at $E_{sum} = 0.8$ was chosen since

the inefficiency and the background are nearly same size for this value as shown in figure 7. From $e^+e^- \to e^+e^-$ Monte Carlo the inefficiency for the total EM energy cut was $0.17 \pm 0.10\%$. This estimation relies on validity of $e^+e^- \to e^+e^-$ Monte Carlo. Alternatively, the inefficiency was checked by using the data; 1) The EM energy cut was removed. 2) To reduce the $\tau^+\tau^-$ background, a cut on the sum of EM energy and charged track momenta (visible energy) was applied instead of total EM energy cut at $0.8E_{cm}$. 3) Then the number of events with EM energy below the EM energy cut was counted. The remaining $\tau^+\tau^-$ backgrounds were estimated by Monte Carlo and subtracted. Figure 8 shows the correlation plot of total EM energy and the sum of momenta, and EM energy distribution after the visible energy cut. The results are summarized in Table 2.

Table 2: Check of ineffciency for EM energy cut. The number of events with E> $0.8E_{cm}$ is 3462. The errors are statistical errors of $e^+e^- \to e^+e^-$ and background estimation.

E_{vis}cut	Observed events E< $0.8E_{cm}$	$\tau^+\tau^-$ expectation	inefficienecy (%)
1.2	31	22.0 ± 5	0.26 ± 0.17
1.4	16	4.3 ± 2	0.34 ± 0.13
e^+e^-M.C			0.17 ± 0.10

Combining the results from Monte Carlo and data, an estimate of inefficiency for the total energy cut of 0.26 ± 0.20 % was obtained.

3.4 Cluster - track matching

In figure 9, distributions of $\Delta\phi$ and $\Delta\theta$ are shown for all possible combinations and for the selected cluster-track combinations. A small fraction of $e^+e^- \to e^+e^-$ final states contain hard photon radiation of nearly full beam energy in which one of the electrons have very low energy(either by hard photon radiation or by hard bremsstrahlung in the material around the beam pipe). There is possibility to loose such events with very low energy electrons. This effect is dependent on the cuts on the minimum P_t and minimum energy of the third EM cluster(E_3) defined for track-cluster matching. This inefficiency was studied using $e^+e^- \to e^+e^-(\gamma)$ Monte Carlo (BABAMC). The 4-vector of the Monte Carlo events were checked and only those events which satisfy the acceptance cuts:$\theta_{acol} < 10^\circ$ and $-0.7 < \cos\theta_e - < 0.7$, were passed through the selection program and the number of events which were rejected by track matching step was counted. The fraction of such events was found to be $0.23 \pm 0.07_{(stat)}\%$. Study was done also with the data. The events for which the selection program failed to find two charged clusters were examined by visual scan. After removing apparent $e^+e^- \to \gamma\gamma$ and the events lost due to bad measurement of Z coordinates of the tracks, there remained 9 candidate events in which either $Pt < Pt_{min}$ or $E_3 < E3_{min}$ out of total 4900 events(0.18 %), which is consistent with the Monte Carlo result. This inefficiency was checked for various choices of the minimum Pt and the minimum E_3. The result for Monte Carlo and the data are compared in figure 10. They are consistent within errors but systematically deviate by ≈ 0.1 %. From these observation it was assumed that the inefficiency for low energy electron(positron) is $0.20 \pm 0.14\%$. The error includes the systematic difference of $E3_{min}$ and Pt_{min} dependences between data and Monte Carlo.

In figure 11, the acoplanarity distribution measured by ϕ_{clust} and ϕ_{track} are compared, showing that the effect of magnetic field seen in ϕ_{clust} distribution is corrected by using ϕ_{track}.

3.5 Tracking losses

Additional 0.1 % of events were found by visual scan in which one of the tracks was badly measured in z-direction (large Z_0 or large $\Delta\theta$) and rejected by the selection cuts. A 100% systematic error was assigned to this type of inefficiency which is not well modeled by Monte Carlo.

3.6 Charge determination

Figure 12 shows the correlation plot of signed momenta of the associated tracks to electron(positron) candidates. For $\approx$ 1.2% of the events, Same sign was assigned to both of the tracks. About half of the same sign events have more than one track in the direction of the cluster due to e^+e^- conversion of hard radiated photons. The rest are mostly caused by bad measurement of tracks near to the CJ wire planes as shown in figure 13. Figure 14 shows the fraction of same sign events as a function of avarage $|\cos\theta|$ of the two charged clusters. This is consistent with a uniform distribution in the angular acceptance of interest. Only events with tracks of opposite sign were used to define the acceptance of e^- direction. To determine cross sections, the loss of events by the confusion of charge determination was corrected at each center of mass energy using the correction factor defined by :

$$C = \frac{N_{++} + N_{--} + N_{+-}}{N_{+-}}$$

where $N_{++}(N_{--})$ are the number of events with same signs and N_{+-} is the number of events with opposite signs obtained from the data sample in which one of the charged clusters is inside the angular acceptance. The difference of the number of events N_{+-} in this approximate acceptance and the exact acceptance was $\approx$ 1 %; any bias coming from this correction could be small. The probability of wrong charge assignment to both of the tracks is negligibly small($<<$ 0.1%).

As a check of this correction procedure, a different approach was tried. When same sign was assigned to both of the particles, the particle with the highest momentum was used to select the sign unless the χ^2 in $r-\phi$ plane is not large, otherwise the other particle was used. The results of these two methods were compared and the number of selected events (corrected for the factor C) differed by only 0.1 %. This we include in the systematic error.

If there were angular dependence of inefficiency it may cause a systematic bias to the measurement of forward-backward asymmetry. A fit of the angular dependence of same sign fraction in figure 14 to a straight line , $\varepsilon = a_0 + a_1|\cos\theta|$, gave $a_0 = 0.0117 \pm 0.0032$ and $a_1 = -0.0021 \pm 0.0066$. Effect of this angular dependent inefficiency was checked by BABAMC Monte Carlo (4-vector) and it was found that the effect is less than 0.0001 for various values of a_0 and a_1 within the 1σ errors of the fit.

Further check of charge determination was to apply additional quality requirements on the charged tracks of opposite sign events.

1. $0.5 < |P|/E_{beam} < 1.5$ for both of the particles
2. $0.6 < |P|/E_{beam} < 1.4$ for both of the particles
3. $|\Delta\phi_{wireplane}| < 2°$, both of the tracks are within $< 2°$ in ϕ from CJ anode plane.
4. $|\Delta\phi_{wireplane}| > 2°$, both of the tracks are separated in ϕ more than 2° from CJ anode plane.
5. $|\Delta\phi_{wireplane}| > 2°$ and $0.5 < |P|/E_{beam} < 1.5$.

The result of forward-backward asymmetry for these different quality requirements are shown in figure 15. They are consistent each other and the differences are less than 0.003.

3.7 Trigger efficiency

Trigger efficiency was checked by counting the number of events triggered by a number of independent triggers. EM trigger (EBTOTHI,EEL(R)HI),track trigger(TBM2,TPTTCL) and TOF trigger (TPTOCL) were studied. It was found that all the selected e^+e^- candidates were triggered by EM trigger. The fraction of events triggered by different triggers are summarized in Table 3. The trigger inefficiency for $e^+e^- \rightarrow e^+e^-$ is $<< 0.1$ %.

Table 3: Number of events triggered by different triggers.

Trigger	Number of events $\lvert\cos\theta\rvert < 0.7$	(%)	Number of events $\lvert\cos\theta\rvert < 0.85$	(%)
e^+e^- candidates	4845		7240	
ECAL	4845	100	7240	100
TT	4562	94.2	6852	94.6
TOF	4824	99.6	6742	93.1

3.8 Summary of efficiency

The inefficiency of event selection discussed so far is summarized in table 4. The total inefficiency to be corrected is 0.69 ± 0.30%.

4 Acceptance cuts

4.1 Absolute value of $\cos\theta$

The absolute accuracy of the determination of the angle at the $\cos\theta$ cut is directly related to the absolute accuracy of the cross section and asymmetry. In this analysis the θ - direction of e^- is determined by the EM cluster. Figure 16 shows the distributions of the cluster $\cos\theta$

Table 4: Summary of inefficiency and its systematic errors.

	Inefficiency(%)	systematic error (%)
Cluster energy cut	0.13	0.08
		< 0.12
Total EM energy cut	0.26	0.20
Low energy tracks	0.20	0.14
Tracking loss	0.10	0.10
Trigger	0.00	$<< 0.1$
total	0.69	0.30

around $\cos\theta = 0.7$ for data and Monte Carlo. The dip-bump structure in the distribution is due to the non linearity of the reconstructed position by weighted average method of energy sharing over lead glass blocks. The peaks correspond to the center of the block and the valleys are the boundaries of the blocks. Geometrically, $\cos\theta$=0.7 correspond very precisely to the center of the block and the systematic bias due to this non linearity is expected to be small. However there is a slight difference of the position of the peak between data and Monte Carlo about $\cos\theta = 0.7$ by $\Delta(\cos\theta) \approx 0.002$. At this stage of analysis it is not clear if it is a real difference or just a fluctuation. Since this difference is comparable to the size of the correction to the measured θ for a detail of the showering effect ($< 0.1°$) made by ROPE EB processor, we take this as a uncertainty in absolute θ measurement as a conservative limit. Effect of this systematic shift of $\cos\theta$ was estimated by Monte Carlo, which gave systematic error of 0.5 % for the cross section and 0.002 for asymmetry. Figure 17 shows the estimated errors as a function of the center of mass energy.

Other source of error in the acceptance is due to the shift of actual beam vertex from the center of the detector; determination of θ by EM cluster assumes that the particles are coming from the center of the detector. Finite size of the vertex is also a problem, especially in Z-direction. The effect of this vertex shift was checked by Monte Carlo 4-vectors. For given Z-displacement of vertex, θ of electron was recalculated assuming the particles are emitted from Z=0. Angular acceptance cut was applied to "measured θ" and the number of accepted events were compared with the number of events with the correct acceptance. Similar study was done for forward-backward asymmetry. In 1990 the average value of Z-vertex was $\Delta Z = 3.3$ mm with similar size of fluctuation, and Z-size was $\sigma_Z = 11.8$ mm. For these values, the error in cross section was 0.1 % and the error in the asymmetry was 0.001 as shown in figure 18.

4.2 Resolution effect

A finite angular resolution may cause a systematic bias to the measured cross section and asymmetry with acceptance cut. This effect was checked by $e^+e^- \rightarrow e^+e^-$ Monte Carlo. Figure 19 shows the angular distribution of electrons for two groups of events: 1) electron is inside the acceptance at 4-vector level and 2) electron is outside the acceptance. For a total of 4748 events 51 events(41 in forward and 10 in backward hemisphere) went out from the acceptance after GOPAL and event selection , and 63 events (38 events in forward and 25 events in backward) came in from outside the acceptance. This result in 0.22 % change of the cross section and 0.004 of the forward-backward asymmetry. Although this changes are compatible with statistical fluctuation, they are included as the systematic uncertainties. Hence

the systematic error due to angular resolution is 0.22 % for the cross section and 0.004 for the asymmetry.

Similar check was done for the acollinearity cut as shown in figure 20. Effect to the cross section was $< \pm 0.04\%$.

Another worry is due to known systematic shift of the reconstructed θ of the charged tracks around $|\cos\theta| \approx 0.7$. This is shown in figure 21. As described in Section 2(event selection) cluster-track matching uses ϕ and θ measurement of the tracks. There are 0.5% of events in which same track is assigned to two near-by clusters. The combination of smaller opening angle between cluster and tracks was taken. A systematic shift of θ_{track} may lead to a wrong choice in selecting cluster-track combination. This was checked by comparing a different criteria to resolve the double track assignment. When a track was assigned to two EM clusters within the $\Delta\phi$ and $\Delta\theta$ cuts, E/P of two combinations was compared and the combination with smaller (E/P - 1.) was taken. In figure 22, a correlation plot of E/P for two possible combinations is shown. Also shown is the E/P correlation for the events without this ambiguity of cluster-track matching as a reference. The number of accepted events were compared for these two methods. The total number of accepted events (4892) did not change. There were one event came in and one event went out. Thus the effect of θ_{track} resolution is < 0.03 %.

5 Backgrounds

5.1 $e^+e^- \rightarrow \tau^+\tau^-$

Number of $\tau^+\tau^-$ background was estimated by KORALZ Monte Carlo. As already shown in figure 6, the low energy part of measured EM energy distribution is well predicted by $\tau^+\tau^-$ Monte Carlo. The fraction of $\tau^+\tau^-$ background is estimated to be $0.23 \pm 0.1\%$. The number of observed events below the EM energy cut at 0.8Ecm is larger than the prediction of Monte Carlo by $\approx$ 15 %. This difference was included in the uncertainty in the background estimate.

5.2 Multihadrons

Multihadron Monte Carlo predicts 0.04 % of background in $e^+e^- \rightarrow e^+e^-$. The multiplicity distribution seen in figure 2 shows about factor two difference between data and Monte Carlo after applying all $e^+e^- \rightarrow e^+e^-$ selection cuts except for the multiplicity cut. This systematic error is included to give a estimate of multihadron background of $0.04 \pm 0.04\%$.

5.3 $e^+e^- \rightarrow \gamma\gamma$

The process $e^+e^- \rightarrow \gamma\gamma$ can be background if both of the photons converted to e^+e^- pairs. The probability of conversion was measured to be $\approx$ 6% for a single high energy photon in $|\cos\theta| < 0.7$ from a study of $e^+e^- \rightarrow \gamma\gamma$ candidate events. The probability of $e^+e^- \rightarrow \gamma\gamma$ events to fake $e^+e^- \rightarrow e^+e^-$ by two converted photons is $< 0.5\%$ which corresponds to < 0.01 % at the Z^0 peak and < 0.04 % at the tails.

A check was done by studying the number of $e^+e^- \to \gamma\gamma$ candidates in the data sample which are rejected by $e^+e^- \to e^+e^-$ selection due to charged cluster requirement. The $e^+e^- \to \gamma\gamma$ candidates were selected by requiring at least one high energy neutral cluster and an additional requirement that there should not be more than one charged cluster in the entire acceptance of EM calorimeter. The $e^+e^- \to \gamma\gamma$ cross section obtained in this way are shown in figure 23 after radiative correction as a function of center of mass energy. A few % of background from $e^+e^- \to e^+e^-(\gamma)$ was estimated [2]. Also shown in the figure is the QED prediction. The agreement with QED is good and this result supports the $e^+e^- \to \gamma\gamma$ background is less than 0.1 %.

5.4 Other backgrounds

The contribution from two photon process $e^+e^- \to e^+e^-e^+e^-$ was checked by passing Monte Carlo events through the $e^+e^- \to e^+e^-$ event selection. For the integrated luminosity of 6.853 pb^{-1} (8000 events), no candidate events were accepted. The contribution from this process is $<< 0.1\%$ and negligible.

Similar check for $e^+e^- \to e^+e^-qq$ also predicted a negligible effect to $e^+e^- \to e^+e^-$ selection.

5.5 Summary of backgrounds

Table 5 summarizes the background from various processes. The energy dependence of $\tau^+\tau^-$ background fraction was estimated from the relative change of $e^+e^- \to e^+e^-$ and $e^+e^- \to \tau^+\tau^-$ cross sections at different center of mass energies,which gave 0.1 %. The total background fraction is $0.27 \pm 0.19\%$.

Table 5: Summary of backgrounds and its systematic errors.

Source of background	background fraction (%)	systematic error (%)
$e^+e^- \to \tau^+\tau^-$	0.23	0.12
Multihadrons	0.04	0.04
$e^+e^- \to \gamma\gamma$		< 0.1
$e^+e^- \to e^+e^-e^+e^-$		$<< 0.1$
energy dependence		0.10
total	0.27	0.19

Effect of the $\tau^+\tau^-$ background to the measurement of forward-backward asymmetry was estimated assuming the angular distribution of $\tau^+\tau^-$ is

$$dN/d\cos\theta = C(1 + \cos^2\theta + \frac{8}{3}a\cos\theta).$$

The factor C was determined from the estimated background fraction and the ratio of cross sections for $e^+e^- \to e^+e^-$ and $e^+e^- \to \tau^+\tau^-$ given by the Standard model. The factor a was determined at each center of mass energy from the Standard model expectation of A_{FB}.

Figure 24 shows the estimate of the effect of $\tau^+\tau^-$ background to e^+e^- forward-backward asymmetry for different background fraction. Measured e^+e^- asymmetries were corrected accordingly.

6 Global checks

6.1 Dependence on EM energy cut

Figure 25 shows the dependence on the total EM energy cut of the number of e^+e^- events after correction for the inefficiency and backgrounds. The resulting corrected numbers of events are not sensitive to small change of the EM energy cut.

6.2 Check by a different selection cut

The efficiency and backgrounds so far discussed are essentially for the center of mass energy near the Z^0 peak where we have Monte Carlo and high statistics of data. To see a possible effect of hard initial bremsstrahlung which becomes important at the energies above the mass of Z^0 to the cut on the total EM energy, a selection without this cut was tried and the results were compared [1].

- Remove the cluster energy cut at $0.5E_{beam}$.
- Remove the total EM energy cut at $0.8E_{cm}$.
- New cluster energy requirements.
  - Energy of the highest energy cluster $E_1 > 0.8E_{beam}$.
  - Energy of the second cluster $E_2 > 0.4E_{beam}$.

Tight cluster energy cut was used to reduce backgrounds. With this condition, the effect of the energy loss due to photon radiation into the beam pipe could be smaller(this requires only 60% of Ecm). On the other hand the background rejection is not as complete as the standard cut. Figure 26 shows the correlation of E_1 and E_2 for the data and Monte Carlo expectation for e^+e^-,$\tau^+\tau^-$ and multihadrons at the Z^0 peak in the barrel region. All the Monte Carlos used here are generated at Z^0 peak and there are no guarantee that their prediction is valid at different energies(we don't have enough Monte Carlos at different energies).

Figure 27 shows the energy distributions of E_1 and E_2, total energy distribution with the standard cuts and the new cluster energy cuts. For most of the CM energies the agreement of data and Monte Carlo is reasonable. Only at the highest energy (M_Z + 3GeV), the e^+e^- peak is shifted to low energy side and the number of low energy events (mainly $\tau^+\tau^-$ background) does not agree with Monte Carlo expectation.

[1] At 4-vector level of BABAMC, the summed energy of electrons and photon within $|\cos\theta| < 0.98$ is never below the energy cut of 0.8Ecm with the acceptance cuts of $|\cos\theta| < 0.7$ and $\theta_{acol} < 10^\circ$. However, the energy spectrum is different from that of peak energy; there are more low energy events due to energy loss in the beam pipe.

Figure 28 shows the fraction of backgrounds from $\tau^+\tau^-$ and multihadrons computed by Monte Carlos of Z^0 peak, renormalized according to the cross sections, as a function of center of mass energy. The number of e^+e^- events obtained by two different selection cuts are compared in figure 29 after correction for the estimated backgrounds and inefficiency. The error bars include statistical fluctuation of number of events which are not common to two different data samples and expected number of background events. They agrees within the errors and deviation is less than 1% except for the energy at M_Z+3GeV where there are a few events just below the total EM energy cut; it is not possible to say whether they are e^+e^- or backgrounds(the momentum sum of these events are slightly lower than the e^+e^- peak, which suggests that they are most likely to be τ pairs). The size of these deviation is much smaller than the statistical error of the cross section itself.

7 Results

The systematic error for the cross section and asymmetry is summarized in table 6 based on the discussions given above.

Table 6: Summary of systematic errors.

Source of errors	Cross section error (%)	Asymmetry error
Efficiency	0.30	< 0.0001
Background	0.19	< 0.001
Acceptance	0.56	0.0046
total	0.66	0.0046

In figure 30 measured angular distribution and acollinearity distribution at the Z^0 peak are shown together with Monte Carlo predictions. Overall normalization of $e^+e^- \rightarrow e^+e^-$ Monte Carlo was corrected by using the cross section given by ALIBABA program by $\approx 3\%$. Small discrepancy seen in the acollinearity distribution may be interpreted as an effect of $O(\alpha)$, nonexponentiated BABAMC Monte Carlo.

We use ALIBABA program [3] for estimating the t-channel exchange and s-t interference contributions to $e^+e^- \rightarrow e^+e^-$ to extract Z^0 decays into e^+e^-. This program calculates the cross section of $e^+e^- \rightarrow e^+e^-$ with kinematical cuts on the direction of final state leptons and acollinearity angle between them. In figure 31 measured differential distributions are compared with ALIBABA prediction. They are the angular distribution of $e^+e^- \rightarrow e^+e^-$ at the Z^0 peak ,corrected for inefficiency and backgrounds, and the acollinearity distribution at several different center of mass energies. The agreement of data and theoretical predictions are good (χ^2 of the difference of angular distribution between data and ALIBABA is 16.2/16) and this is a support to use ALIBABA program for the analysis of $e^+e^- \rightarrow e^+e^-$ data.

With the selection cuts, efficiency and background estimation discussed in previous sections, the cross section and forward-backward asymmetry were calculated. A total of 4701 events were used for cross section and 4892 events for the asymmetry.

The cross section was obtained by:

$$\sigma_{ee} = \frac{1}{L}\frac{N_{ee}(1-R_{bkg})}{(1-\varepsilon)}C$$

, where N_{ee} is the observed number of e^+e^- candidates, L is the integrated luminosity, R_{bkg} is estimated background fraction, ε is inefficiency of event selection and C is the correction factor($\approx 1.2\%$) to the loss of events due to same sign tracks(section 3.6).

The forward-backward asymmetry,A_{FB} was obtained from the number of foward event,N_F, and the number of backward events, N_B.

$$A_{FB} = \frac{N_F - N_B}{N_F + N_B} + C_{bkg}$$

where C_{bkg} is the correction for background as discussed in section 5.5.

Table 7 and 8 summarize the results. Asymmetries are combined with 1989 data and given in 9. They are plotted in figures 32 and 33. Fill to fill dependences of the cross sections at different center of mass energies are shown in figure 34. The χ^2 of deviation of cross section at the Z^0 peak is 70.1/58 (fills with more than 9 events are used to calculate χ^2).

Table 7: $e^+e^- \rightarrow e^+e^-$ cross section within kinematical acceptance of $|\cos\theta_e| < 0.7$ and $\theta_{acol} < 10°$. Luminosity values are preliminary. The final numbers are given in the physics note of Z^0 line shape.

E_{cm}(GeV)	Luminosity (nb^{-1})	N_{ee}	Cross section (nb)
88.22	480.64 ± 3.20	164	0.353 ± 0.028
89.23	631.27 ± 3.71	306	0.487 ± 0.028
90.23	394.93 ± 2.96	315	0.814 ± 0.046
91.22	3321.65 ± 8.70	3322	1.017 ± 0.018
92.22	451.04 ± 3.26	265	0.603 ± 0.037
93.22	556.09 ± 3.65	202	0.367 ± 0.026
94.22	554.95 ± 3.68	127	0.232 ± 0.021
	6390.57 ± 12.08	4701	

8 Summary

With the event selection criteria described above, a total of 4701 (4892) $e^+e^- \rightarrow e^+e^-$ candidate events were selected from the data taken in 1990. They are summarized in tables 7,8 and 9. The systematic errors for the cross section and asymmetry are summarized in table 6.

Table 8: $e^+e^- \rightarrow e^+e^-$ forward-backward asymmetry for 1990 data with acceptance cuts $|\cos\theta_e| < 0.7$ and $\theta_{acol} < 10°$.

E_{cm}(GeV)	N_F	N_B	A_{FB}
88.22	116	48	0.415 ± 0.071
89.22	204	102	0.334 ± 0.054
90.22	197	118	0.251 ± 0.055
91.22	1920	1593	0.093 ± 0.017
92.22	146	119	0.102 ± 0.061
93.22	99	103	-0.020 ± 0.070
94.21	79	48	0.244 ± 0.086
Total	2761	2131	

Table 9: $e^+e^- \rightarrow e^+e^-$ forward-backward asymmetry,1989 and 1990 combined. Acceptance is $|\cos\theta_e| < 0.7$ and $\theta_{acol} < 10°$. Luminosity is preliminary. The final numbers are given in line shape physics note.

E_{cm}(GeV)	N_F	N_B	A_{FB}
88.24	133	61	0.372 ± 0.067
89.23	213	108	0.328 ± 0.053
90.24	235	149	0.225 ± 0.050
91.03	80	64	0.112 ± 0.083
91.23	2017	1704	0.084 ± 0.016
91.53	80	68	0.081 ± 0.082
92.23	166	142	0.078 ± 0.057
93.23	117	119	-0.008 ± 0.065
94.25	97	63	0.217 ± 0.078
Total	3138	2478	

References

[1] OPAL Collaboration, M.Z. Akrawy et al., Phys. Lett. B235 (1990) 379.
Physics note 90-16 for singapore conference 1990.

[2] OPAL Collaboration, M.Z. Akrawy et al., Phys. Lett. B241 (1990) 133.
K. Kawagoe, OPAL physics note 90-09,09A

[3] Bhabha line shape program ALIBABA, W.J.P. Beenakker, F.A. Berends and S.C. van der Marck (Institut-Lorentz, University of Leiden, POB 9506, 2300 RA Leiden, The Netherlands).

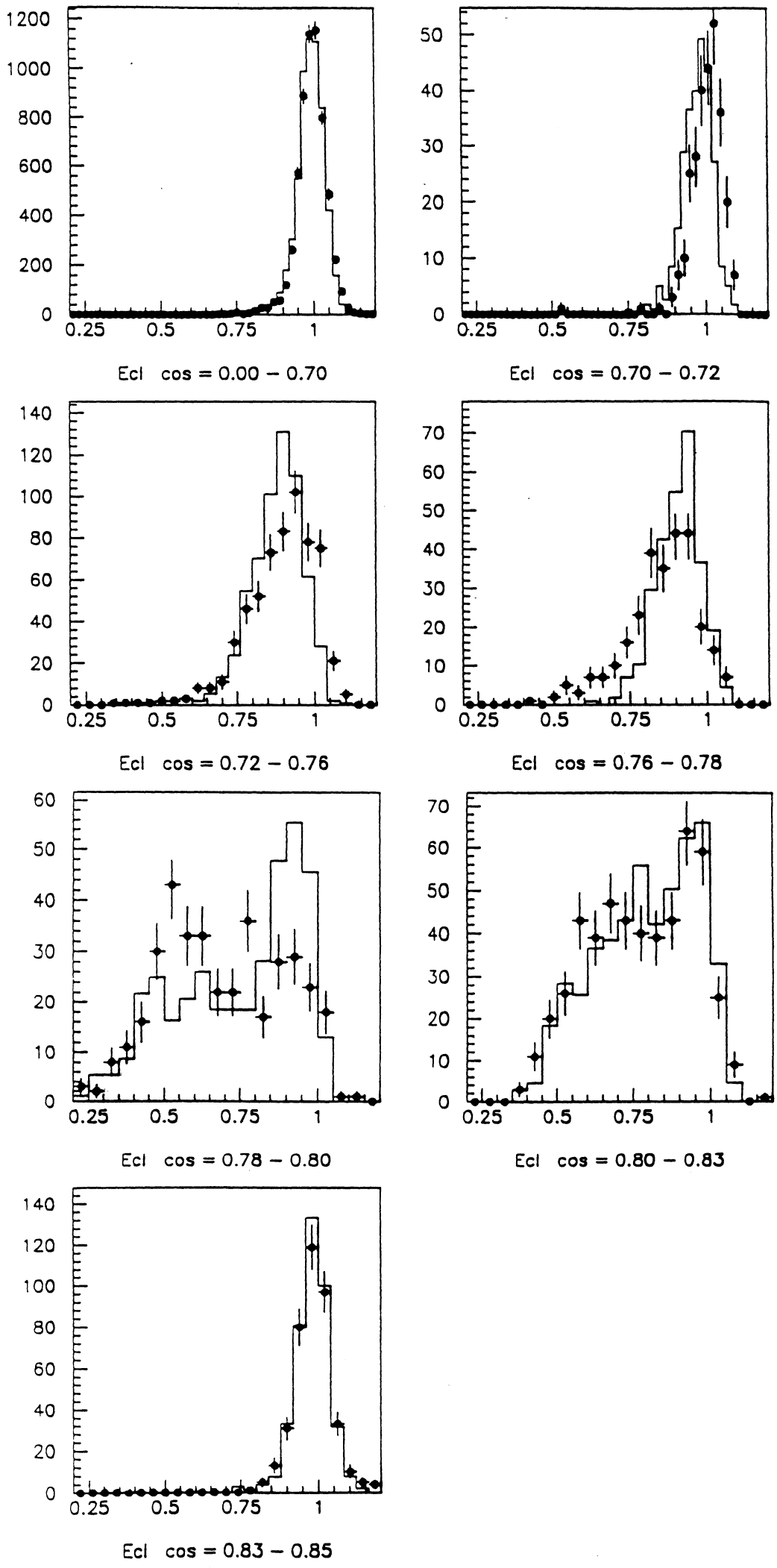

Figure 1: Cluster energy distribution from $e^+e^- \to e^+e^-$ data sample shown separately for 7 different $\cos\theta$ regions. The solid histograms are Monte Carlo and the points with error bar are data. To reduce background from $\tau^+\tau^-$ only events with both of the charged tracks have

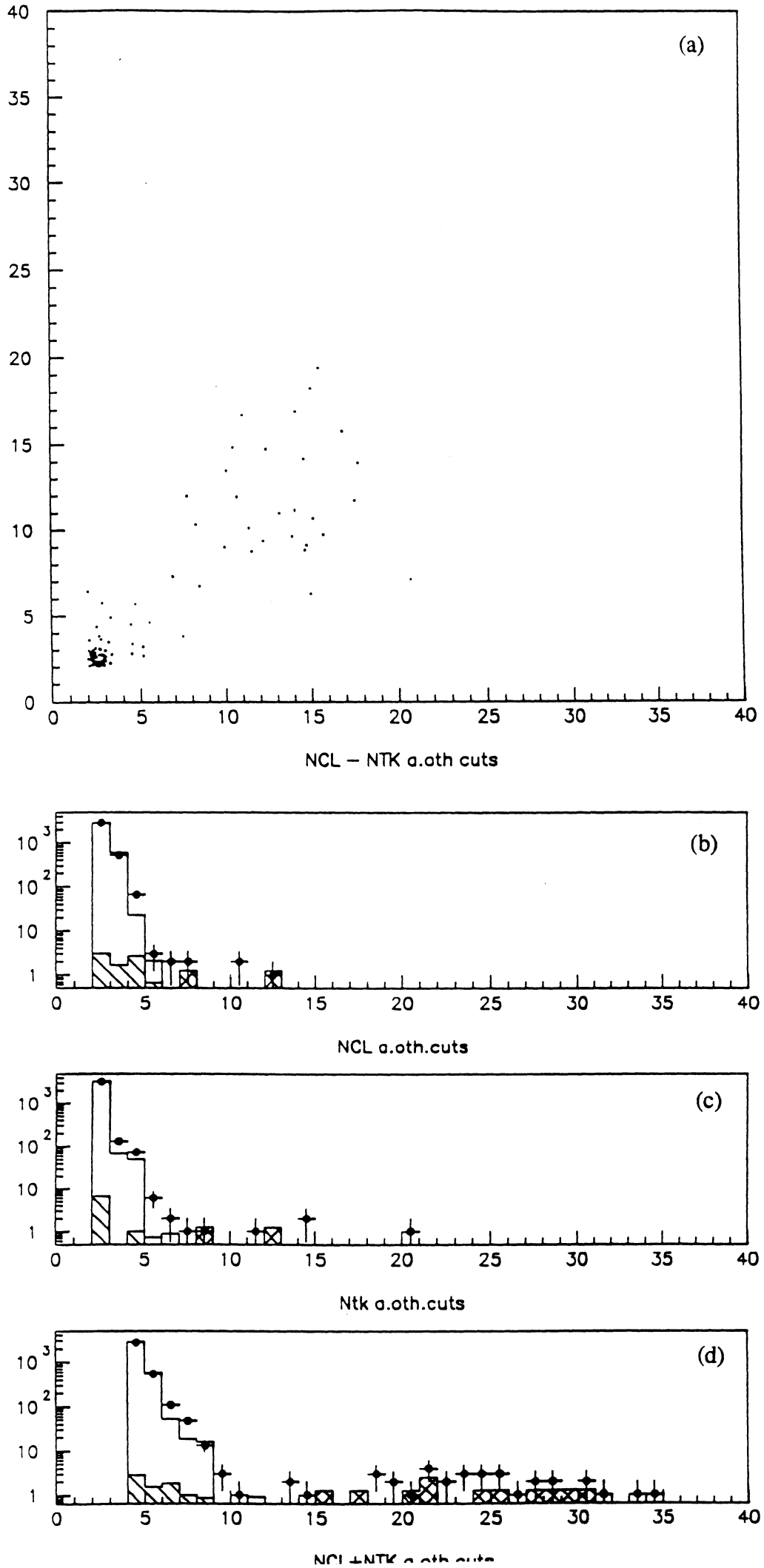

Figure 2: Multiplicity distribution after all other cuts: (a) Correlation plot of N_{clust} and N_{track}; (b) N_{clust}, (c) N_{track} and (d) $N_{clust} + N_{track}$. The solid histograms are Monte Carlo and the points with error bar are the data.

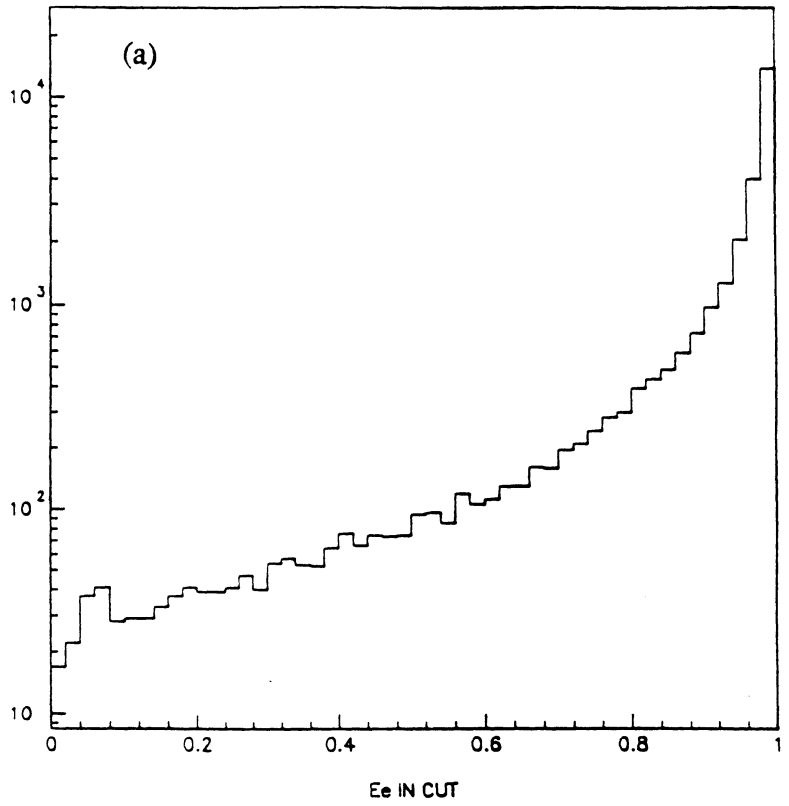

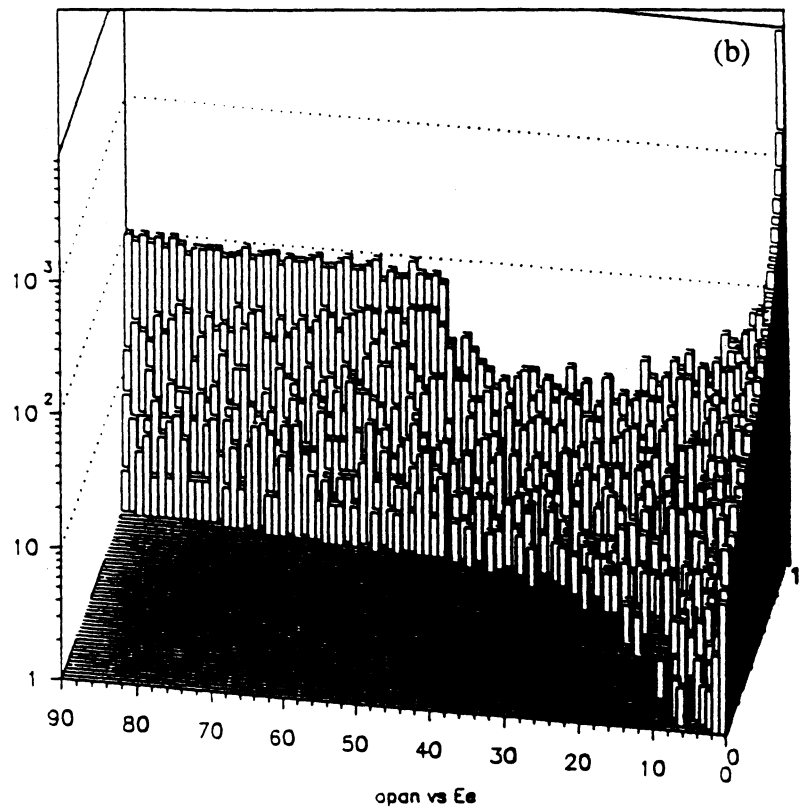

Figure 3: (a) Distribution of electron(positron) energy obtained by BABAMC. (b) Correlation of E_e and $\theta_{e\gamma}$.

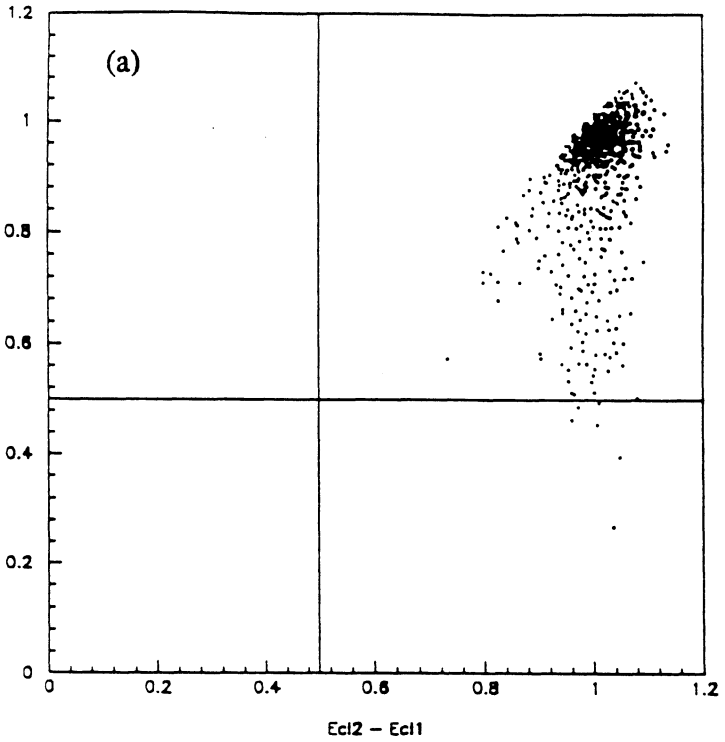

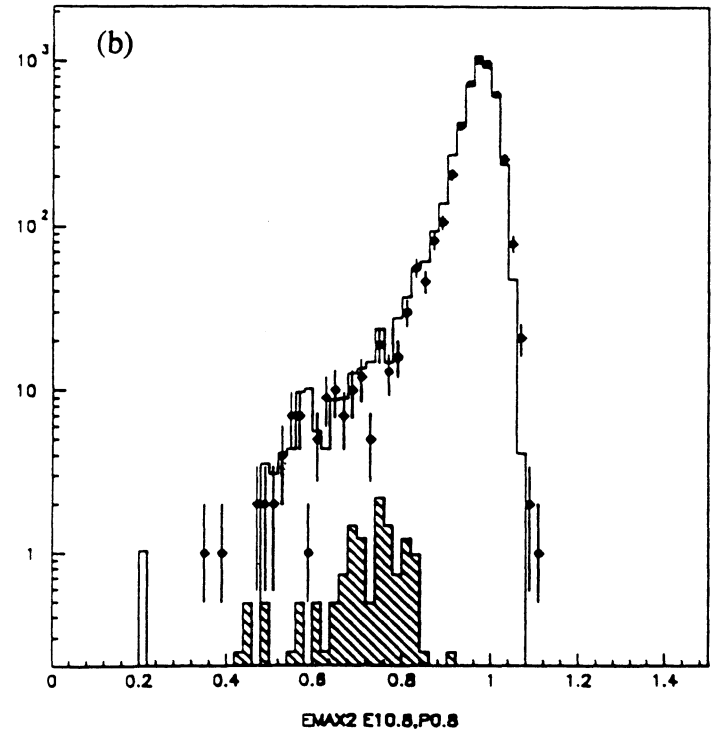

Figure 4: (a) Correlation of energies of the highest energy(E_1) and the next highest energy(E_2) clusters calculated by BABAMC. (b) The energy distribution of the second cluster E_2. Solid histogram is Monte Carlo and points with error bar are data without cut on E_2.

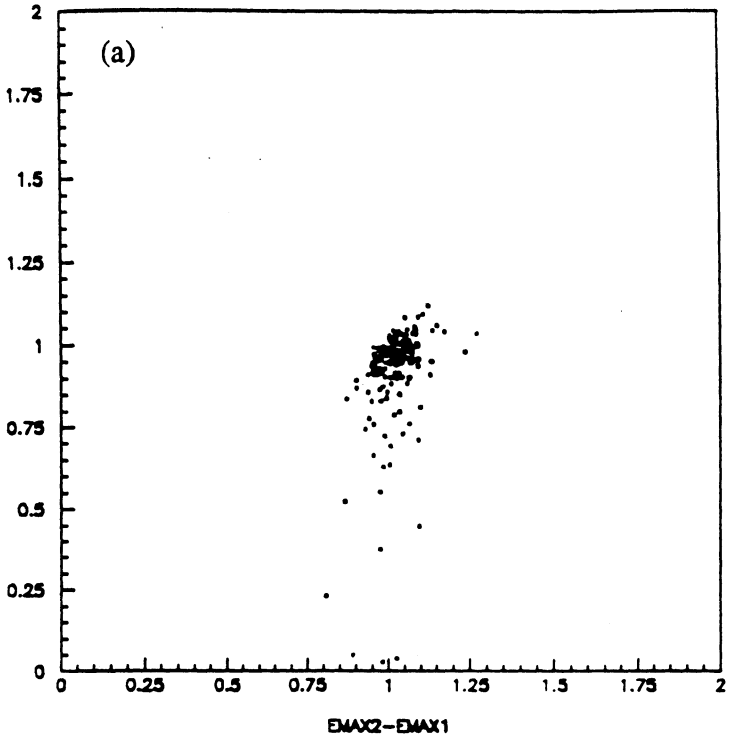

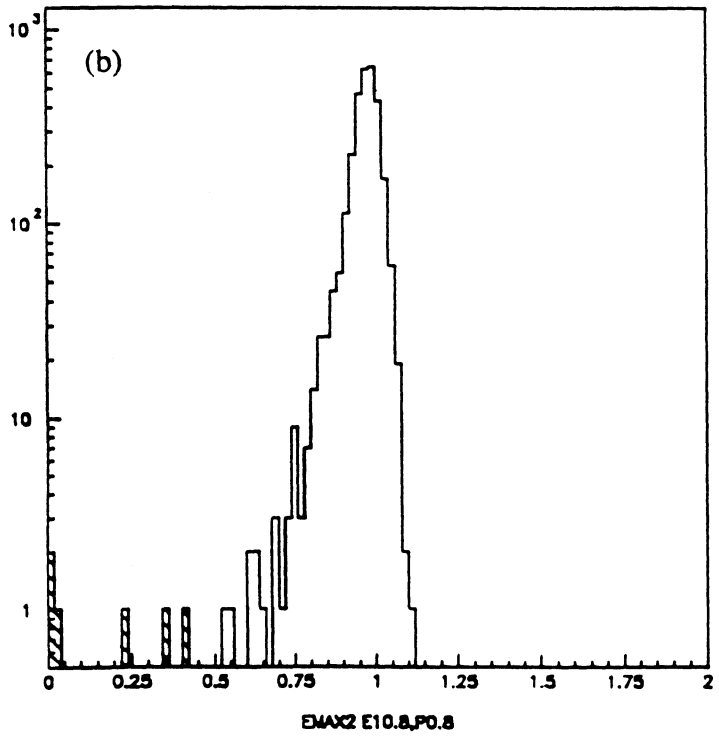

Figure 5: Correlation of E_1 and E_2 without energy cut on E_2 and E_{sum}. $P/E_{beam} > 0.8$ was required for both of the tracks.

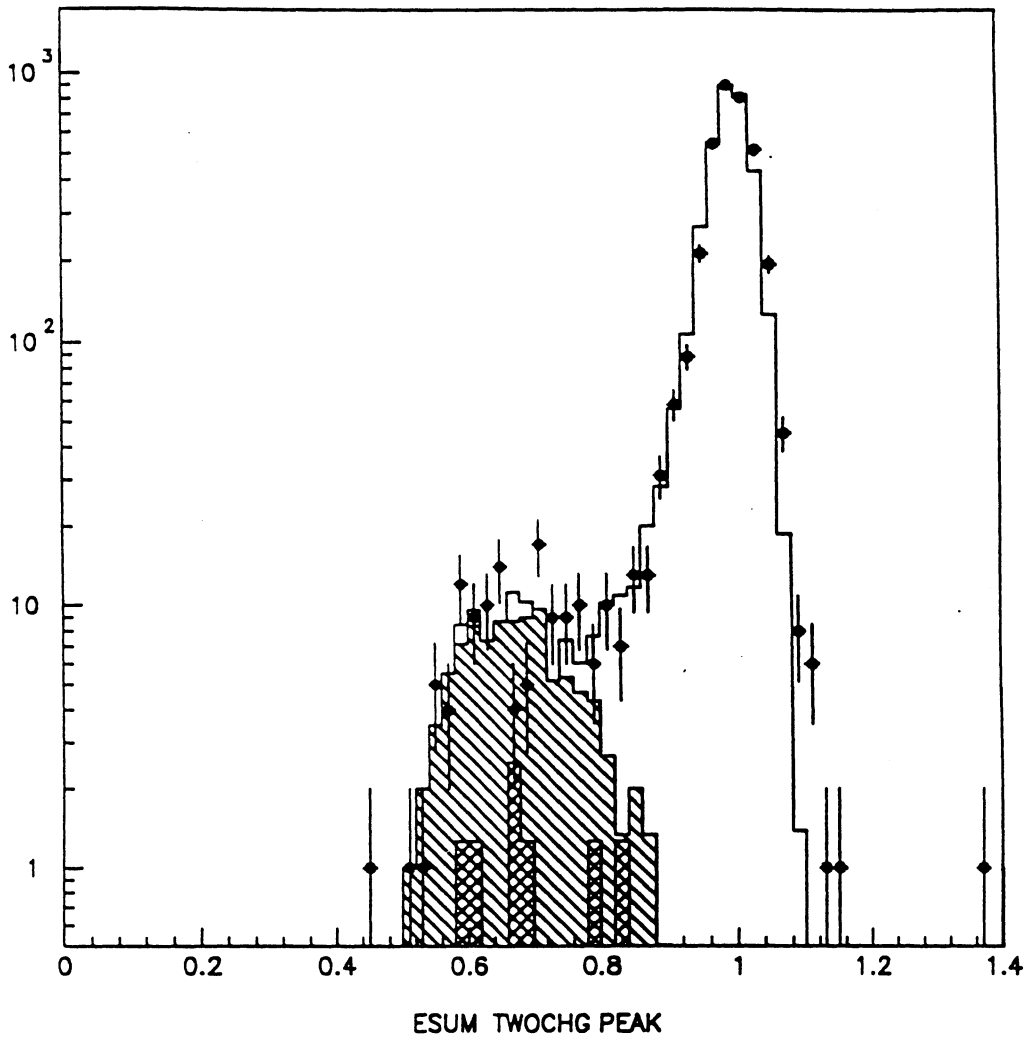

Figure 6: Distribution of total EM energy. Solid histogram is Monte Carlo expectation for $e^+e^- \to e^+e^-, e^+e^- \to \tau^+\tau^-$ and multihadrons. The hatched histogram shows the contribution from $e^+e^- \to \tau^+\tau^-$ and the cross hatched histogram is multihadrons.

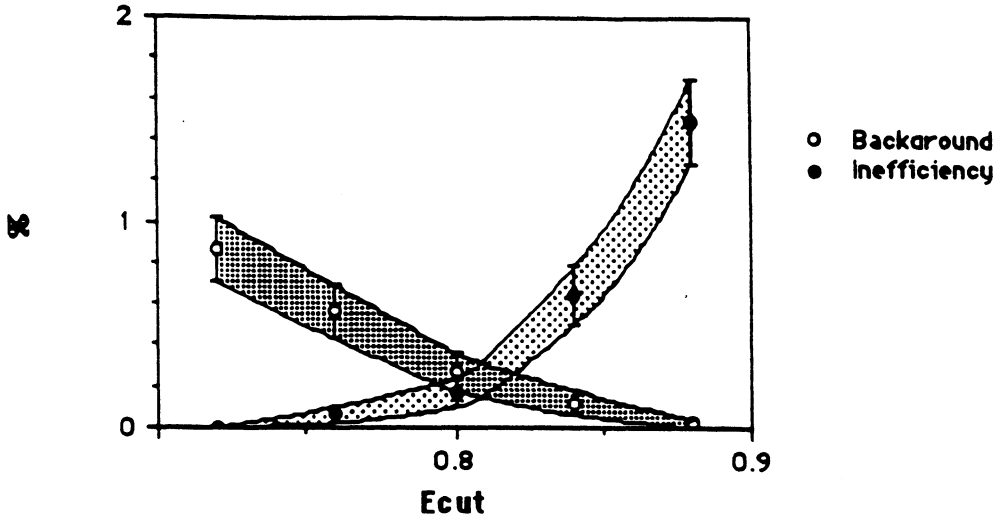

Figure 7: Monte Carlo estimation of background fraction and inefficiency of $e^+e^- \rightarrow e^+e^-$ selection for various values of E_{sum} cut.

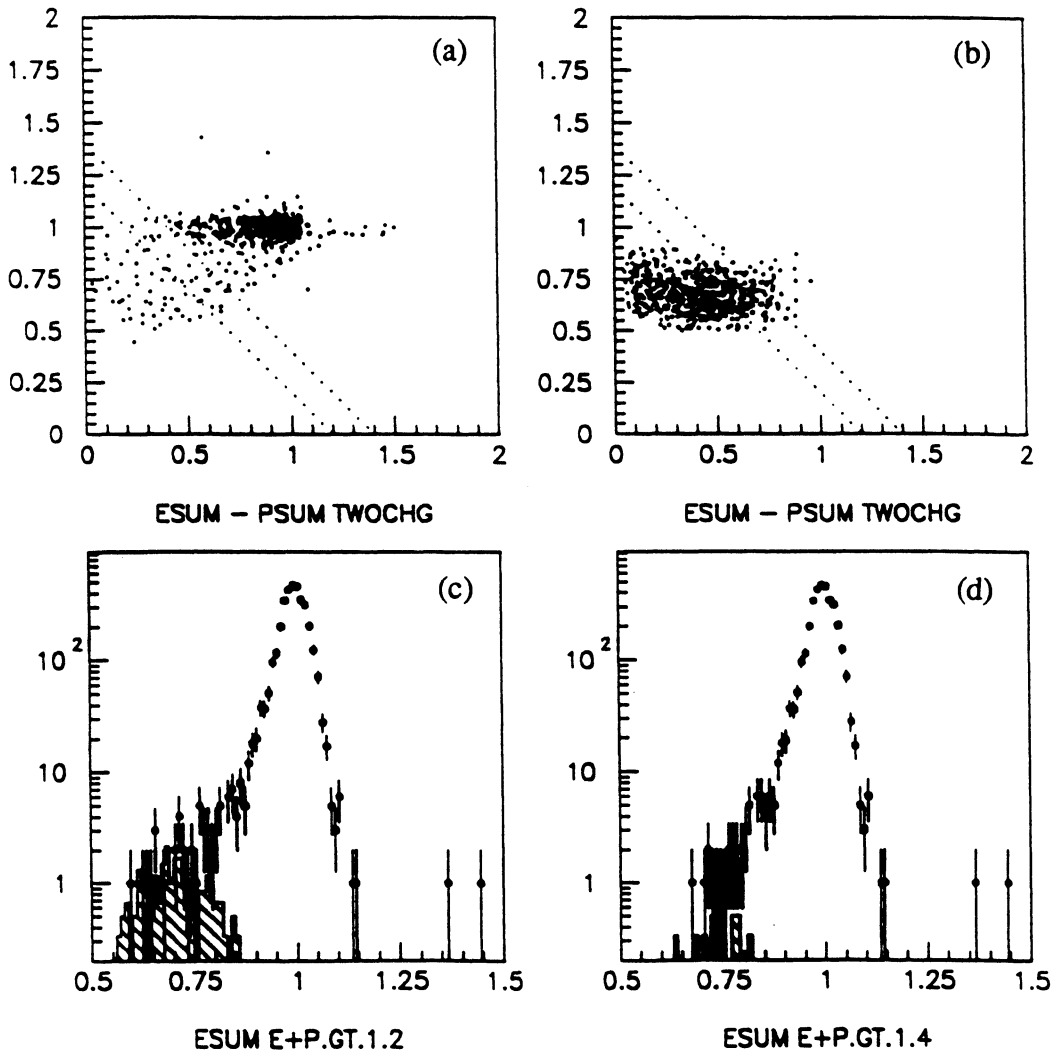

Figure 8: Correlation of total EM energy and the sum of track momenta for (a) data after all other cuts, and (b) $\tau^+\tau^-$ Monte Carlo with the same cuts as (a). The EM energy distribution after cut on the visible energy (sum of the EM energy and track momenta): (c) $E_{vis} > 1.2$ and (d) $E_{vis} > 1.4$. The hatched area is Monte Carlo expectation for $\tau^+\tau^-$ background.

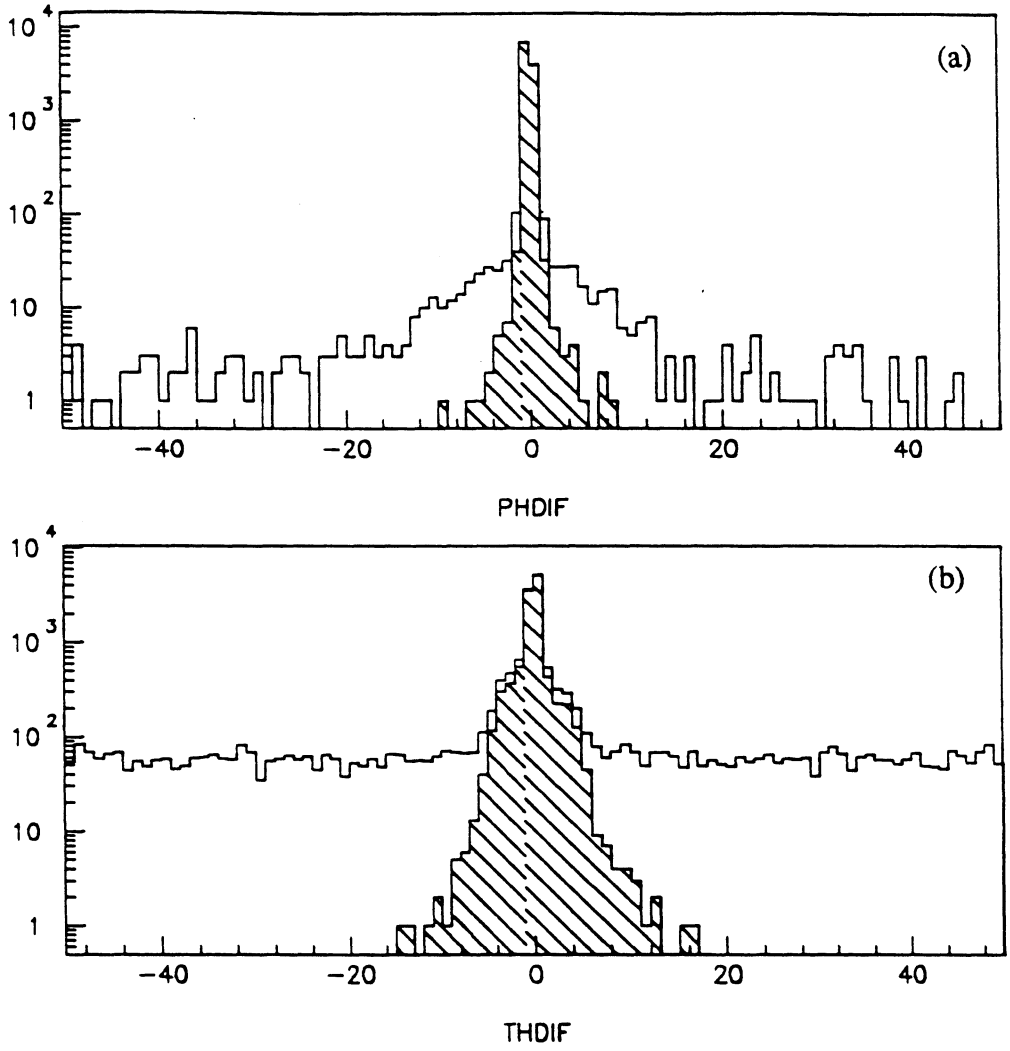

Figure 9: (a) $\Delta\phi$ and (b) $\Delta\theta$ distribution. Open histograms are for all possible combinations of clusters and tracks. The hatched histograms are for the matched cluster and track.

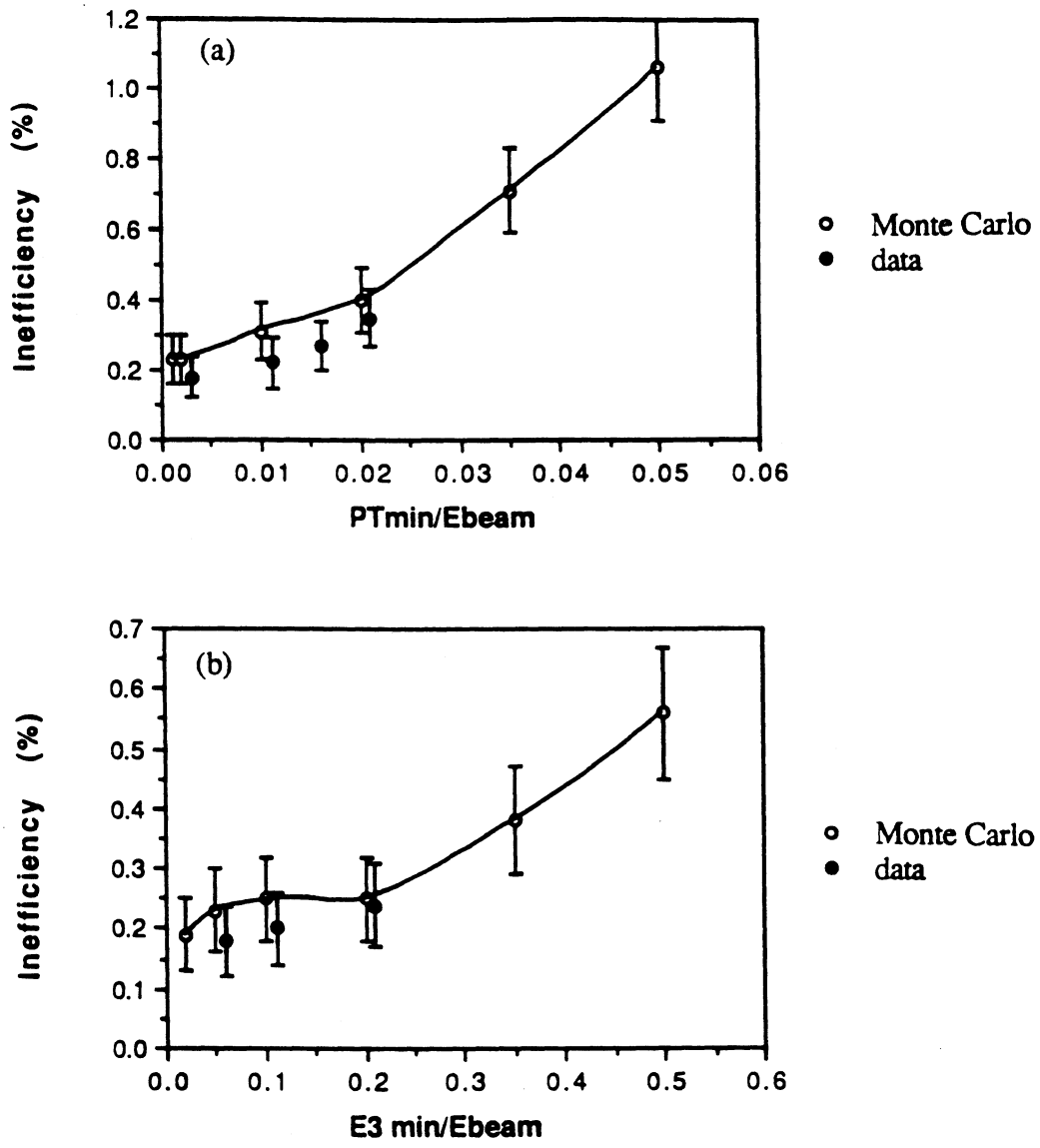

Figure 10: Dependence of inefficiency as a function of (a) minimum E_3 and (b) minimum P_T. The points with open circles are Monte Carlo and the closed circles are estimation from the data.

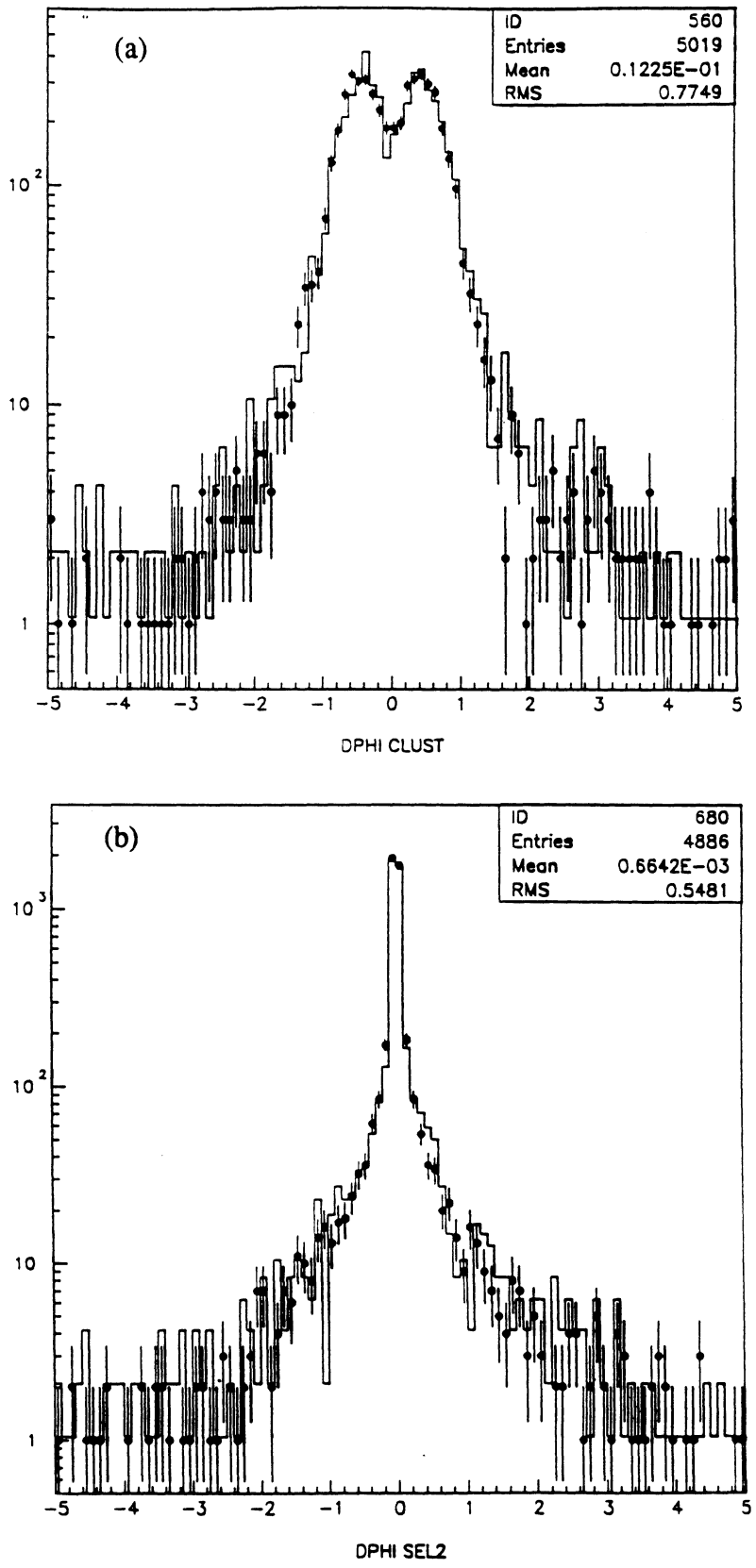

Figure 11: Acoplanarity distribution measured by (a) EM clusters and (b) tracks, compared with BABAMC predictions (solid histograms).

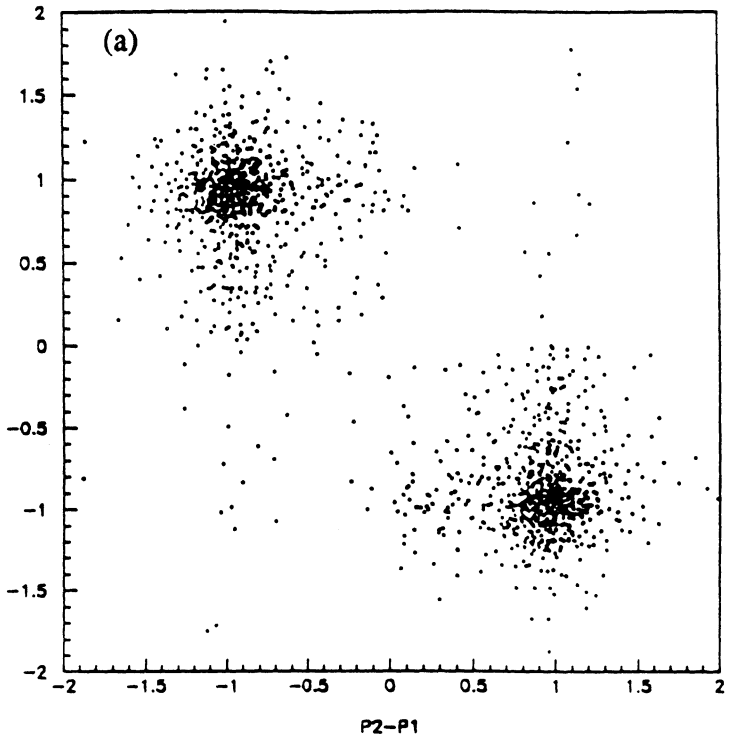

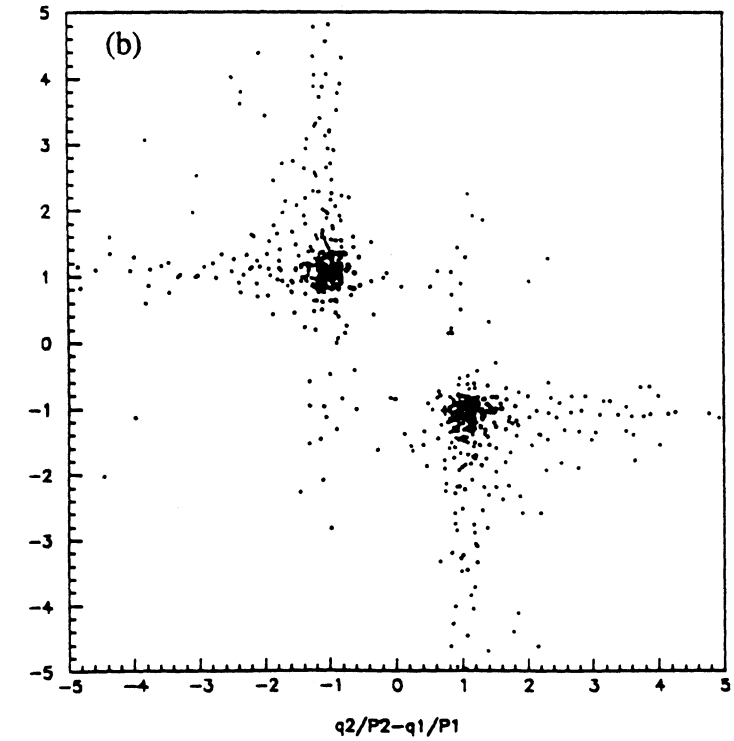

Figure 12: a) Correlation of signed momenta of two charged clusters from $e^+e^- \rightarrow e^+e^-$ candidates. b) Correlation of 1/P.

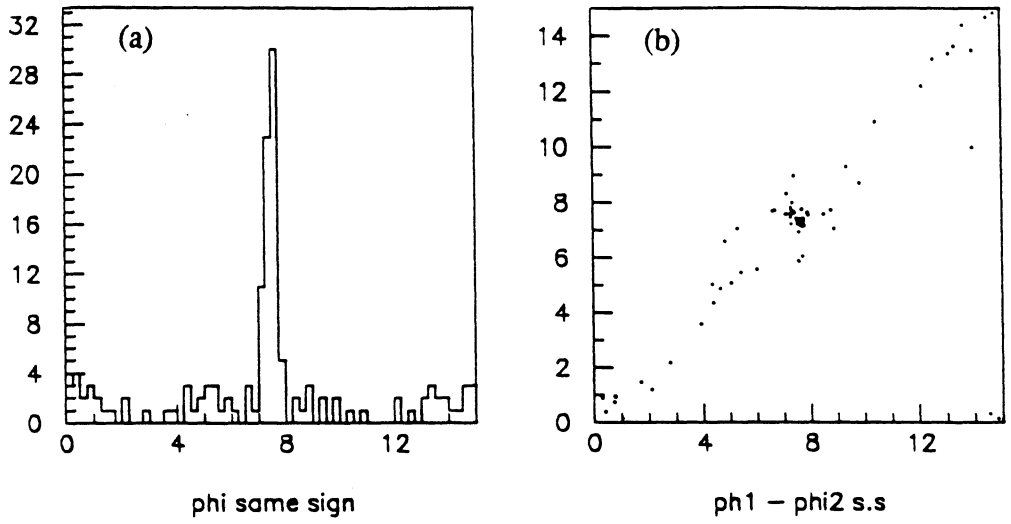

Figure 13: (a)ϕ distribtion of clusters for the event with same sign tracks. (b)Correlation of ϕ_1 and ϕ_2.

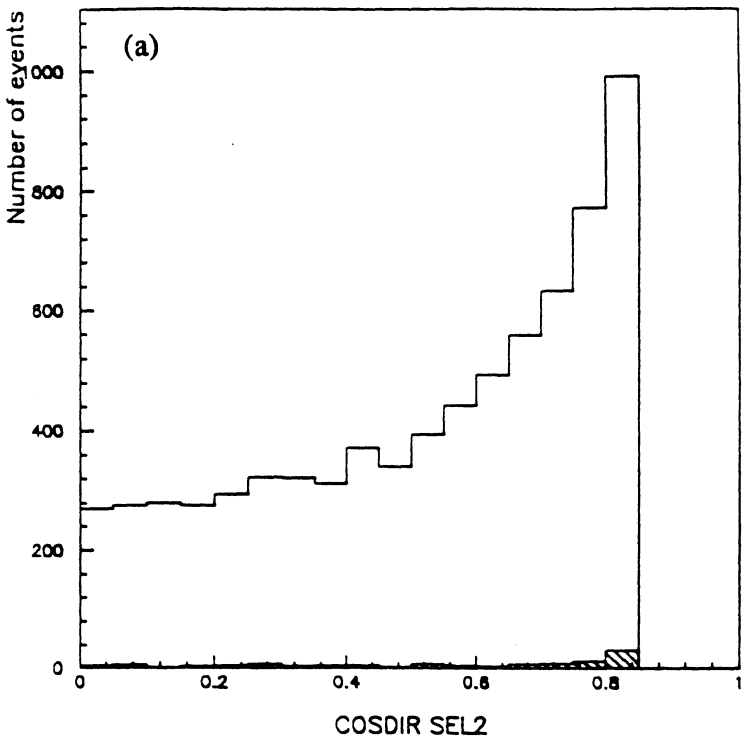

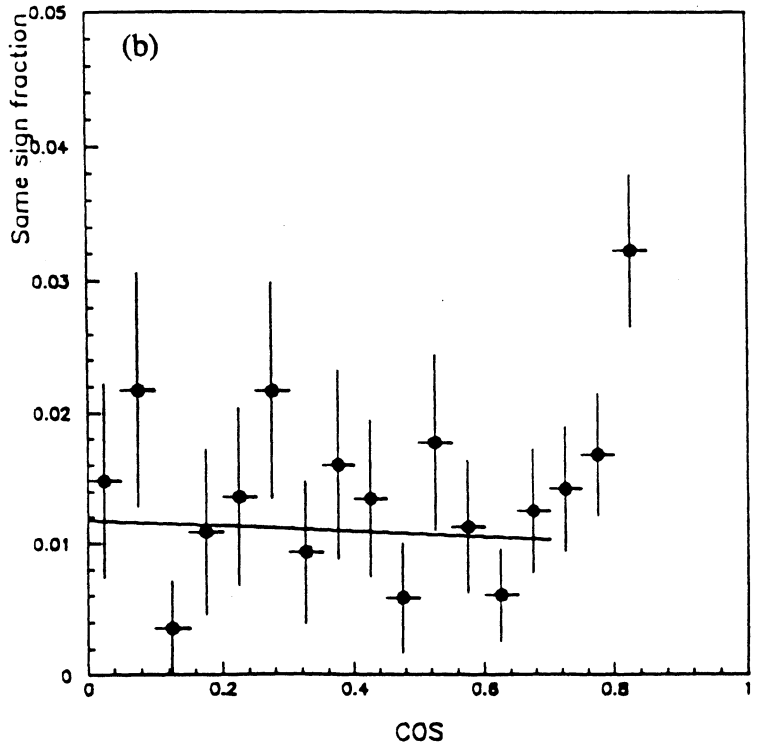

Figure 14: (a) Angular distribution of $e^+e^- \to e^+e^-$ candidates. The hatched histogram shows the events with same signs were assigned to both of tracks. (b) Fraction of the same sign events as a function of $\cos\theta$.

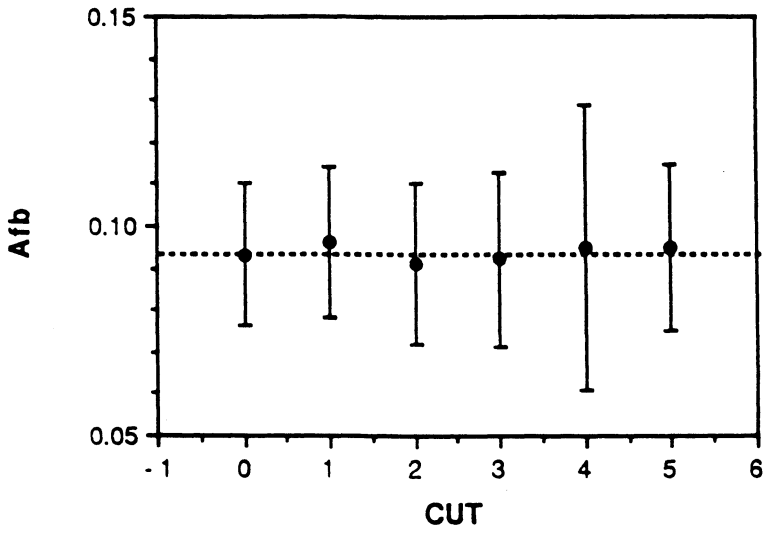

Figure 15: Comparison of forward-backward asymmetry at the Z^0 peak with additional requirements on the track quality. Cut-0 is the standard selection. other cuts are described in the text.

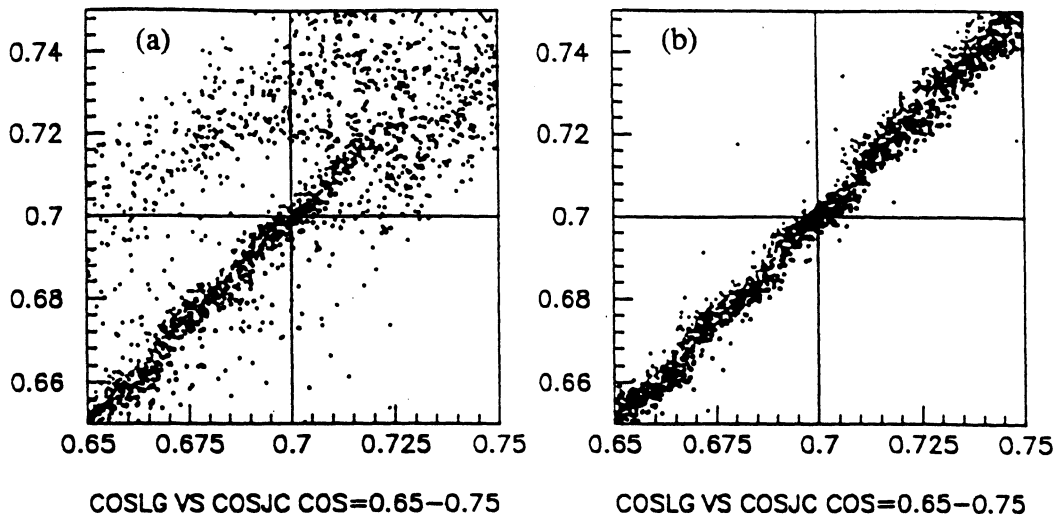

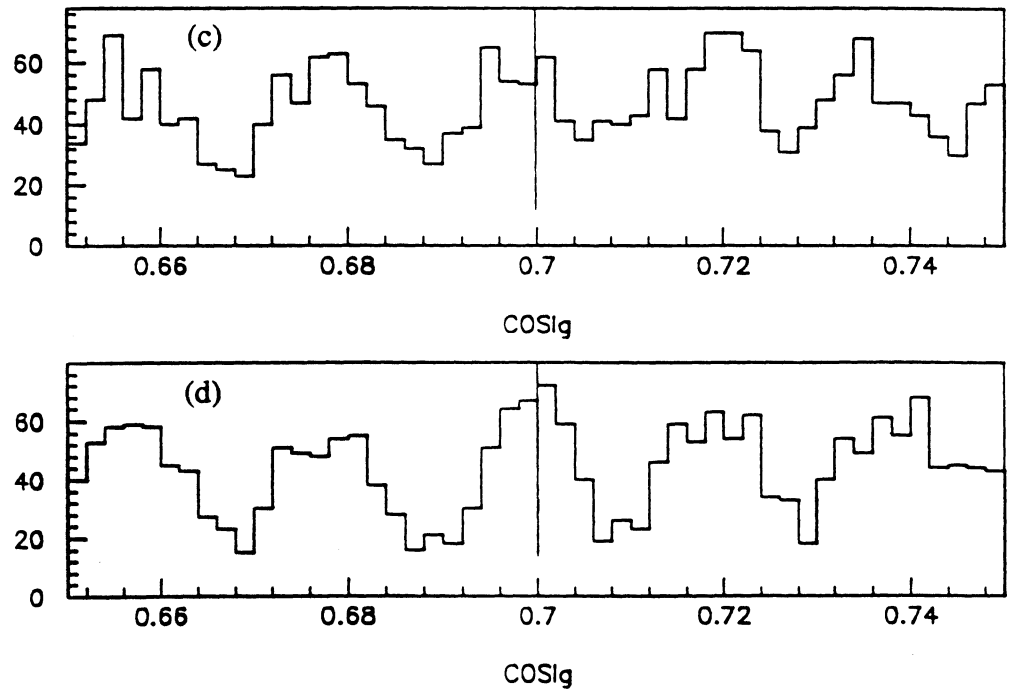

Figure 16: Correlation of $\cos\theta$ measurement by clusters and tracks: (a) $e^+e^- \rightarrow e^+e^-$ candidates and (b) Monte Carlo. Distribution of $\cos\theta_{clust}$ around $\cos\theta = 0.7$: (c) data and (d) Monte Carlo.

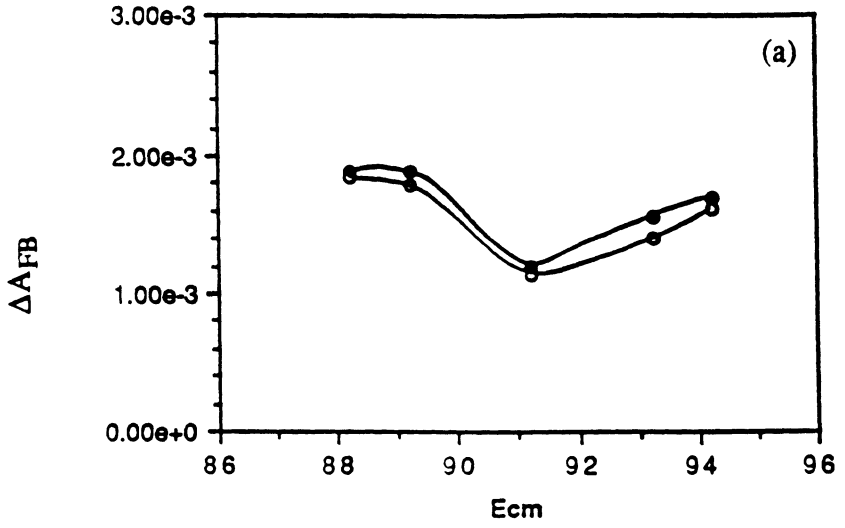

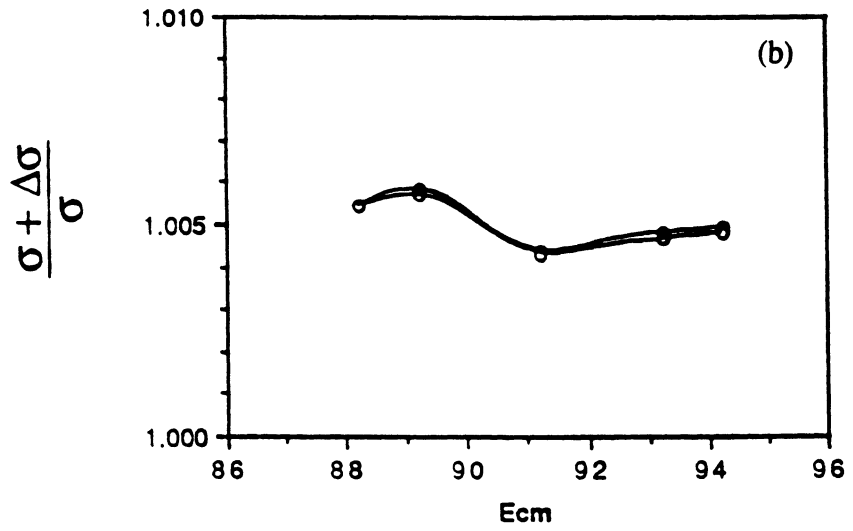

Figure 17: Effect of systematic error in the measured $\cos\theta$, ($\Delta\cos\theta = 0.002$) to a) forward-backward asymmetry and (b) cross section.

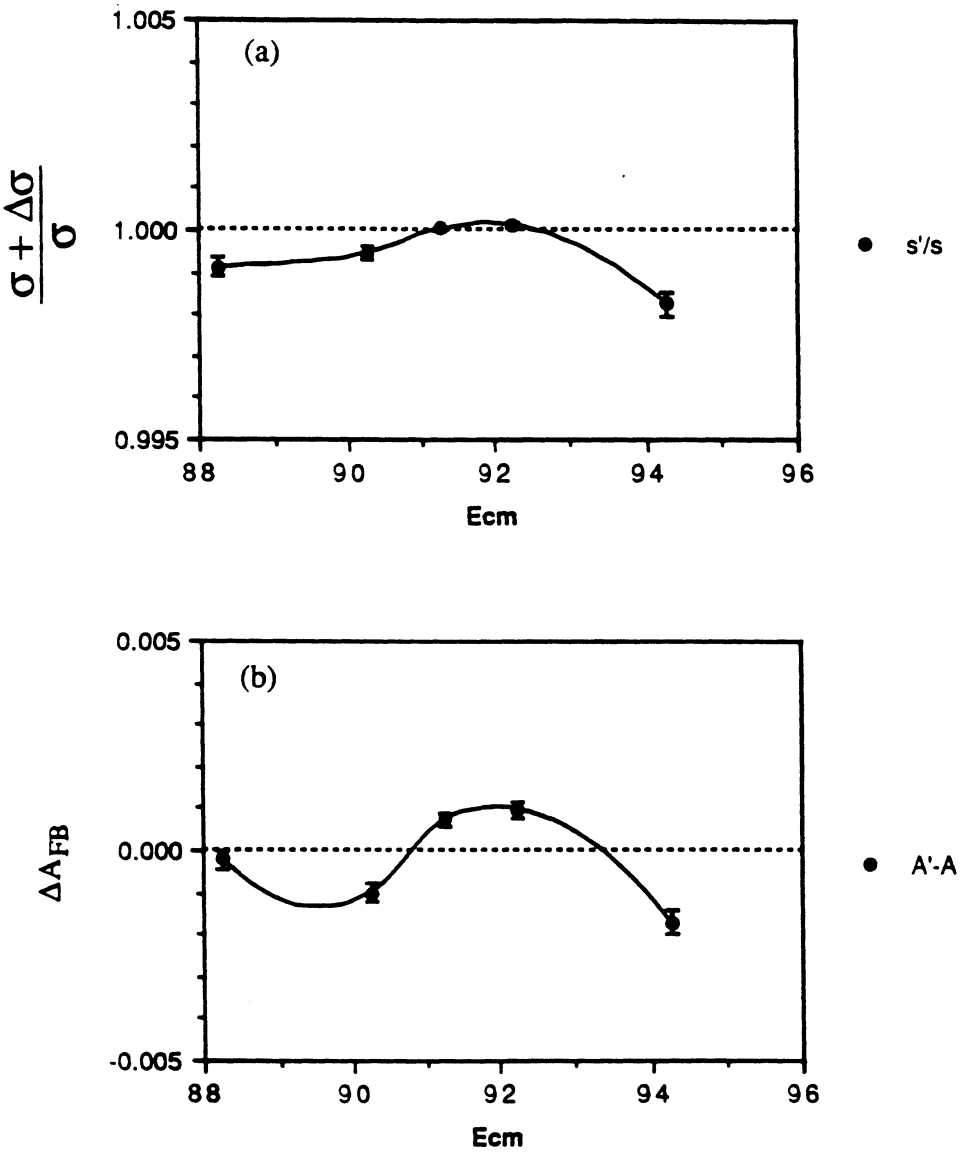

Figure 18: Effect of Z-displacement of the beam vertex and its finite size in Z-direction to (a) cross section and (b) forward-backward asymmetry as a function of center of mass energy estimated using BABAMC. ΔZ = 3.3 mm and σZ =11.8 mm.

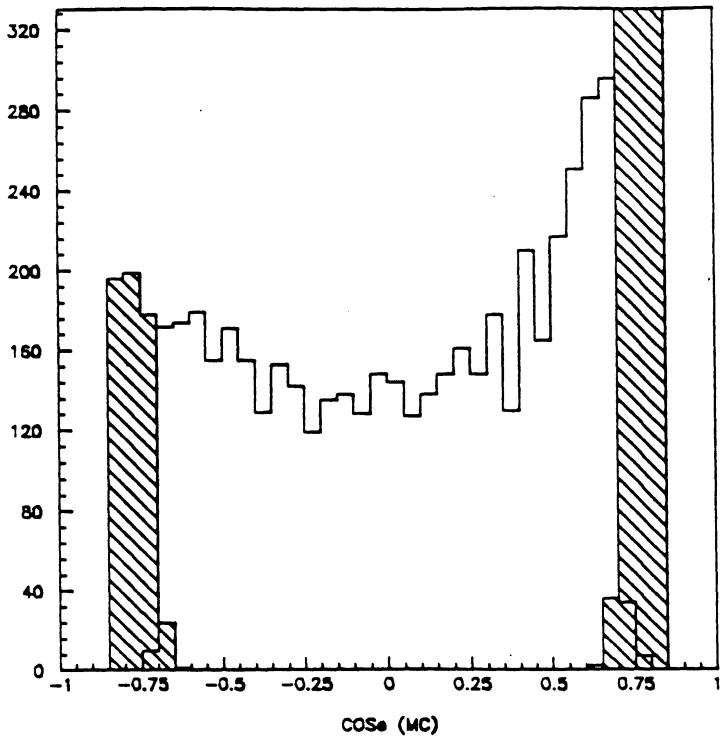

Figure 19: Monte Carlo prediction of the effect of angular resolution. Open histogram is for the events which, at 4-vector level, are inside the angular acceptance. The hatched histogram shows the distribution of the events which are outside of the acceptance at 4-vector level.

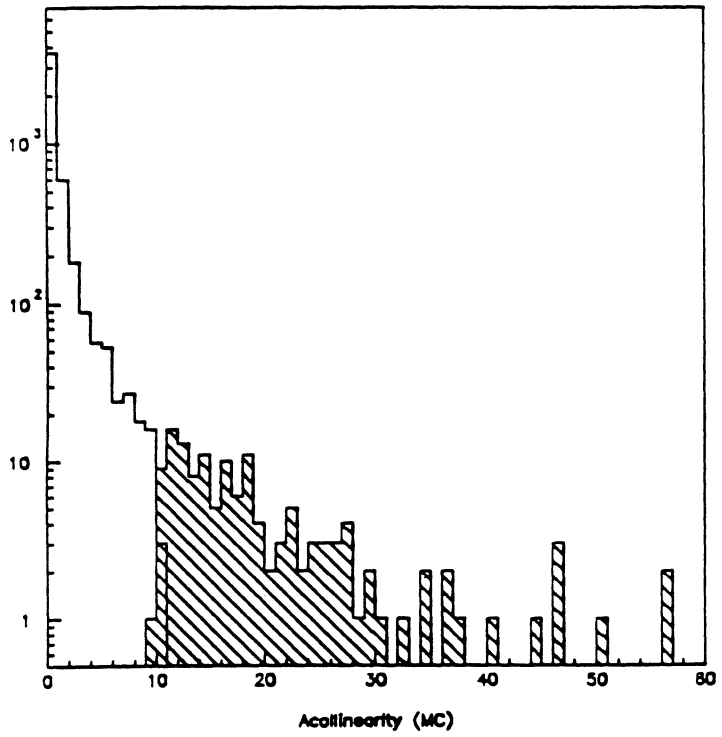

Figure 20: Monte Carlo prediction of acollinearity distribution for $e^+e^- \rightarrow e^+e^-$. Open histogram is for the events which, at 4-vector level, are inside the acollinearity cut. The hatched histogram shows the distribution of the events which are outside of the cut at 4-vector level.

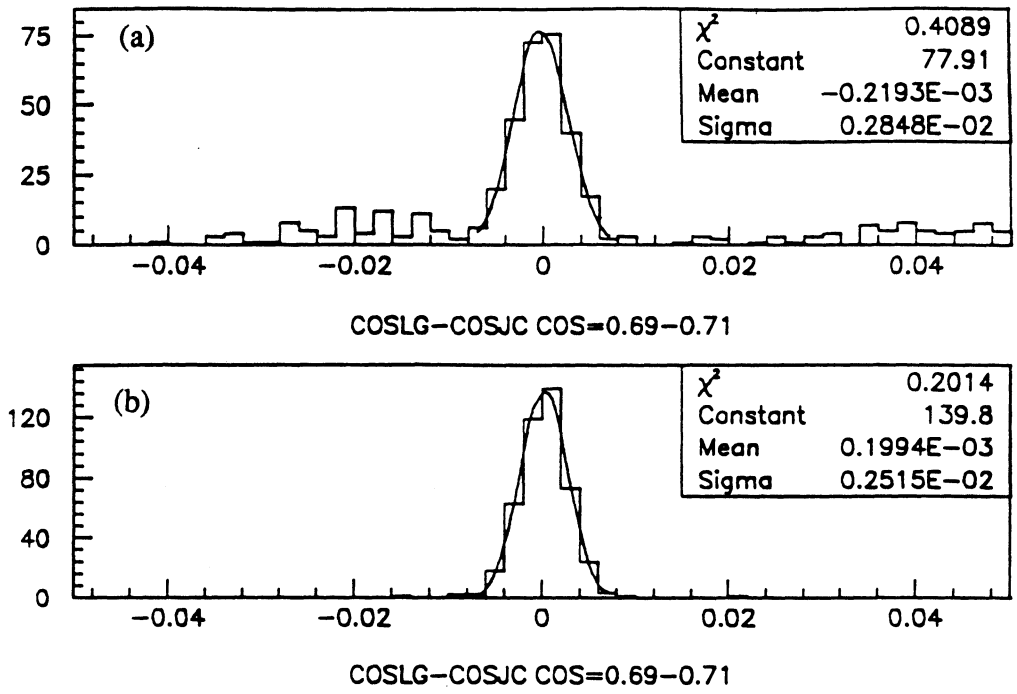

Figure 21: Difference between $\cos\theta_{track}$ and $\cos\theta_{clust}$ in the region $0.69 < |\cos\theta| < 0.71$: (a) data and (b) Monte Carlo. (c) $\theta_{track} - \theta_{clust}$ as a function of ϕ in two CJ sectors for $0.58 < |\cos\theta| < 0.76$.

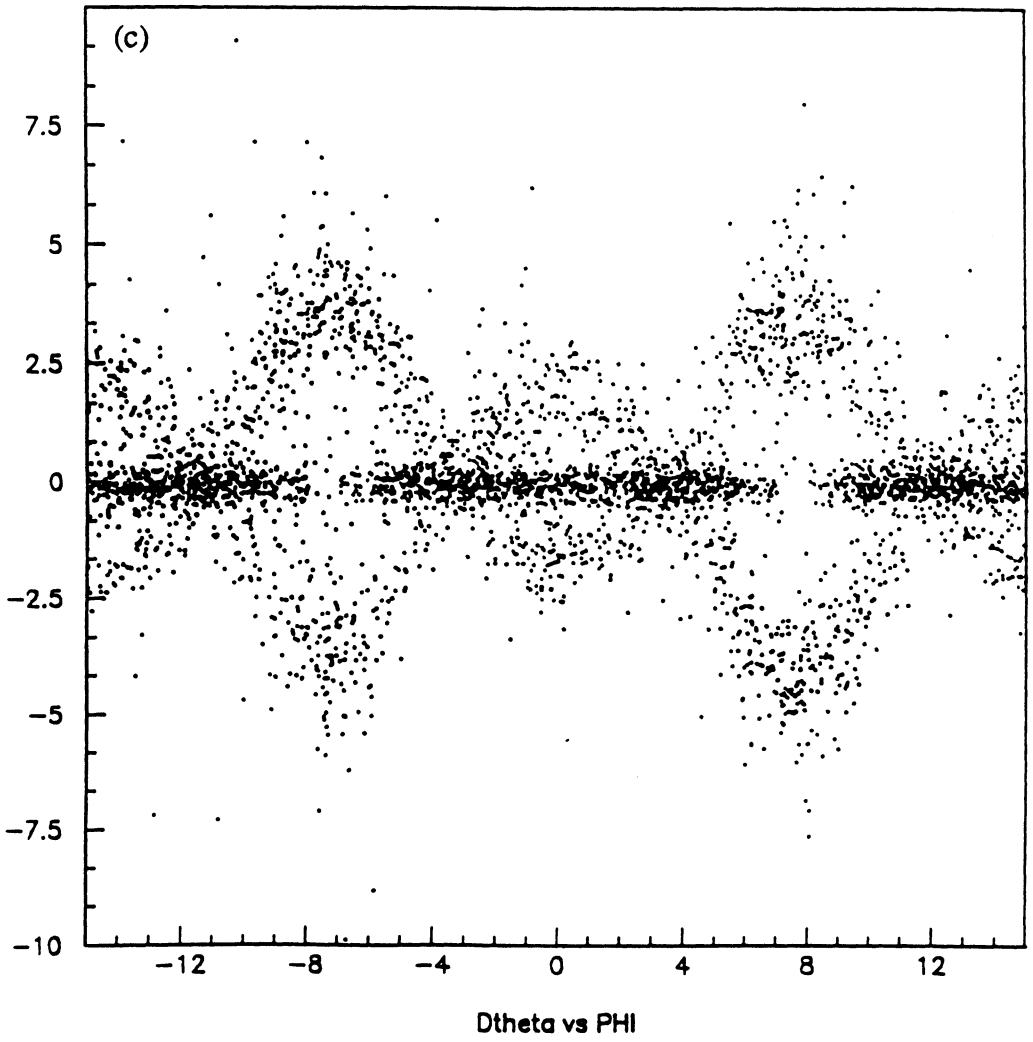

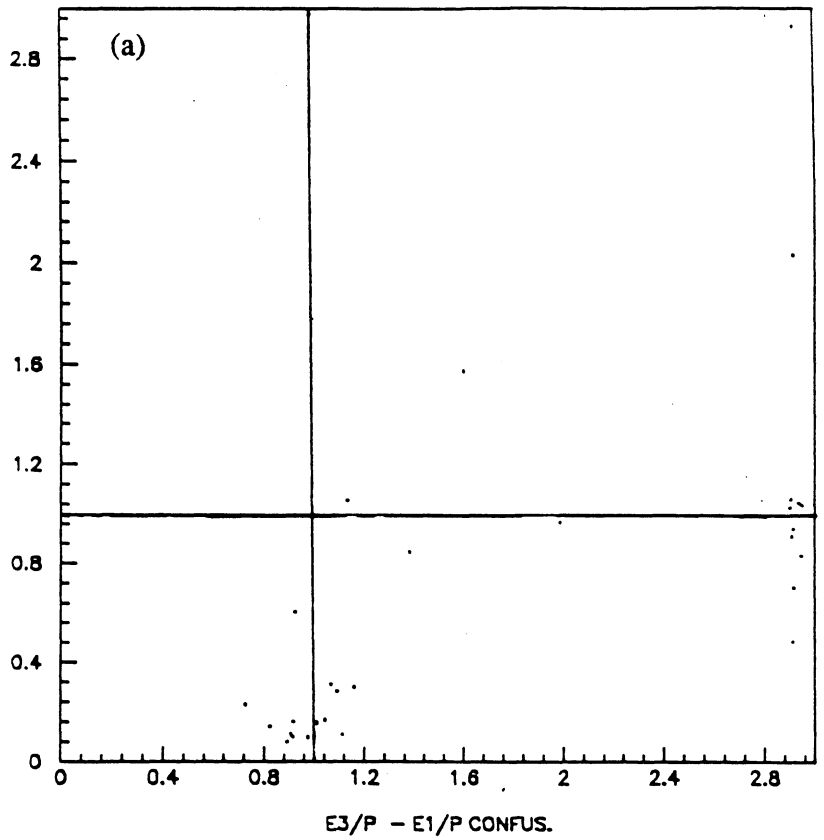

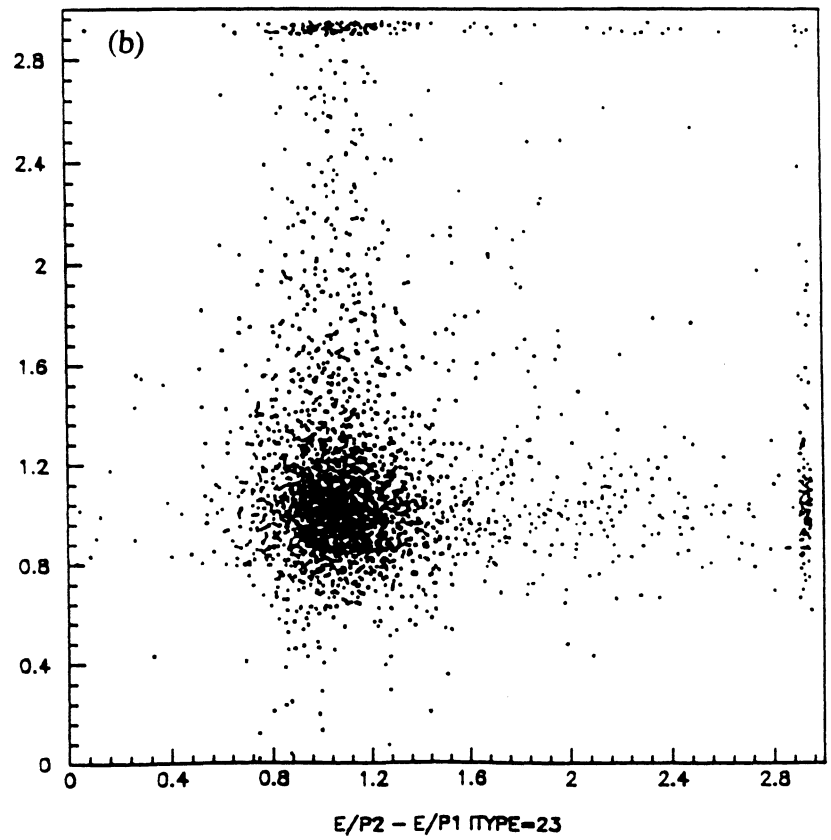

Figure 22: (a) Correlation of two possibilities of E/P in case a track was assigned to two near by clusters. The vertical axis is for the smaller cluster energy. (b) E/P of two back-to-back

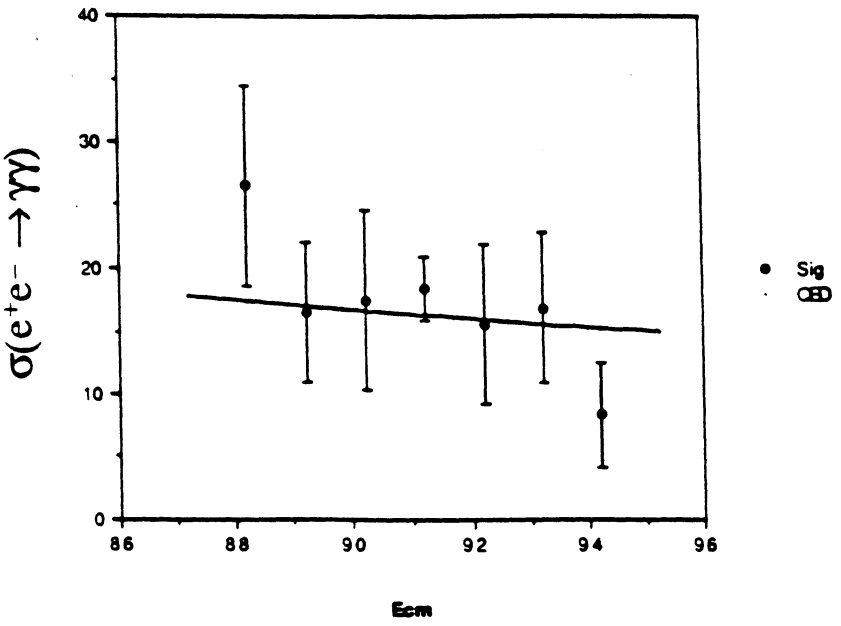

Figure 23: Measured cross section for $e^+e^- \rightarrow \gamma\gamma$ with acceptance cuts; $|\cos\theta| < 0.7$ and $\theta_{acol} < 10°$, after radiative correction plotted as a function of center of mass energy. The solid line shows the QED prediction.

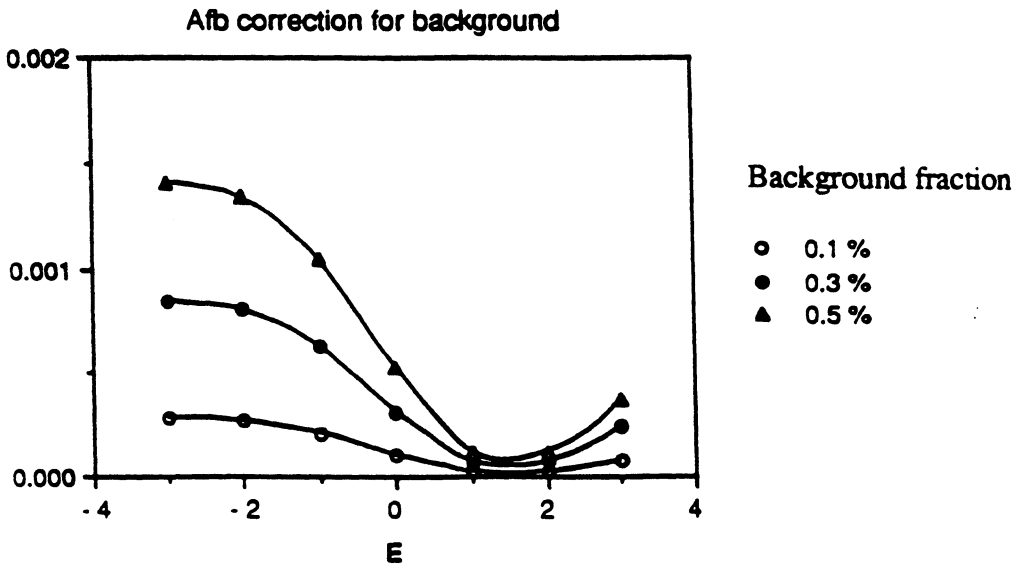

Figure 24: Correction for $\tau^+\tau^-$ background to A_{FB}^{ee} as a function of center of mass energy shown for three different values of background fraction at the Z^0 peak.

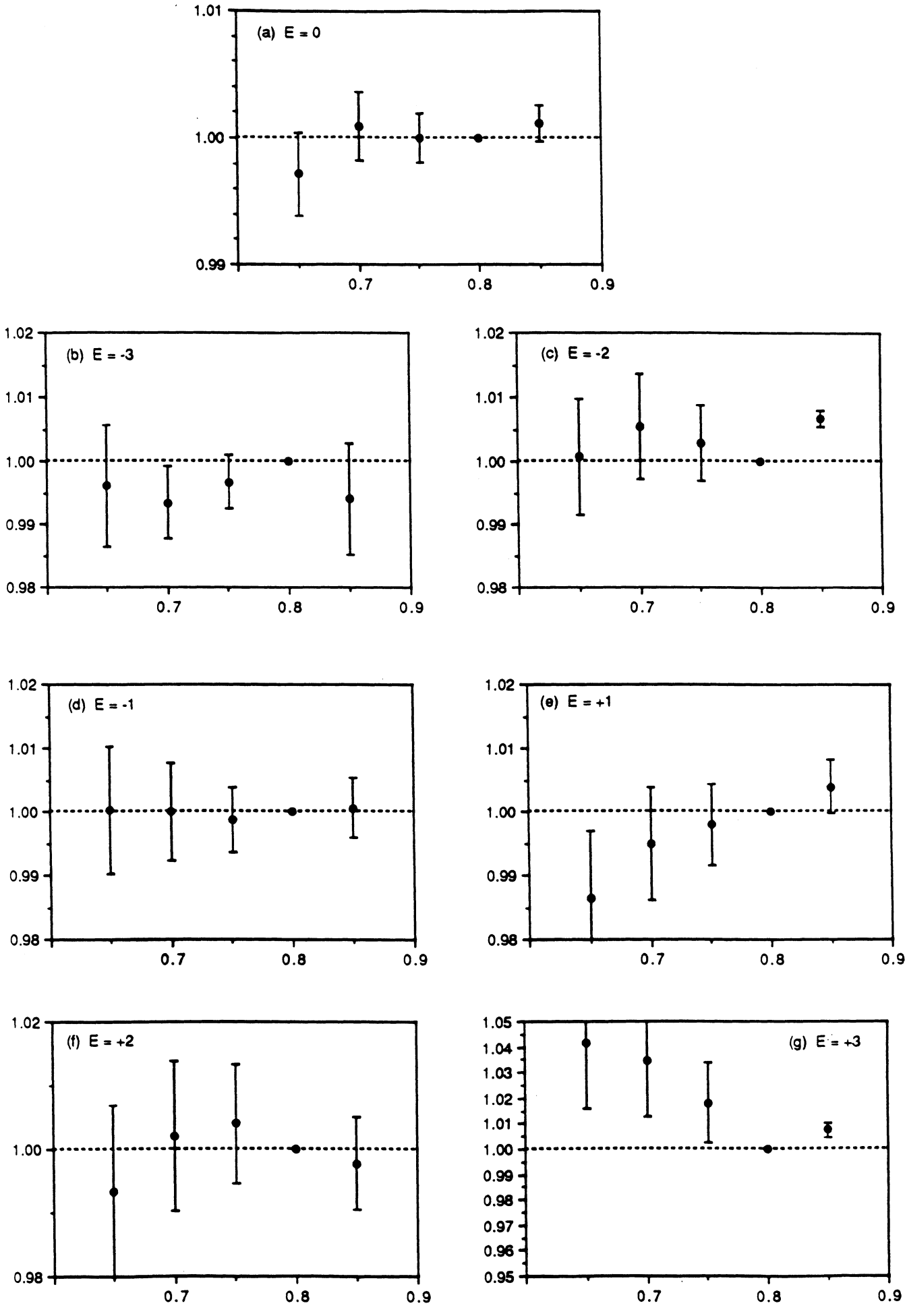

Figure 25: Dependence on the total EM energy cut of the selected number of e^+e^- events after correction for background and inefficiency

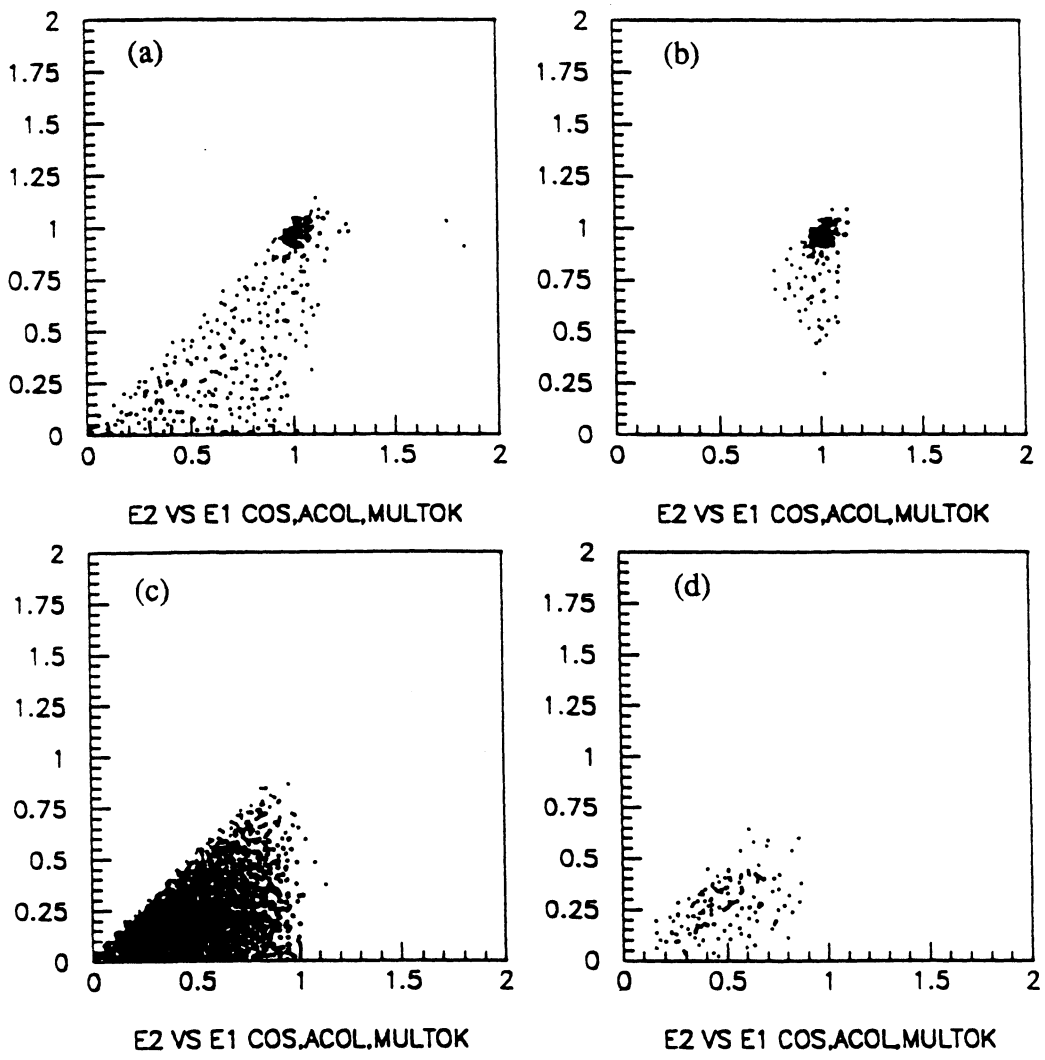

Figure 26: Correlation plot of the highest cluster energy and the next highest cluster energy, (a) data, (b) e^+e^- Monte Carlo, (c) $\tau^+\tau^-$ Monte Carlo, and (d) multihadron Monte Carlo.

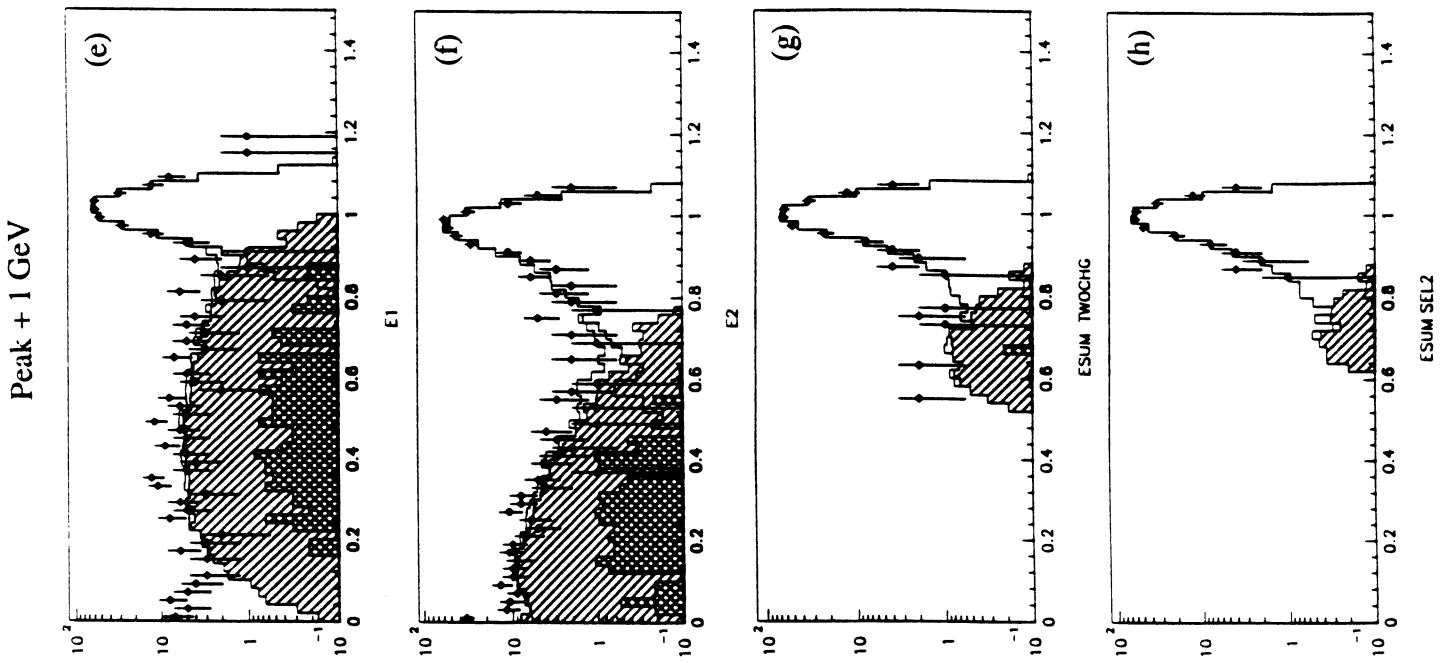

Figure 27: Distribution of the cluster energy E_1, the highest cluster energy and E_2, the energy of the second cluster, after other cuts(multiplicity, acceptance, acollinearity), compared with Monte Carlo. Also shown is the total EM energy with two different cluster energy cuts:(E_1, E_2)=(0.5 , 0.5) and (0.8 , 0.4). The hatched histogram is $\tau^+\tau^-$ contribution and cross hatched histogram is multihadrons as predicted by Monte Carlo. (a)-(d) at Z^0 peak, (e)-(h) at E_{cm} = +1 GeV, (i)-(l) at E_{cm} = +2 GeV and (m)-(p) at E_{cm} = +3 GeV.

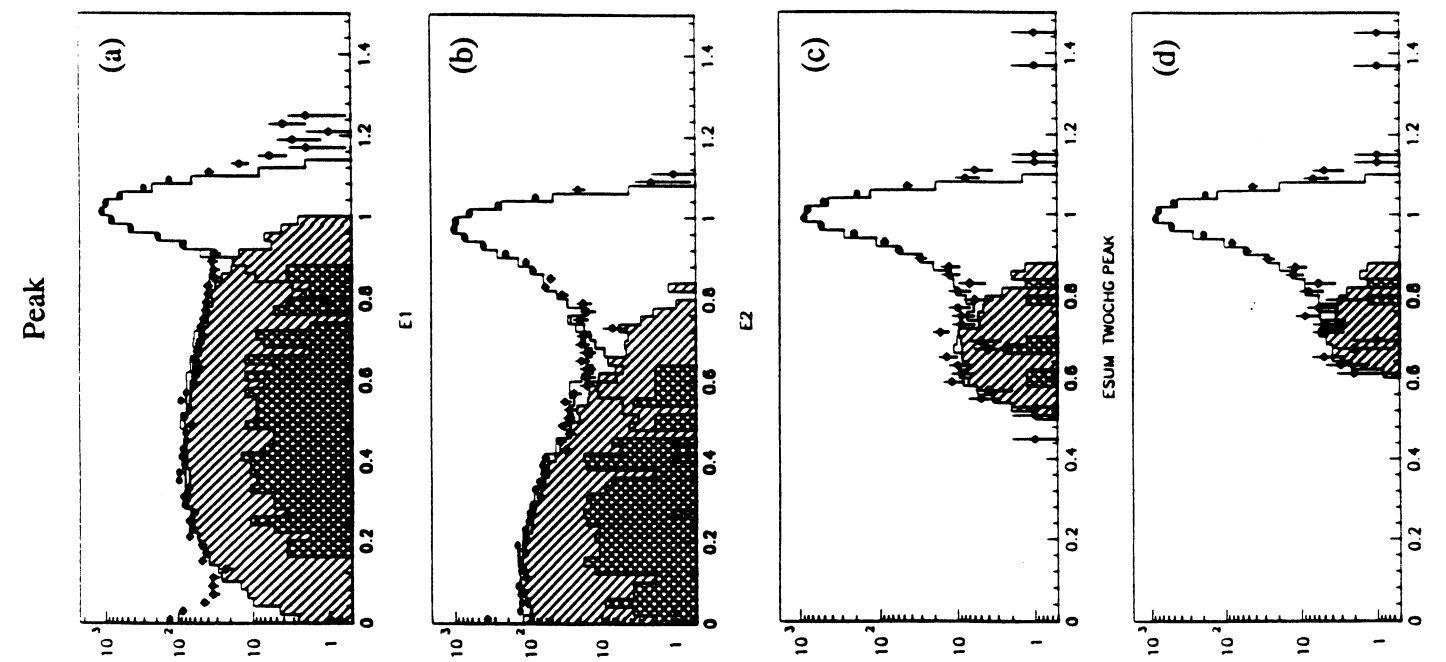

Peak + 2 GeV

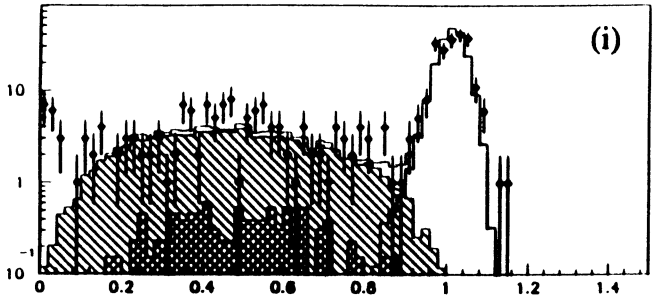

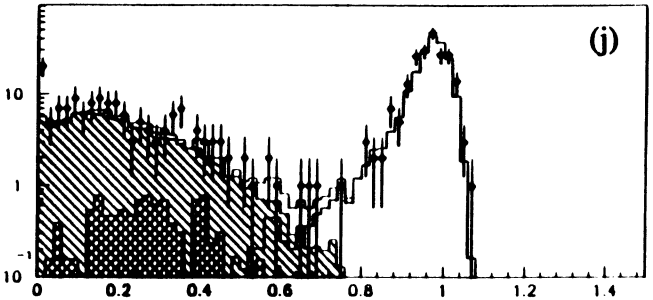

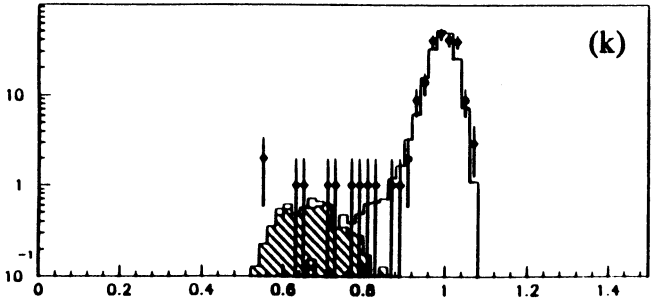

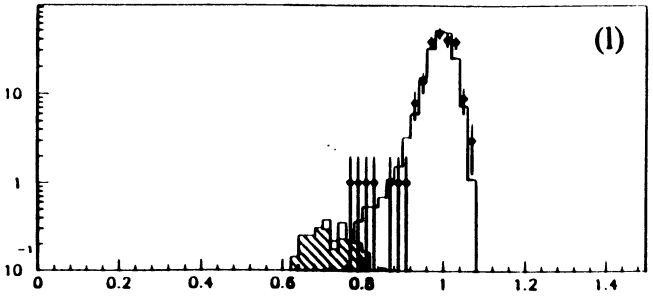

Peak + 3 GeV

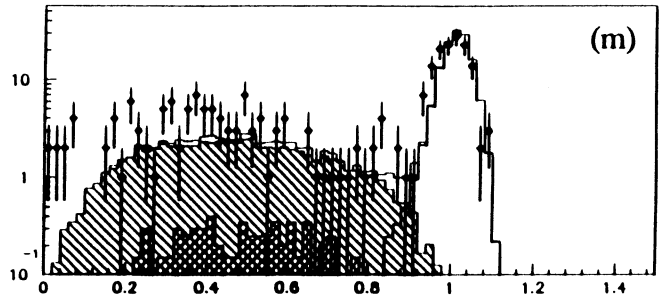

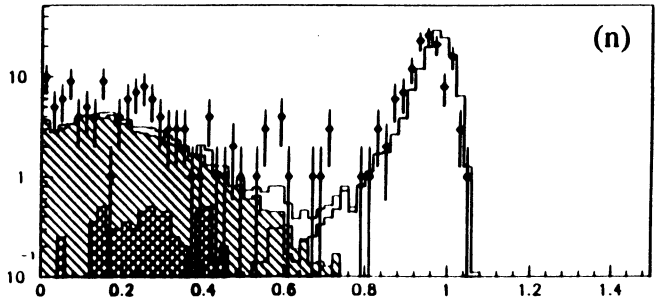

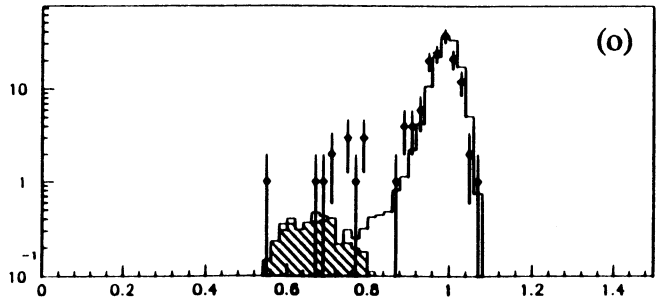

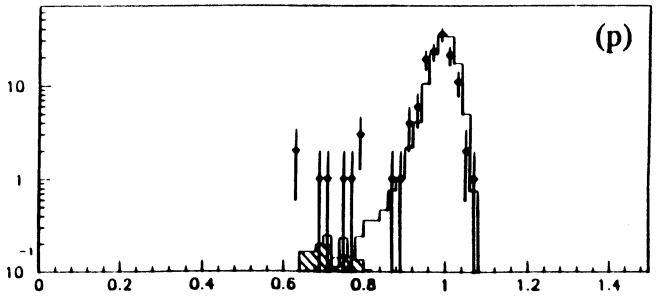

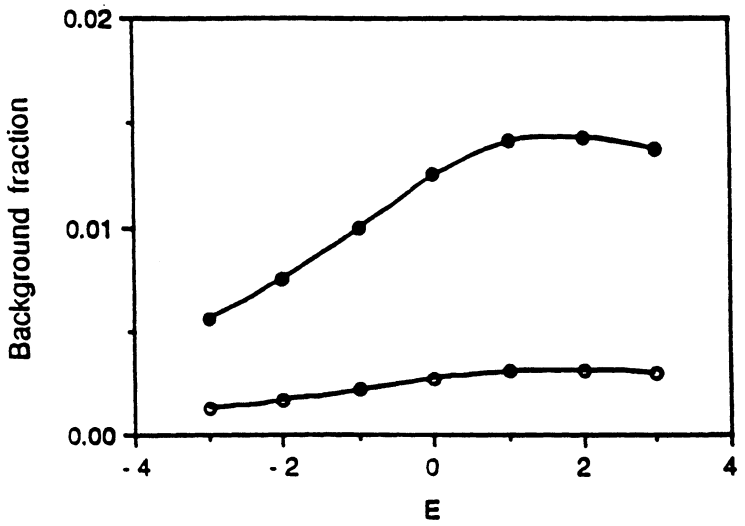

Figure 28: Estimated background fraction as a function of center of mass energy. The open circles are for the standard selection and the closed circles are for the selection with cluster energy cuts alone.

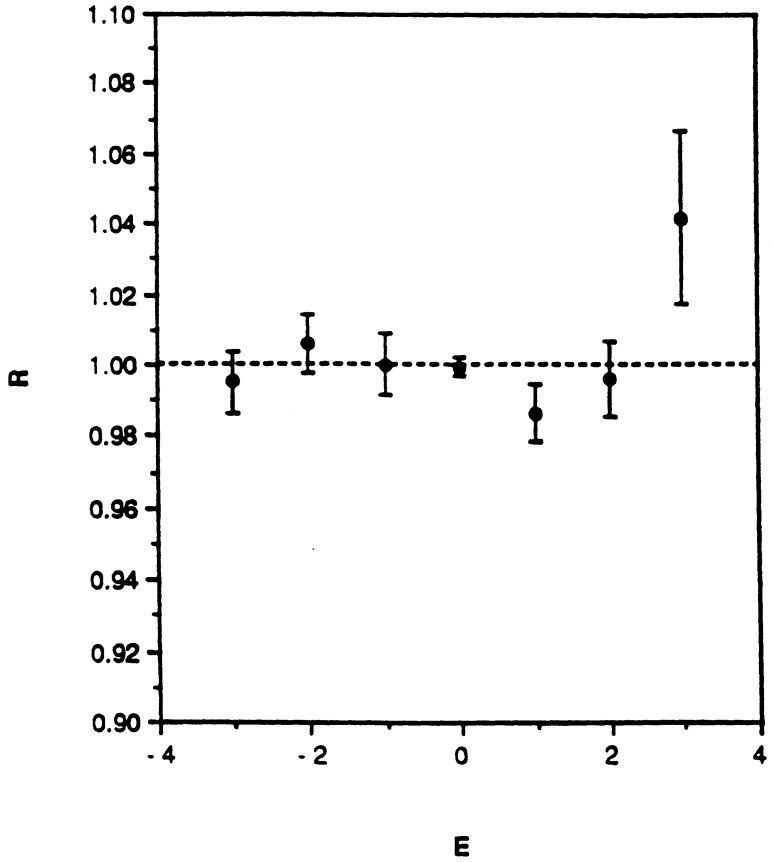

Figure 29: Comparison of two different event selection as described in the text(Cluster energy cut alone / total EM energy cut).

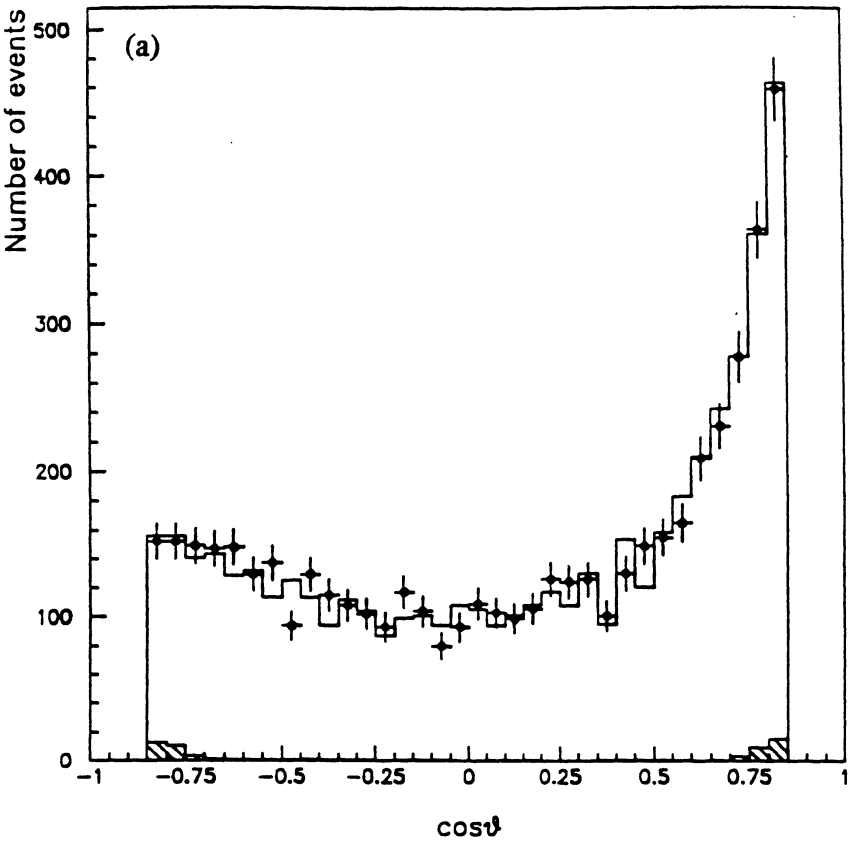

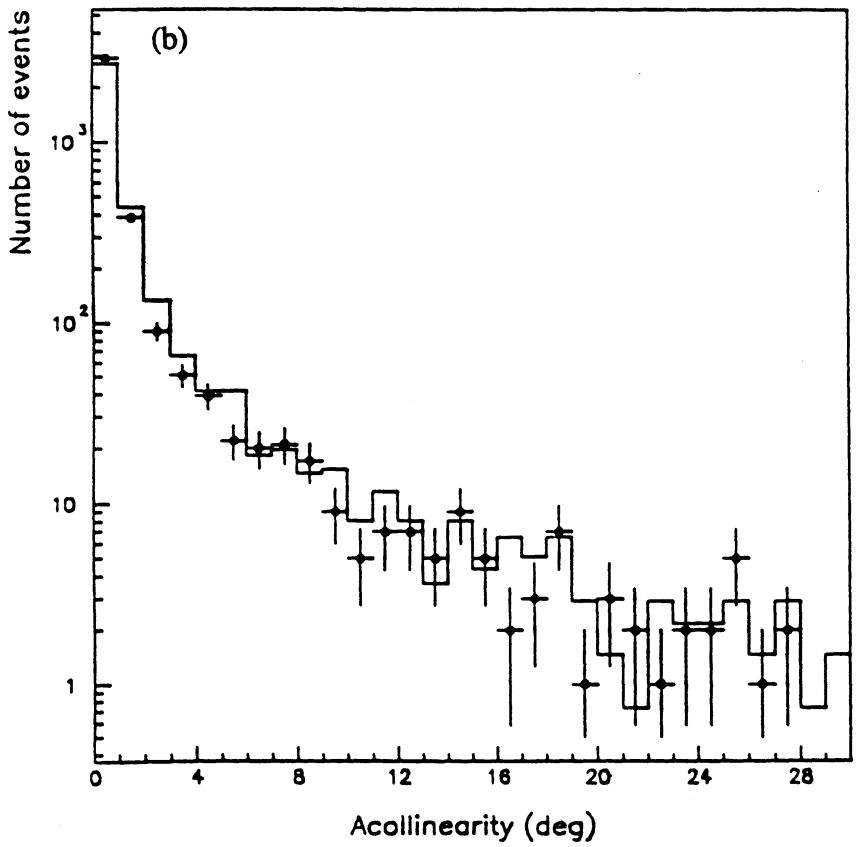

Figure 30: (a) Angular distribution and (b) acollinearity distribution at the Z^0 peak compared with Monte Carlo(BABAMC)(histogram). The hatched histogram shows the contribution from backgrounds.

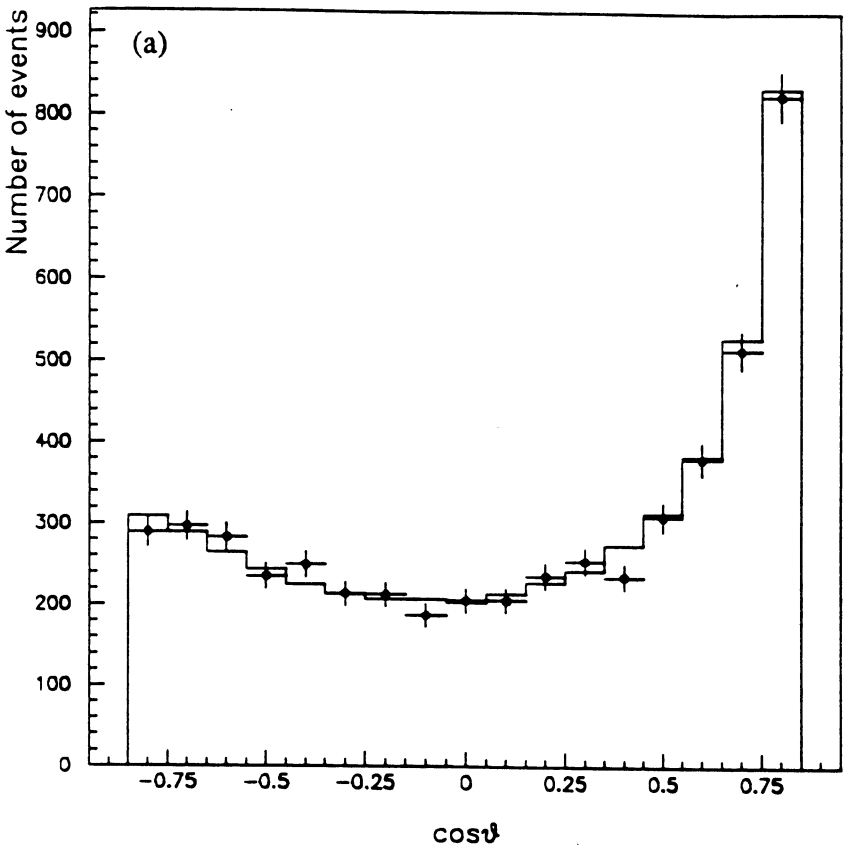

Figure 31: (a) Angular distribution at Z^0 peak compared with ALIBABA prediction(histogram). Data are corrected for inefficiency and backgrounds. (b)-(h) acollinearity distribution at seven different center of mass energies compared with ALIBABA. Discrepancy seen at small angles may be interpretted as an effect of angular resolution which is not corrected for these plots.

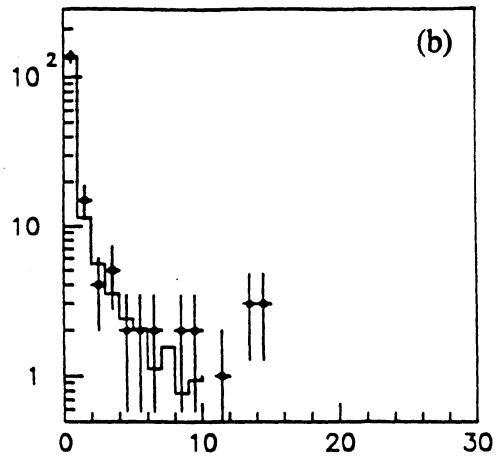

Acol ee −3

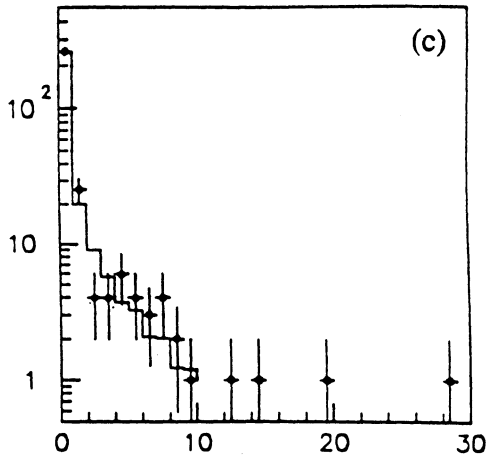

Acol ee −2

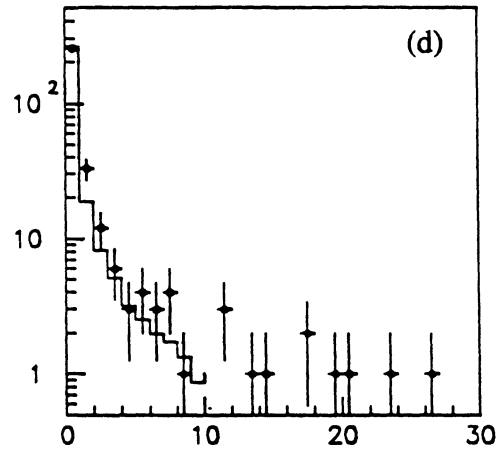

Acol ee −1

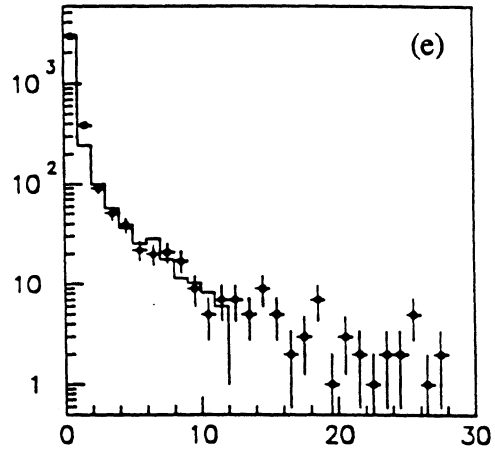

Acol ee , peak

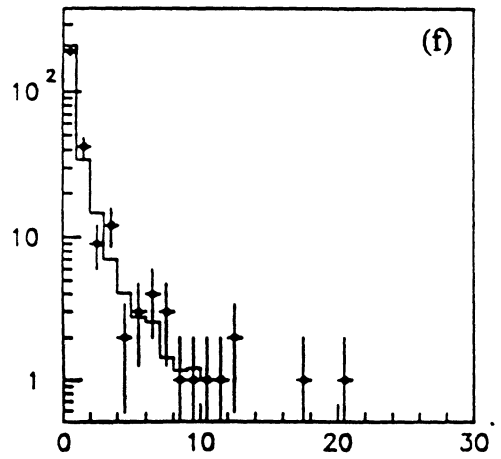

Acol ee +1

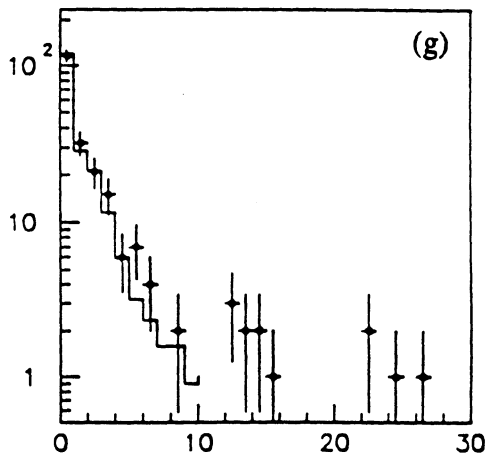

Acol ee +2

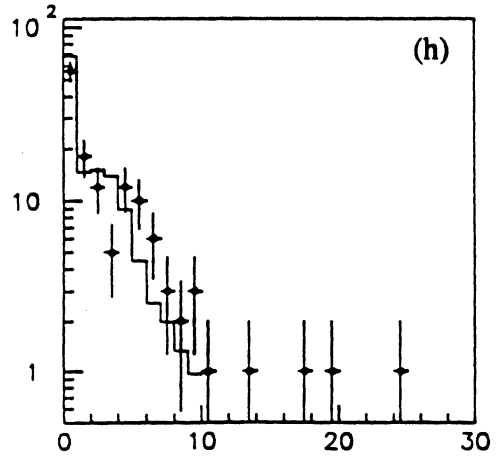

Acol ee +3

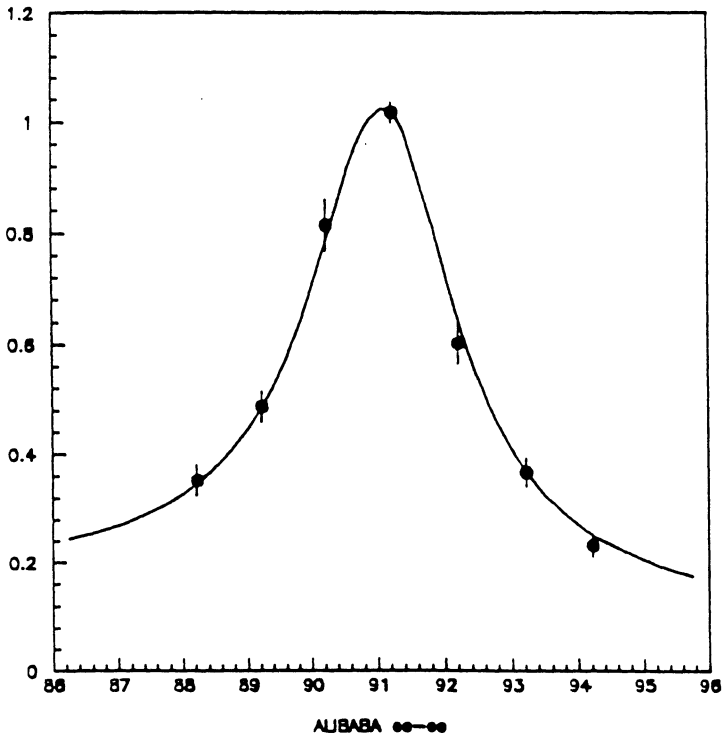

Figure 32: Measured cross section for $e^+e^- \rightarrow e^+e^-$ in the acceptance cut of $-0.7 < \cos\theta_{e^-} < 0.7$ and $\theta_{acol} < 10°$ as a function of center of mass energy. The solid curve is ALIBABA prediction for $M_Z = 91.17$ GeV and $M_T = M_H = 100$GeV.

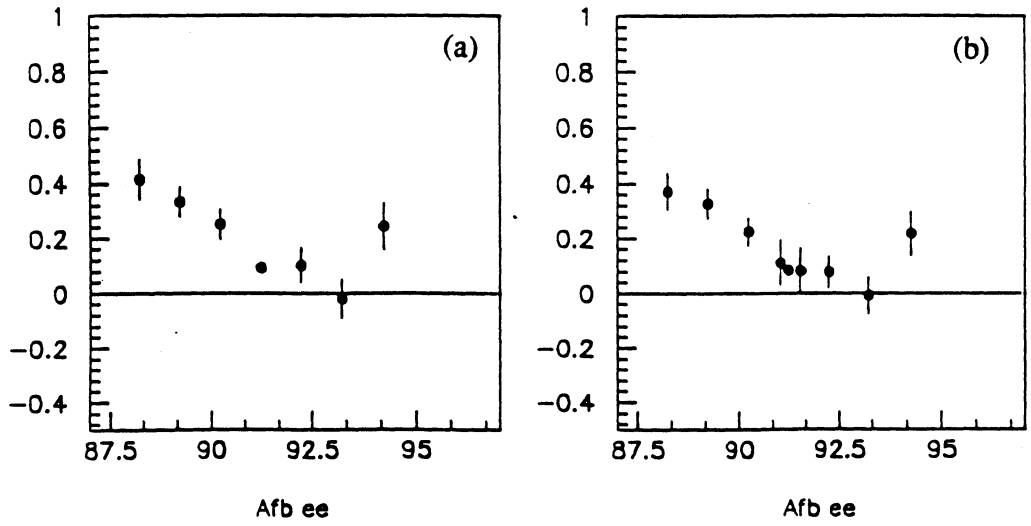

Figure 33: Measured forward-backward asymmetry for $e^+e^- \rightarrow e^+e^-$ in the acceptance of $-0.7 < \cos\theta_{e^-} < 0.7$ and $\theta_{acol} < 10°$ as a function of center of mass energy. (a) 1990 data and (b) 1989 and 1990 combined

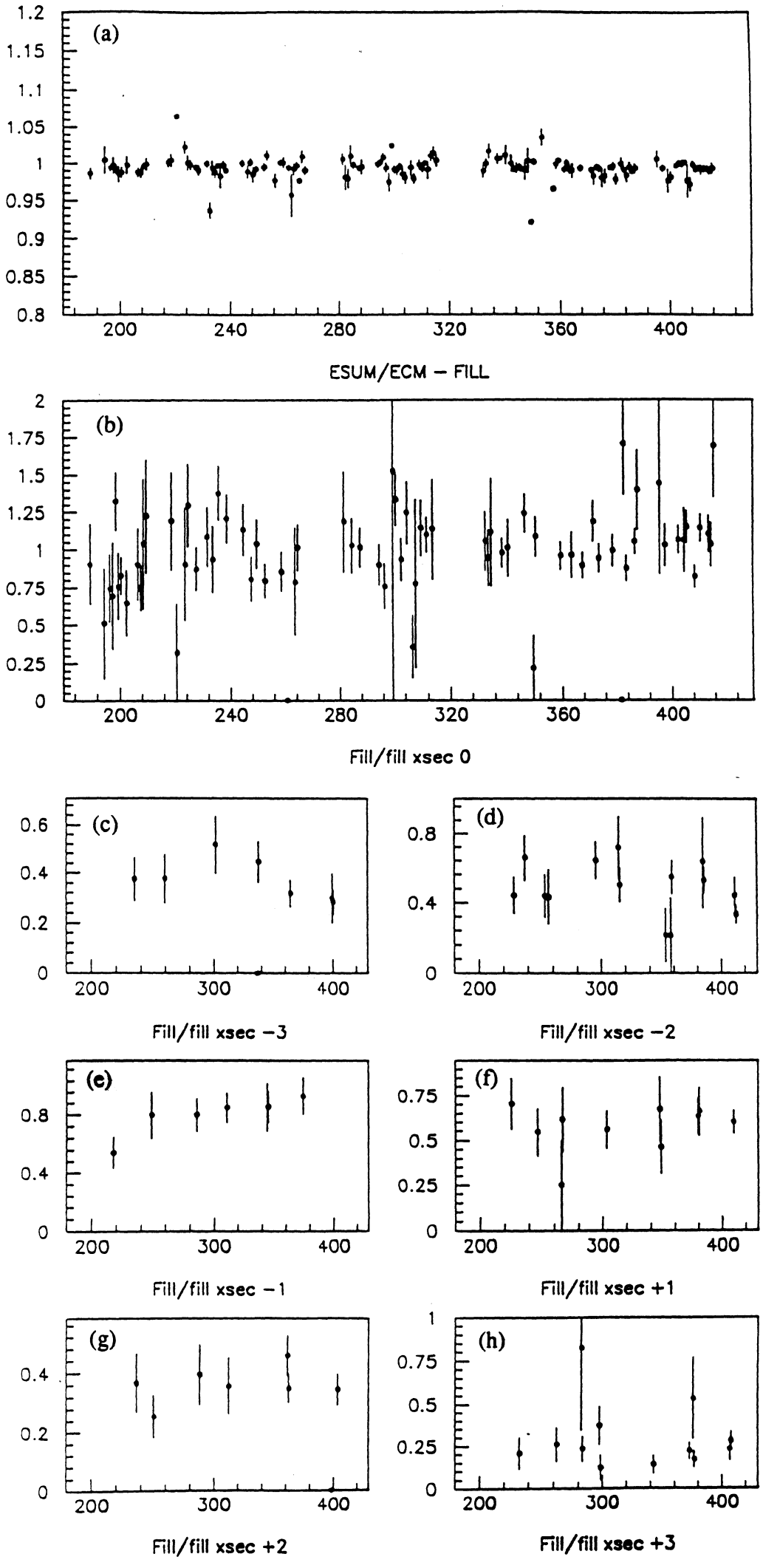

Figure 31: Fill to fill fluctuation of (a) average E_{sum} of $e^+e^- \to e^+e^-$ candidates and (b)-(h) measured cross section, plotted for seven different center of mass energies.